INTERFACIAL ELECTRON-TRANSFER REACTIONS AT SEMICONDUCTOR ELECTRODES

Thesis by

Thomas W. Hamann

In Partial Fulfillment of the Requirements

for the Degree of

Doctor of Philosophy

CALIFORNIA INSTITUTE OF TECHNOLOGY

Pasadena, California

Defended July 20, 2006

ACKNOWLEDGMENTS

First of all, I am grateful to my advisor, Nate Lewis, for his instruction and encouragement during my scientific journey in the interesting field of semiconductor electrochemistry. I have come to marvel at his quick mind, depth of knowledge, and enthusiasm for understanding this world. Nate's critical analysis and requirement to "really nail it" taught me to think through everything very carefully and set my scientific standards at a high level. Finally, I appreciate the freedom of inquiry and exploration that I enjoyed; even though it led to many mistakes and dead-ends, they proved as instructive as the successes.

I am also thankful to Bruce Brunschwig; he has been a great teacher, mentor, and colleague to me and his good nature has made him a pleasure to work with. I admire his patience in explaining things and meticulous attention to details. No matter how busy he was, Bruce always seemed willing to spend hours with me working through whatever problem I brought him, and I have benefited greatly from these interactions. I am also thankful to my former advisor, Hans van Willigen, for introducing me to the pleasure and rigors of scientific research. It is one of my continued goals to emulate his thoroughness, integrity, and humility, which I believe are the ideal characteristics of a scientist.

It is my honor to thank my committee members, Geoff Blake, Harry Gray, and Jacqueline Barton, who are all not only great scientists and teachers, but very nice people. I want to thank everyone in the Lewis group, old and new. I have benefited from the help, advice, and/or conversation of every single member I have known. I especially thank Florian Gstrein for showing me how to do electrochemistry experiments and introducing me to ZnO, and Agnes Juang, Dave Michelak, and Lauren Webb for teaching me how to work with and functionalize silicon and use the XPS. Finally, I appreciate the many stimulating conversations and arguments over coffee or drinks with Nick Prokopuk, Watson, and Will Royal, which was a great diversion from lab.

Lastly, I thank all my family and friends for their love and support, Svetlana for her belief in me, and especially my parents for creating and raising me.

ABSTRACT

Differential capacitance versus potential and current density vs. potential measurements were used to determine the energetics and kinetics, respectively, of the interfacial electron-transfer processes of n-type ZnO electrodes in contact with aqueous solutions. The electron-transfer rate constant, k_{et}, vs. driving force was investigated employing a series of non-adsorbing, one-electron, outer-sphere redox couples with formal reduction potentials spanning approximately 900 mV in the band-gap region. The data were well-fit by a parabola generated using classical Marcus theory with a reorganization energy, λ, of 0.67 eV. The dependence of k_{et} on λ was determined using a series of compounds with similar formal reduction potentials, but reorganization energies that span approximately 1 eV. The interfacial electron-transfer rate constant decreases as the reorganization energy of the acceptor species increases and a plot of the logarithm of the electron-transfer rate constant vs. $\frac{\left(\lambda + \Delta G^{0'}\right)^2}{4\lambda k_B T}$ is linear with a slope of ≈ -1. Changes in solution pH were used to shift the band-edge positions of ZnO electrodes relative to solution-based electron acceptors having pH-independent redox potentials. This strategy allowed investigation of the pH-induced driving-force dependence of k_{et} in the normal and inverted regions. It was further found that introduction of the tert-butyl functionality on osmium tris-bipyridyl decreased the self-exchange rate constant, determined from NMR line-broadening measurements, by a factor of 50 and the interfacial electron-transfer rate constant by 100, compared to that of the analogous methyl-substituted complex. The results indicate that the tert-butyl group can act as a spacer on an outer-sphere redox couple to significantly decrease the electronic coupling of the electron-transfer reaction both in self-exchange and interfacial electron-transfer processes. Methyl-terminated, n-type, (111)-oriented Si surfaces in contact with an electron acceptor having a pH-independent redox potential were used to verify that the band edges of the modified Si electrode were fixed with respect to changes in solution pH. These results, taken together, provide strong evidence that interfacial electron-transfer rate constants at semiconductor electrodes are in excellent agreement with the predictions of a Marcus-type model of interfacial electron-transfer reactions.

TABLE OF CONTENTS

LIST OF SCHEMES

Number *Page*

LIST OF FIGURES

LIST OF TABLES

Summary

This thesis describes the investigation of heterogeneous charge-transfer reactions. A simple example, which is examined in detail herein, is the transfer of an electron from a semiconductor electrode to a non-adsorbing molecular species dissolved in solution. In addition to basic scientific interest, interfacial electron transfer is an important step in many technological applications such as solar energy conversion and storage devices. As an example of particular importance, photoelectrochemical cells provide the most efficient wet chemical method presently known to convert solar energy into chemical or electrical energy. The transfer of an electron across the semiconductor/liquid interface is a key process in the operation of both fuel-forming and regenerative photoelectro-chemical energy conversion systems. Therefore, a detailed understanding of the factors that control interfacial electron-transfer reactions is crucial to the development of improved solar energy devices.

A microscopic description of electron-transfer reactions has been developed by Rudy Marcus.[1-3] Numerous experimental studies on homogeneous intermolecular and intramolecular donor-acceptor (D-A) systems, have provided strong evidence in support of Marcus theory.[4-6] In contrast, studies of heterogeneous charge-transfer reactions at semiconductor electrodes have shown mechanistic behavior consistent with Marcus theory, but experimental confirmation has been lacking due to non-ideal electrode behavior, redox species adsorption, and other issues at semiconductor electrode surfaces.

Fermi's golden rule was used to extend the Marcus formalism to the case of electron-transfer reactions across the semiconductor/liquid interface giving the following expression:[7]

$$k_{et} = \frac{2\pi}{\hbar}\frac{1}{(4\pi k_B T\lambda_{sc})^{1/2}}\left(\overline{H^2_{AB,sc}}\right)\beta_{sc}^{-1}\left\{\frac{l_{sc}}{d_{sc}^{2/3}(6/\pi)^{1/3}}\right\}\left[\exp\left\{\frac{-[(\overbrace{\mathbf{E}_{CB}-qE^{o'}}^{\Delta G^{0'}})+\lambda_{sc}]^2}{(4k_B T\lambda_{sc})}\right\}\right] \quad (1)$$

where β_{sc} is the coupling attenuation factor, l_{sc} is the effective coupling length in the semiconductor, λ_{sc} is the reorganization energy of the acceptor species near the semiconductor electrode, and d_{sc} is the atomic density of the solid. The quantity $\overline{H^2_{AB,sc}}$ represents the square of the matrix element that couples reactant and product states at energy **E**, averaged over all degenerate states in the semiconductor in a plane parallel to the electrode surface. $\overline{H^2_{AB,sc}}$ is assumed to be independent of energy over the range of interest.[7] The subscript "sc" indicates parameters for a semiconductor electrode. The quantity $\Delta G°'$ is the change in standard interfacial free energies, where $\mathbf{E}_{CB}$ is the energy of the conduction band and $E^{o'}(A/A^-)$ is the formal reduction potential of the (A/A^-) redox system. The exponent's prefactor can be combined into the term $k_{et,max}$, which is the rate constant at optimal exoergicity, defined when $-\Delta G°' = \lambda_{sc}$. The overall objective of the work presented in this thesis is the experimental test of predictions from the Marcus model of electron transfer as applied to semiconductor/liquid junctions. Specifically, investigations of the interfacial electron-transfer rate constant as a function of $\Delta G°'$, λ_{sc}, and $\overline{H^2_{AB,sc}}$, and the determination of $k_{et,max}$ will be presented herein.

In Chapter 1 the driving force dependence of interfacial electron-transfer reacations at ZnO electrodes is investigated. Rate constants have been measured for a series of one-electron outer-sphere redox couples, whose potentials span approximately 900 mV in the band gap region of ZnO, in contact with n-type ZnO electrodes. NMR line-broadening experiments were performed to determine the reorganization energies of the compounds in the same medium as that used to determine the interfacial kinetics at ZnO. These measurements allow for a detailed investigation of the dependence of the rate constant for electron transfer on driving force in both the normal and Marcus

inverted region, for a homologous series of outer-sphere redox-active compounds at an "ideally" behaving semiconductor/electrode interface.

Chapter 2 addresses another basic prediction of the Marcus model for interfacial electron-transfer reactions at semiconductor electrodes, specifically that the interfacial electron-transfer rate constant should be strongly dependant on the reorganization energy, λ_{sc}, of the acceptor species in solution. At constant driving force, k_{et} should decrease as λ_{sc} increases in the normal region, and k_{et} should increase as λ_{sc} increases in the inverted region. In order to verify this basic theoretical prediction, we have synthesized a series of one-electron redox couples having relatively constant potentials in the band-gap region of ZnO and having reorganization energies that span approximately 1 eV. Charge-transfer rate constants have been measured for these systems in contact with n-type ZnO electrodes. This investigation provides a detailed comparison of interfacial electron-transfer reactions at an "ideally" behaving semiconductor/electrode interface with the predictions of Marcus theory for such systems.

Chapter 3 examines another method of changing the driving force by holding the energetics of the redox couple constant while changing the chemical state of the semiconductor surface. A pH-dependent variation of the conduction band edge energy is expected for metal oxide electrodes due to the protonation/deprotonation equilibrium of –OH sites on the oxide surface. The driving force for interfacial electron-transfer reactions can thus be conveniently tuned by varying the solution pH. We have evaluated the pH-dependence of the rate constants for interfacial charge transfer at single crystal ZnO electrodes in contact with the dissolved, outer-sphere redox species $[Co(bpy)_3]^{3+/2+}$ and $[Ru(bpy)_2(MeIm)_2]^{3+/2+}$ (where MeIm = 1-methyl imidazole). The redox couples $[Co(bpy)_3]^{3+/2+}$ and $[Ru(bpy)_2(MeIm)_2]^{3+/2+}$ are of specific interest because prior measurements of the band-edge positions at n-type ZnO electrodes indicate that $[Co(bpy)_3]^{3+/2+}$ should be in the normal region, whereas $[Ru(bpy)_2(MeIm)_2]^{3+/2+}$ should be in the inverted region.[6] The charge-transfer rate constant for $[Co(bpy)_3]^{3+/2+}$ is therefore

expected to increase, while the rate constant for $[Ru(bpy)_2(MeIm)_2]^{3+/2+}$ is expected to decrease, as the band-edge position is made more negative, and therefore the interfacial driving force is increased, by increasing the pH of the solution.

Chapter 4 presents an investigation of homogeneous and heterogeneous electron-transfer rate constants to randomly dissolved osmium polypyridyl complexes. The homogeneous and interfacial electron-transfer rate constants between osmium polypyridyl complexes that are relatively unhindered are compared with complexes that have tert-butyl groups. The self-exchange measurements in solution were performed by conventional NMR line-broadening analysis, yielding information on the relative contributions of electronic coupling vs. outer-sphere reorganization energy on affecting the electron-transfer rate of the self-exchange process. The interfacial charge-transfer kinetics for metal complexes using these two different ligand systems have also been investigated in our work using semiconductor electrodes. The changes in the steric properties of the ligands used in the present study provide an elucidation of the potential role of the electronic coupling in affecting the interfacial electron-transfer rate constants in such systems.

Chapter 5 describes the covalent modification of Si surfaces via a two-step chlorination-methylation method to introduce kinetically stable CH_3-Si bonds onto Si surfaces. This process eliminates the pH dependence of the Si band-edge positions, and additionally facilitates use of the Si under conditions in which it otherwise would be rapidly oxidized to produce pH-dependent surface potentials. This methylation process additionally allows for the experimental measurement of the interfacial electron-transfer kinetics in media, which cannot be probed at reactive, oxidizable, H-terminated Si surfaces, and has produced another system that reveals “ideal” kinetics behavior at the semiconductor/liquid contact.

REFERENCES

(1) Marcus, R. A. *J. Chem. Phys.* **1965**, *43*, 679-701.

(2) Marcus, R. A. *Ann. Rev. Phys. Chem.* **1964**, *15*, 155-196.

(3) Marcus, R. A. *J. Chem. Phys.* **1956**, *24*, 966-978.

(4) Closs, G. L.; Calcaterra, L. T.; Green, N. J.; Penfield, K. W.; Miller, J. R. *J. Phys. Chem.* **1986**, *90*, 3673-3683.

(5) Closs, G. L.; Miller, J. R. *Science* **1988**, *240*, 440.

(6) Fox, L. S.; Kozik, M.; Winkler, J. R.; Gray, H. B. *Science* **1990**, *247*, 1069.

(7) Royea, W. J.; Fajardo, A. M.; Lewis, N. S. *J. Phys. Chem. B* **1997**, *101*, 11152-11159.

(8) Bansal, A.; Li, X. L.; Lauermann, I.; Lewis, N. S.; Yi, S. I.; Weinberg, W. H. *J. Am. Chem. Soc.* **1996**, *118*, 7225-7226.

CHAPTER 1

Measurement of the Free Energy Dependence of Interfacial Charge-Transfer Rate Constants Using ZnO/H_2O Semiconductor/Liquid Contacts

1.1 INTRODUCTION

A. Background

The Marcus semi-classical description of outer-sphere electron-transfer reactions has been studied extensively for electron-transfer processes between molecular donor and acceptor species.[1] Agreement between theory and experiment has been demonstrated in numerous cases.[2-5] In contrast, there have been relatively few studies of electron transfer at semiconductor/liquid contacts. Current vs. potential data for electron transfer from ZnO to deuterated and normal thianthrene acceptors was interpreted in terms of the Marcus theory.[6] Transient absorption data for a series of TiO_2-$Fe(CN)_5L$ contacts that showed increasing excited-state lifetimes with increasing relative driving force was presented as evidence of the inverted region.[7]

For non-adsorbed, outer-sphere redox species, extraordinarily low defect densities at the semiconductor/liquid interface are required to prevent adsorption and surface-state related reactions from dominating the observed interfacial kinetics processes.[8,9] Carefully prepared (100)-oriented n-type Si/CH_3OH viologen$^{2+/+}$ contacts have shown the predicted dependence of interfacial charge-transfer rate constants, k_{et}, on changes in standard interfacial free energies, $\Delta G^{\circ\prime}$,[10] for driving forces up to, and slightly beyond, that of optimal exoergicity. However, measurements at higher driving forces were precluded because redox couples having more positive potentials than the valence band edge of Si oxidize the Si surface and/or induce carrier inversion processes that prevent changes in interfacial driving force as the Nernstian potential of the electrolyte is increased.[11] Similar considerations limit the experimentally accessible range of driving forces for InP electrodes.[12] Such considerations are expected to complicate kinetics measurements at high exoergicity for other small band gap (<2 eV) semiconducting electrodes as well.

The metal oxide semiconductor ZnO is an attractive material to mitigate these drawbacks, and thereby allow direct investigation of the behavior of k_{et} at large interfacial exoergicities. The wide band gap of ZnO (3.3 eV) allows for a large variation in the driving force and ZnO is not susceptible to the oxidation or passivation processes that are prevalent in small band gap semiconductors.

Several studies using ZnO electrodes in the 1960s noted a linear relationship between the logarithm of the current density, *J*, and the applied potential, *E*, with a slope of *E* vs. *J* of 60 mV/decade, indicating that ZnO/liquid contacts exhibit an "ideal" first-order dependence on the electron concentration at the surface of the semiconductor.[13-16] However, only a few of the redox couples studied, notably $Fe(CN)_6^{3-/4-}$, showed a first-order dependence of the interfacial rate on the concentration of the redox acceptor species in solution. This latter condition is also required to allow a straightforward interpretation of the observed interfacial current density. Another important result of these earlier ZnO studies is that a relatively small frequency dispersion was observed in the differential capacitance measurements, allowing a reliable determination of the surface electron concentration and, additionally, a reliable measurement of the position of the band edges versus a fixed reference electrode. In addition, corrosion or passivation of the surface of the ZnO electrodes was minimal. Subsequent attempts to extract rate constants from steady-state *J* vs. *E* data were thwarted because most of the simple metal-ion-based redox systems that were investigated, such as Ce^{4+} (in HNO_3 and H_2SO_4), $IrCl_6^{2-}$, V^{3+} (in HCl), and $Ag(NH_3)_2^+$, are known to adsorb onto hydroxylated surfaces or to involve inner-sphere electron-transfer pathways. Little follow-up of these early experiments has apparently occurred over the subsequent four decades.

In this work, the interfacial electron-transfer kinetics of a ZnO semiconductor/liquid interface at low and high driving forces has been studied. To achieve this goal, we have synthesized a series of one-electron outer-sphere redox couples having potentials that span approximately 900 mV (Figure 1.1) in the band gap region of ZnO.

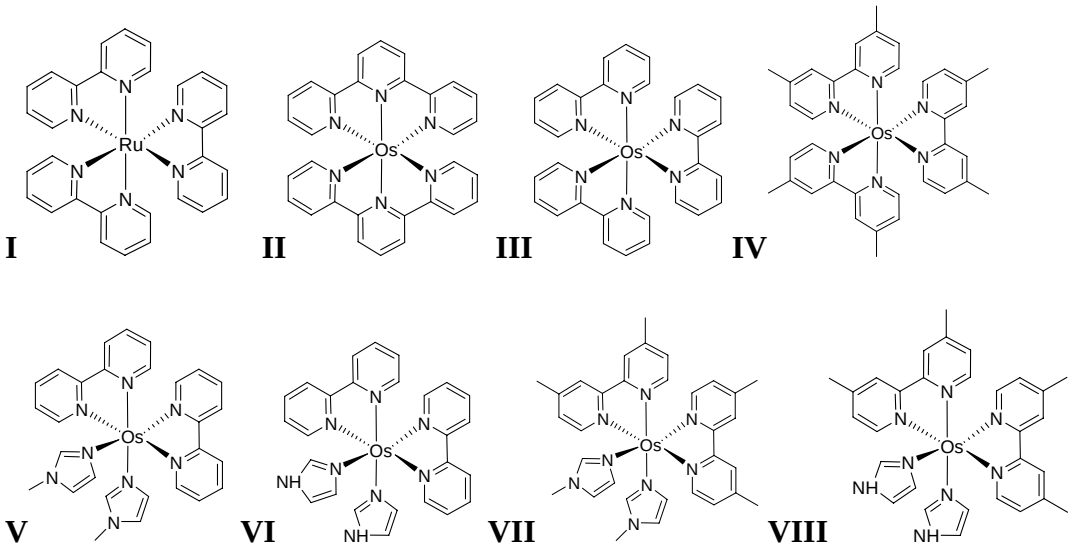

Figure 1.1 Numerical symbols and chemical names of the redox compounds used in this study given in order of decreasing potential. **I** $[Ru(bpy)_3]^{3+/2+}$, **II** $[Os(terpy)_2]^{3+/2+}$, **III** $[Os(bpy)_3]^{3+/2+}$, **IV** $[Os(Me_2bpy)_3]^{3+/2+}$, **V** $[Os(bpy)_2(MeIm)_2]^{3+/2+}$, **VI** $[Os(bpy)_2(Im)_2]^{3+/2+}$, **VII** $[Os(Me_2bpy)_2(MeIm)_2]^{3+/2+}$, **VIII** $[Os(Me_2bpy)_2(Im)_2]^{3+/2+}$.

Rate constants have been measured for such systems in contact with n-type ZnO electrodes. NMR line broadening experiments were performed to determine the reorganization energies of the compounds in the same medium as that used to determine the interfacial kinetics at ZnO. Such measurements have allowed a detailed investigation of the dependence of the rate constant for electron transfer on driving force in both the normal and Marcus inverted region, for a homologous series of outer-sphere redox-active compounds at an "ideally" behaving semiconductor/electrode interface.

B. Rate Laws and Models for Charge-Transfer Processes

Scheme 1.1 depicts the thermodynamic and kinetics parameters that describe electron-transfer processes at a non-degenerately-doped n-type semiconductor/liquid interface. No electronic states are present in the band gap region of an ideal semiconductor, so only electrons that are thermally excited to the conduction band for an n-type material can participate in majority-carrier-based electron-transfer events. At forward bias, the net flux of electrons from the conduction band to randomly dissolved acceptors in solution is given by[17]

$$J(E) = -qk_{et}[\mathrm{A}]n_s \tag{1}$$

where J is the current density (A cm^{-2}), E is the applied potential (V) relative to a saturated calomel electrode, SCE, q is the charge of an electron (1.6022×10^{-19} C), k_{et} is the electron-transfer rate constant (cm^4 s^{-1}), [A] is the acceptor concentration (cm^{-3}), and n_s is the electron concentration (cm^{-3}) at the surface of the semiconductor. The concentrations of the acceptor, [A], and of the electrons in the conduction band at the surface of the semiconductor, n_s, appear explicitly in the expression for the current density, thus yielding a second-order rate law for the charge-transfer process.

The value of n_s is related to the potential difference between E and the potential of the conduction band edge, $\mathbf{E}_{cb}/q$, through a Boltzmann-type relationship:[8]

$$n_s = N_c e^{\frac{(\mathbf{E}_{cb} - qE)}{k_B T}} \tag{2}$$

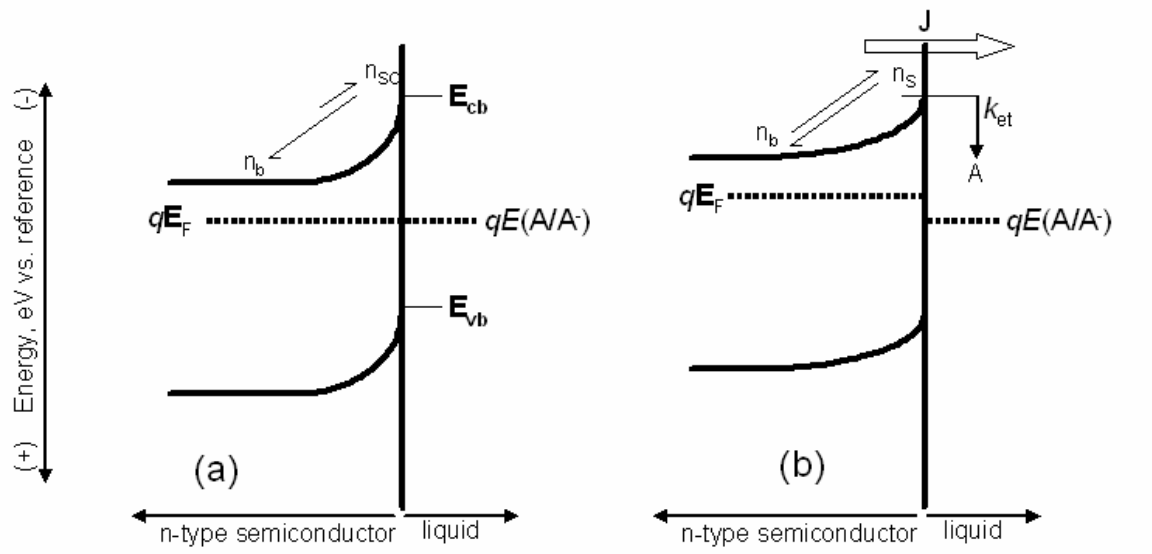

Scheme 1.1 Energy vs. distance for an n-type semiconductor in contact with a redox species (A/A^-). Formation of a space-charge region produces a spatially dependent electric potential drop in the solid. $\mathbf{E}_{cb}$ and $\mathbf{E}_{vb}$ are the energies of the conduction and valence band edges, respectively, and $E(A/A^-)$ is the Nernstian potential of the redox species (A/A^-). The value of $\Delta G^{o'}$, the standard free energy change for interfacial charge transfer, is given by $\Delta G^{o'} = \mathbf{E}_{cb} - qE^{o'}(A/A^-)$, where $E^{o'}(A/A^-)$ is the formal reduction potential of the (A/A^-) redox system. The surface and bulk electron concentrations are denoted as n_s and n_b, respectively. (a) At equilibrium, the electode potential, E, is such that the Fermi level of the semiconductor, $\mathbf{E}_F$, equals $qE(A/A^-)$, and $n_s = n_{so}$, where n_{so} is the surface electron concentration at equilibrium of the solid/liquid interface. (b) If a potential is applied such that the junction is biased away from equilibrium, n_s is not equal to n_{so}, and a non-zero net current, J, flows across the semiconductor/liquid interface.

where k_B is Boltzmann's constant, T is the temperature, $\mathbf{E}_{cb}$ is the energy of the conduction band edge, and N_c is the effective density of states in the conduction band of the semiconductor. Hence, application of a potential to an ideally behaving semiconductor electrode interface effects a change in the observed current density (i.e., the charge-transfer rate) by changing the value of the electron concentration at the surface of the solid, as opposed to changing the rate constant, or the energetics, of the interfacial charge-transfer process.

If J is shown to follow eq (1), with knowledge of n_s and [A], the value of k_{et} can be calculated from the observed steady-state J vs. E data. Unlike the situation for metallic electrodes, the relatively small, and controllable, value of the electron concentration at the semiconductor surface affords the ability to avoid redox coupled mass-transport limitations on the charge-transfer flux even for reactions at optimal exoergicity. Hence, rate measurements at semiconductor electrodes can be performed using simple steady-state methods with dissolved redox species, even for relatively large values of the interfacial charge-transfer rate constant.

1.2 EXPERIMENTAL

A. Electrodes

Hydrothermally grown, n-type, <0001>-oriented, ZnO single crystals having dimensions approximately 10 × 10 × 0.5 mm were purchased from Commercial Crystal Laboratories, Inc. (Naples, FL). The resistivity of the crystals was reported by the manufacturer to be between 10^1 and 10^4 Ω cm. The ZnO crystals were clear with either a light green or yellow color, likely due to differences in unintentional impurities. ZnO crystals with light green color tended to give better results than yellow.

Electrochemical experiments reported in this work were confined to the Zn-rich surface of such electrodes. Due to the limited number of high-quality ZnO single crystals

available, a meaningful statistical approach was not feasible. For conciseness, results are reported here for a single electrode; several other electrodes, however, were prepared and measured with reproducible results. The crystal was first polished with water-based diamond suspensions of grain size 6, 3, and 1 μm, for 15, 30, and 45 minutes, respectively. The crystal was then chemically polished in a silica/KOH suspension (0.05 μm, pH > 10, South Bay Technology Inc., San Clemente, CA) for 30 minutes. Ga-In eutectic was used as an ohmic contact and silver print (GC electronics 22-201, Rockford IL) was used to connect the Ga-In to a tinned copper wire. White epoxy was used to seal the ZnO electrode assembly in a glass tube. The resulting electrode area was determined by digitizing photographs of a microruler and of the exposed ZnO surface. An area of 0.51 cm^2 was determined with an estimated error of 0.03 cm^2. Before use, the electrode was etched for 7 min in concentrated phosphoric acid (Aldrich), rinsed with 18 MΩ cm resistivity water (Barnstead NANOPure), and blown dry with $N_{2(g)}$.

B. Electrolyte Solutions

Electrochemical experiments were carried out in a 55 mM phthalate buffer prepared by adding 12 mL of 1.0 M KOH(aq) to 250 mL of 0.11 M potassium hydrogen phthalate (5.76 g) solution, followed by dilution to 500 mL. The pH was then adjusted to pH = 4.99 using 1 M KOH(aq). The ionic strength was adjusted to 1.0 M by adding 37.4 g of KCl (Aldrich, 99+%) to provide the supporting electrolyte for the electrochemical measurements.

C. Redox Compounds

Ammonium hexachloroosmate(IV), 2, 2'-bipyridine (bpy), 4,4'-dimethyl 2, 2'-bipyridine (Me_2bpy), terpyridine (terpy), imidazole (Im), 1-methyl imidazole (MeIm), NH_4PF_6, and $(n\text{-}C_4H_9)_4NCl$ (TBAC) were purchased from Aldrich and used as received. All solvents were reagent grade and were used as received. $Ru(bpy)_3Cl_2 \cdot 6H_2O$, **I**, (Figure 1) was purchased from Strem Chemicals and used as received. All other compounds were made following modified literature procedures, as described briefly below.[18,19]

*i. Synthesis of $[Os(terpy)_2](PF_6)_2$ **(II)**, $[Os(bpy)_3](PF_6)_2$ **(III)**, and $[Os(Me_2bpy)_3](PF_6)_2$ **(IV)***

In a 50 mL round bottom flask, 3.5 equivalents of bpy or Me_2bpy, or 2.5 equivalents of terpy, were added to $(NH_4)_2[OsCl_6]$ (0.25g; 0.56 mmol) dissolved in 25 mL of ethylene glycol. The solution was heated to reflux for 1 hr with rapid stirring under Ar, and was then cooled to room temperature. Then 2-3 equivalents of NH_4PF_6(aq) were added, and the resulting PF_6^- salt precipitate of the desired compound was filtered, yielding a dark green product that was washed with cold water and diethyl ether.

*ii. Synthesis of $[Os(bpy)_2(MeIm)_2](PF_6)_2$ **(V)**, $[Os(bpy)_2(Im)_2](PF_6)_2$ **(VI)**, $[Os(Me_2bpy)_2(MeIm)_2](PF_6)_2$ **(VII)**, and $[Os(Me_2bpy)_2(Im)_2](PF_6)_2$ **(VIII)***

In a 50 mL round bottom flask, 2 equivalents of bpy or Me_2bpy were added to $(NH_4)_2[OsCl_6]$ (1.1g / 2.3 mmol) in 30 mL of ethylene glycol. The solution was heated to reflux for 1 hr with rapid stirring under Ar, and was then cooled to room temperature. To reduce any Os(III) species that may have formed, approximately 100 mL of cold 1 M aqueous $Na_2S_2O_4$ was slowly added, and the solution was cooled for 1 hr in an ice bath. The dark precipitate was collected by vacuum filtration, washed with cold water and diethyl ether, and used in further reactions without additional purification.

To make the imidazole complexes, in a 100 mL round bottom flask, 5-20 equivalents of Im or MeIm were then added to the dried product, $[OsCl_2bpy_2]$ or $[OsCl_2Me_2bpy_2]$, in 50 mL of ethylene glycol. The solution was heated to reflux for 2-3 hrs with rapid stirring under Ar and was then cooled to room temperature. Then 2-3 equivalents of NH_4PF_6(aq) were added, and the resulting PF_6^- salt precipitate was filtered, yielding a dark brown product that was washed with cold water and diethyl ether.

iii. Purification and Characterization of the Os Complexes

Metal complexes **II-VIII** were purified on an activated neutral alumina column using acetonitrile as the eluent. For **II-IV,** a dark green band was collected, whereas **V-VIII** yielded a brown band. The solvent was removed *in vacuo*. The residue was

dissolved in a minimal amount of acetone and the complex was precipitated by addition of diethyl ether. The product was then filtered and dried under vacuum. Yields in excess of 80% were obtained for **II-IV** and yields were in excess of 30% for **V-VIII**. Elemental analysis yielded the following (calculated): **II**. C 37.99 (38.06), H 2.41 (2.56), N 8.89 (8.88); **III**. C 37.93 (37.98), H 2.73 (2.55), N 8.64 (8.86); **IV**. C 41.81 (41.86), H 3.49 (3.51), N 7.89 (8.14); **V**. C 35.15 (35.15), H 3.07 (2.95), N 11.34 (11.71); **VI**. C 33.56 (33.63), H 2.46 (2.60), N 11.77 (12.07); **VII**. C 39.22 (37.95), H 3.67 (3.58), N 11.23 (11.06); **VIII**. C 36.65 (36.59), H 3.31 (3.28), N 11.13 (11.37).

Compounds were converted to the chloride salt by dissolving in acetone followed by addition, while stirring, of a concentrated solution of tetra-butylammonium chloride in acetone. The chloride salt precipitated out of solution, was filtered, washed with acetone and ether, and then dried *in vacuo*. Elemental analysis yielded the following (calculated): **II**·$2H_2O$ C 47.42 (47.18), H 3.18 (3.17), N 11.12 (11.00); **III**·$4H_2O$ C 45.04 (44.95), H 4.02 (4.02), N 10.48 (10.48); **IV**·$4H_2O$ C 44.57 (48.81), H 4.26 (5.01), N 10.10 (9.49); **V**·$4H_2O$ C 39.63 (41.53), H 3.72 (4.48), N 13.15 (13.84); **VI**·$2H_2O$ C 41.41 (41.88), H 3.66 (3.78), N 14.24 (15.03); **VII**·$2H_2O$ C 47.33 (46.32), H 4.94 (4.86), N 12.20 (13.50); **VIII**·$2H_2O$ C 45.01 (44.94), H 4.48 (4.53), N 12.33 (13.98). Since chloride salts can adsorb water, water was added to the molecular formula to account for the analysis results.

NMR, mass spectroscopic, and cyclic voltammetric data were collected on all of the compounds of interest. Analytic NMR measurements were made on a Varian 300 MHz spectrometer. Spectra were obtained of the PF_6^- salts in CD_3CN and of the Cl^- salts in D_2O. The expected integration and shifts of the proton peaks of the ligands were observed for both types of salts. NMR of the chloride salts indicated the presence of the expected ligands and the lack of hydrogen-containing impurities, other than water.

Electrospray mass spectroscopic data (Table 1.1) were collected for compounds **II-VIII**, and confirmed the composition of the materials. The major peaks were also

Table 1.1 Mass spectroscopic and cyclic voltammetric results for redox couples. Mass peaks of singly charged ions are given for 2+ ions that were reduced from the matrix; 1+ ions were also observed in all spectra with a m/z one-half that of the calculated mass.

Ion	Calc. Mass	Observed m/z	$E^{o'}$ (V vs. SCE)
I	n/a	n/a	1.001
$\mathbf{II}^{2+}$	328	329	0.673
$\mathbf{III}^{2+}$	330	330	0.572
$\mathbf{IV}^{2+}$	372	372	0.385
$\mathbf{V}^{2+}$	333	334	0.248
$\mathbf{VI}^{2+}$	319	320	0.248
$\mathbf{VII}^{2+}$	361	362	0.111
$\mathbf{VIII}^{2+}$	347	348	0.106

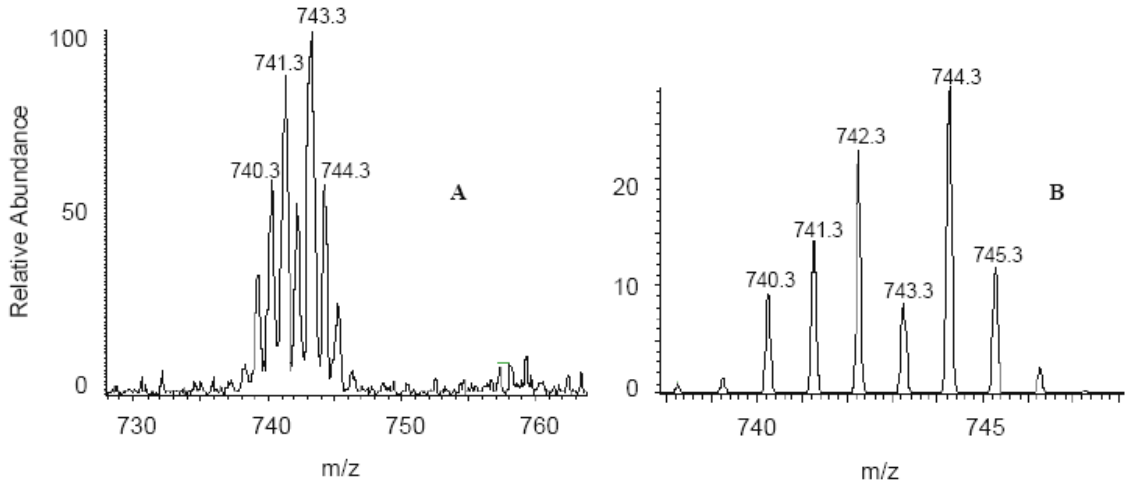

Figure 1.2 (A) electrospray mass spectrum of $[Os(Me_2bpy)_3]^+$ from $[Os(Me_2bpy)_3]Cl_2$, (B) simulated isotopic peak distribution for the molecular ion $[OsC_{36}H_{36}N_6]^+$.

isotopically resolved and compared to theoretical spectra for the compounds of interest. Figure 1.2 displays the peaks observed for $[Os(Me_2bpy)_3]^+$ along with the theoretically predicted spectrum of this species. The $[Os(Me_2bpy)_3]^+$ ion was produced by reduction of $[Os(Me_2bpy)_3]^{2+}$ by the matrix; peaks corresponding to $[Os(Me_2bpy)_3]^{2+}$ were also observed. Differences in mass between the predicted and observed spectra are due to the loss of a hydrogen atom. The agreement between the observed and calculated spectra and isotopic patterns confirmed the composition of each compound.

The formal reduction potential, $E^{o\prime}(A/A^-)$, of each compound (Table 1) was determined using cyclic voltammetry in buffered H_2O with 1 M KCl electrolyte in an ice bath. A graphite disc electrode was used as the working electrode, a platinum mesh was employed as the counter electrode, and an SCE, in a separate cell at room temperature, was used as the reference electrode. Scans were taken from -0.1 V to 1.1 V vs. SCE at a scan rate of 50-75 mV s^{-1}. An error of ± 5 mV was estimated for $E^{o\prime}(A/A^-)$ of each redox couple, as determined from the cyclic voltammetry data.

D. NMR Line Broadening Experiments

NMR spectra were measured on a Varian 500 MHz spectrometer. Since these results were used in the interpretation of electrochemical measurements, the conditions of the two experiments were matched as closely as possible. Measurements were carried out at 3-4 °C in buffered D_2O solutions that contained 1 M KCl. The deuterated buffer was prepared as follows: NaOD in D_2O was added drop-wise, until the pH reached 4.50, to a solution of 0.134 g of d-phthalic acid dissolved in 10 mL D_2O (78 mM).

Diamagnetic Os(II) samples of **IV** were prepared by dissolving sufficient **IV**, as the Os(II) chloride salt, to make a 10 mM solution in D_2O that contained 1 M KCl. An aliquot of this solution was oxidized by exposure to $Cl_2(g)$ until the solution turned bright red. To remove dissolved $Cl_2(g)$, the solution was purged with Ar(g), and the resulting sample was used as the pure paramagnetic Os(III) sample of **IV**. Both the diamagnetic and paramagnetic solutions were then diluted by 50% with the buffer solution. Aliquots

of the paramagnetic solution were added to the diamagnetic solution and the resulting solutions were used as mixed samples. Several solutions with different concentrations of paramagnetic species were prepared in this fashion.

Diamagnetic samples of **V** and **VIII** were prepared from the Os(II) chloride salt by making a 5 mM solution in a deuterated buffer (2.5 mM, 1 M KCl). Bulk electrolysis was employed to oxidize controlled amounts of the complex of interest, and aliquots were taken after each bulk electrolysis step. The mass-transport-limited currents recorded with a platinum microelectrode were used to verify the mole fractions of diamagnetic and paramagnetic species of each aliquot. The pure paramagnetic sample was prepared by bulk electrolysis carried out to completion, as verified by the lack of significant anodic faradaic current in the resulting solution.

For data analysis, NMR free-induction decays were imported to Mestrec software and a Fourier transform was performed. Spectra were then exported to Sigma Plot software for analysis. All reported peak positions and line widths were derived from non-linear least-squares fits of the peak of interest to a Lorentzian line shape. Errors given in the spectral parameters are the standard errors from the peak fitting routine, propagated for the determination of the error in k_{ex}.

The line-width method[20] was used for proton signals that were not complicated by coupling. Because the osmium polypyridyl compounds of interest in this study are in the fast-exchange regime, the chemical shifts of mixed species were assumed to vary linearly with the mole fraction of species in the solution.[20] Accurate mole fractions, therefore, can be determined by the ratio of the frequency shift to the contact shift[21]

$$X_p = |\nu - \nu_d| / \Delta\nu \qquad (3)$$

where X_p and X_d are the mole fractions of paramagnetic and diamagnetic species, respectively (with $X_d = 1 - X_p$), ν is the frequency shift of a proton peak in the mixed sample, ν_d is the corresponding peak shift in the pure diamagnetic sample, and $\Delta\nu$ is the

shift difference between the peaks of the pure paramagnetic and diamagnetic samples ($\Delta\nu = \nu_p - \nu_d$).

E. Electrochemical Measurements

All buffers were deaerated prior to use by purging with Ar, and electrochemical measurements with ZnO were performed under an Ar atmosphere. ZnO electrodes were etched and then immersed in the supporting electrolyte for at least 5 min before being transferred to the electrochemical cell. All experiments were carried out in an ice bath with a solution temperature of ≈ 3 ºC. The Os(III) compounds were created in situ via bulk electrolysis using a carbon mesh working electrode to create a 5mM concentration; a 5% error in [A] was estimated. The concentration of acceptor, [A], was varied by diluting an aliquot of the redox solution with buffer. The Nernstian potential of the solution, $E(A/A^-)$, changed by less than 3 mV during each measurement and by less than 15 mV following dilution. The J vs. E data and the open-circuit potential of each electrode were recorded before and after each set of differential capacitance measurements.

Differential capacitance measurements were performed with a Schlumberger Instruments Model 1260 Impedance Gain-Phase Analyzer interfaced to a Model SI1287 potentiostat. Measurement parameters were adjusted to minimize the exposure of the electrode to acidic media, as it is known that ZnO can dissolve in acidic solutions.[22] The C_{diff}^{-2} vs. E behavior of the semiconductor/liquid contact was recorded for DC biases that were stepped in 100 mV increments over the potential range of 0.1 to 0.8 V vs. SCE. A 10 mV AC signal was superimposed on the DC bias. Each capacitance measurement consisted of frequency sweeps from 10^2 to 10^4 Hz in equally spaced log steps.

To deduce the space-charge capacitance, impedance spectra were fitted to an equivalent circuit that consisted of the cell resistance, R_s, in series with two parallel components: the resistance to charge transfer, R_{sc}, and the space-charge capacitance, C_{sc}. Because C_{sc} is much less than the differential capacitance, C_{diff}, of either the Helmholtz

layer or the double layer, C_{diff} was set equal to C_{sc}.[11] A linear regression was used to fit the C_{diff}^{-2} vs. E data in accordance with the Mott-Schottky equation:[17]

$$C_{sc}^{-2} = \frac{2}{q\varepsilon\varepsilon_o N_D A_s^2}\left(E - E_{fb} - \frac{k_B T}{q}\right) \quad (4)$$

where ε is the static dielectric constant (8.65 for ZnO),[23] ε_o is the permittivity of free space, N_D is the dopant density of the semiconductor, A_s is the surface area of the semiconductor electrode, and E_{fb} is the flat-band potential of the semiconductor/liquid contact. Values for N_D and E_{fb} were obtained from the slope, and from the x-intercept adjusted by $k_B T/q$, respectively. With knowledge of N_D and E_{fb}, the energy of the conduction band edge, $\mathbf{E}_{cb}$, was determined using the expression

$$\mathbf{E}_{cb} = qE_{fb} + k_B T \ln\left(\frac{N_D}{N_c}\right) \quad (5)$$

where $N_c = 3.5 \times 10^{18}$ cm^{-3} for ZnO.[24] The interfacial free energy for charge-transfer under standard conditions, $\Delta G^{o'}$, was then computed for each redox system by subtracting $\mathbf{E}_{cb}$ from $qE^{o'}(A/A^-)$.

The J vs. E data were obtained with a Schlumberger Instruments Electrochemical Interface Model SI1287 potentiostat. Two scans at a rate of 20 mV s^{-1} were measured. IR corrections were applied to all of the J vs. E data, despite the negligible effect due to the low currents in the region of interest. The cell resistance, R_{cell}, was obtained from the fit of the impedance spectra to the equivalent circuit. The data for the low driving force redox couples, **VII** and **VIII**, were also corrected for the concentration overpotential,[25] calculated from the mass-transport-limited cathodic and anodic current densities, $J_{l,c}$ and $J_{l,a}$, respectively, that were measured with a one-sided Pt-foil electrode of known area, according to eq (6) and (7):

$$\eta_{conc} = \left(\frac{k_B T}{nq}\right)\left\{\ln\left(\frac{J_{l,a}}{-J_{l,c}}\right) - \ln\left(\frac{J_{l,a} - J}{J - J_{l,c}}\right)\right\} \quad (6)$$

$$E_{corr} = E - iR_{cell} - \eta_{conc} \quad (7)$$

1.3 RESULTS

A. Measurements of Self-Exchange Rate Constants Using NMR Line Broadening

Figure 1.3 displays the fit of the methyl peak of **IV** to a Lorentzian line shape for a solution of the diamagnetic Os(II) complex and for a solution containing both the Os(II) and Os(III) forms of the complex. The self-exchange rate constant, k_{ex}, was calculated from[20]

$$k_{ex} = \frac{4\pi X_d X_p (\Delta\nu)^2}{\left(W_{dp} - X_d W_d - X_p W_p\right) C} \tag{8}$$

where W_{dp} is the line width (full width at half maximum) of the mixed species resonance peak, W_p and W_d are the line widths of the paramagnetic and diamagnetic peaks respectively, and C is the total concentration of exchanging species. The line width of the diamagnetic species was ≈ 3-5 Hz. The reported values of k_{ex} are averages of measurements on at least three compositionally different mixed samples. A value of k_{ex} was also determined from the line broadening of the methyl and of the 3,3' proton peak, as both are uncoupled. This analysis produced a value of $k_{ex} = 1.1 \times 10^8$ M^{-1} s^{-1} (Table 1.2) for **IV** in buffered D_2O (pH = 4.5) at 3 ºC and 1 M ionic strength.

Self-exchange rate constants were also determined for compounds **V** and **VIII**. Both of these compounds have uncoupled methyl protons, facilitating a straightforward analysis of the NMR data. Values of k_{ex} were calculated to be 7×10^7 $M^{-1}s^{-1}$ for **V** and **VIII** (Table 1.2).

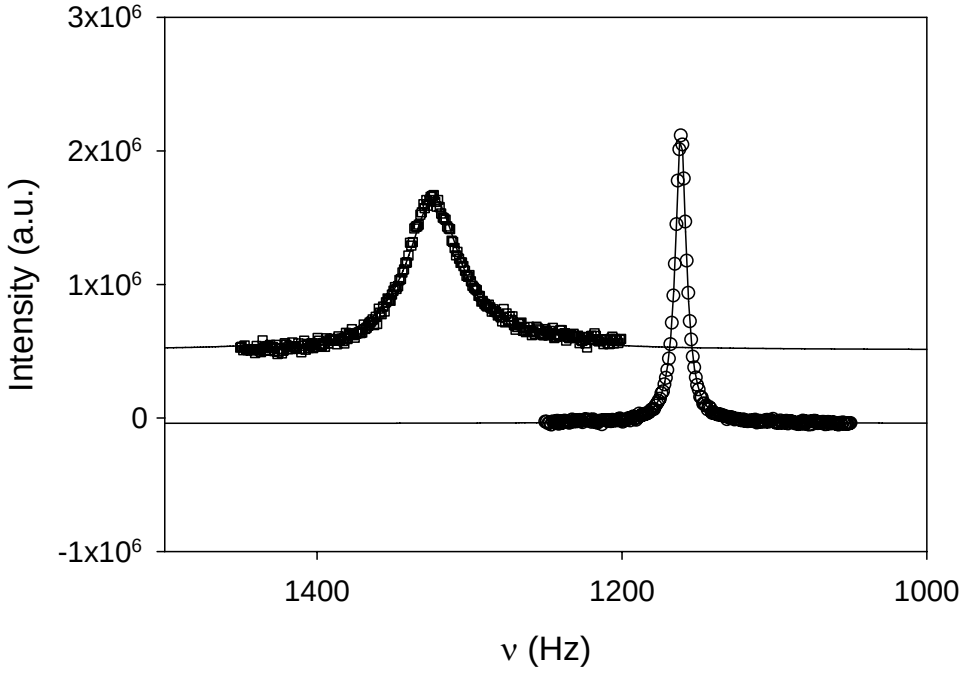

Figure 1.3 ^{1}H NMR spectra of the methyl proton peak of $Os(Me_2bpy)_3^{2+}$ (circles) and of a mixture of $Os(Me_2bpy)_3^{2+}$ and $Os(Me_2bpy)_3^{3+}$ (squares). The lines indicate the results of non-linear least-squares fitting of each spectrum.

Table 1.2 Relevant parameters, self-exchange rate constants, and reorganization energies from ^{1}H NMR line-broadening measurements in buffered D_2O (pH = 4.5) with an ionic strength of 1 M at 3 ºC. The quantity ν_d is the shift of the pure diamagnetic species, $\Delta\nu$ is the shift difference between the diamagnetic and paramagnetic species, and W_p is the paramagnetic line width. The subscripts Me and 3,3' designate results from the methyl protons and 3,3' protons, respectively, for compound **IV**.

	ν_d (Hz)	$\Delta\nu$ (Hz)	W_p (Hz)	$k_{ex} \times 10^{-7}$ (M^{-1} s^{-1})	λ_{se} (eV)
IV_{Me}	1161	8297	194	11.3 ± 0.7	0.64 ± 0.01
$IV_{3,3'}$	4064	4892	155	12 ± 3	0.64 ± 0.02
V	1643	5079	101	7.3 ± 0.8	0.68 ± 0.01
VIII	1122	3857	141	7.1 ± 0.7	0.69 ± 0.01

B. Electrochemical Data

i. Differential Capacitance vs. Applied Potential Measurements

Figure 1.4 presents representative Bode plots for some of the semiconductor/liquid junctions studied in this work. Data are shown for two applied potentials, 0.8 V and 0.2 V vs. SCE. The Bode plots of the impedance magnitude, |Z|, were linear over at least two orders of magnitude variation in ac signal frequency, *f*, having slopes of ≈ -1 and phase angles of the current vs. ac voltage of ≈ -90°. The observed impedance of these systems was thus dominated by a single capacitive circuit element, with $Z_{im} \approx (2\pi f C_{diff})^{-1}$.[11]

To obtain values for C_{sc}, which is taken to be equal to C_{diff}, the impedance spectra were fitted over the frequency range of 10^2 to 10^4 Hz to the equivalent circuit described above. No frequency dependence of the capacitance was observed, resulting in very small errors (< 1%) for each fit. The series resistance of the system, R_s, was essentially constant for all measurements, with a value of 850 Ω. This series resistance can be accounted for by the ohmic resistance of the sample because the measured impedance of other electrodes prepared from crystals from the same batch was ≈ 1 kΩ.

Figure 1.5 displays Mott-Schottky plots in the form of C_{diff}^{-2} vs. E data for all contacts grouped and weighted by their respective (negligible) errors. All of the plots were linear, as predicted by eq (4). The resulting slope and intercept of a linear least-squares fit were used to extract values for N_d and E_{fb}, respectively. The standard errors resulting from the fit were used to calculate the errors in N_d and E_{fb}, producing values of $E_{fb} = -0.10 \pm 0.01$ V vs. SCE and $N_d = (5.8 \pm 0.6) \times 10^{14}$ cm^{-3}. Equation (5) was then used to calculate a value for $\mathbf{E}_{cb}/q = -0.31 \pm 0.01$ V vs. SCE. The invariance of the capacitance data at a fixed electrode potential for all of the compounds, despite the large variation in Nernstian potential of the cells, confirms that the band-edge position is invariant (the "ideal" model) rather than changing with the solution potential (the Fermi level pinning situation).

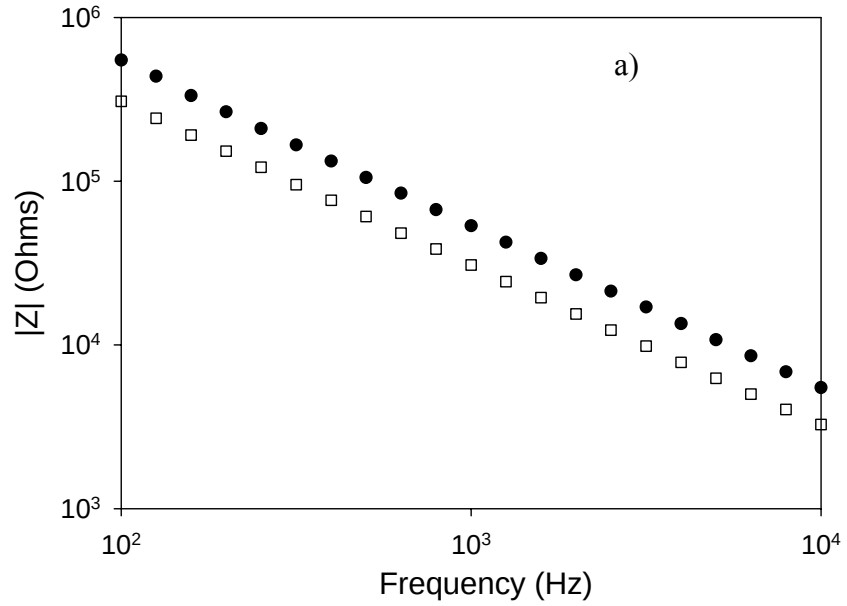
a)
|Z| (Ohms)
10^6
10^5
10^4
10^3
10^2
10^3
10^4
Frequency (Hz)

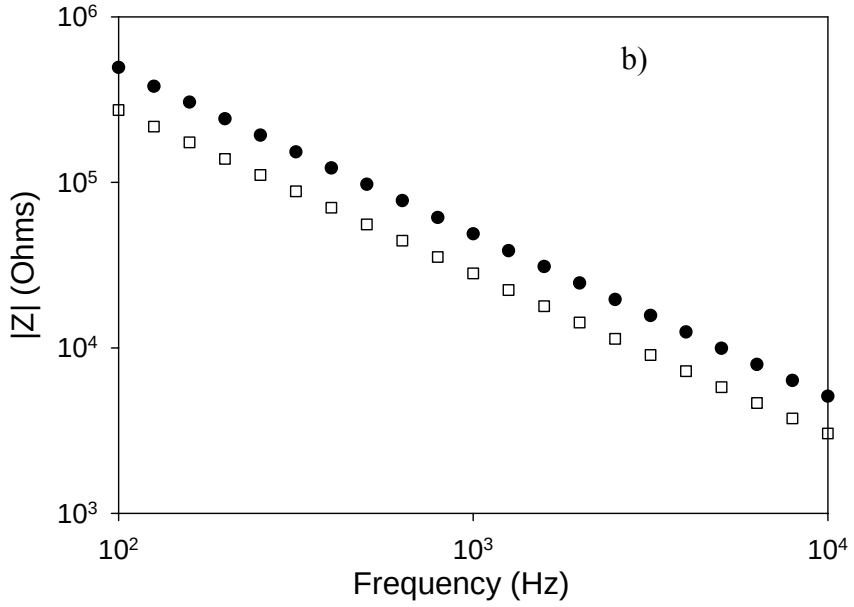
b)
|Z| (Ohms)
10^6
10^5
10^4
10^3
10^2
10^3
10^4
Frequency (Hz)

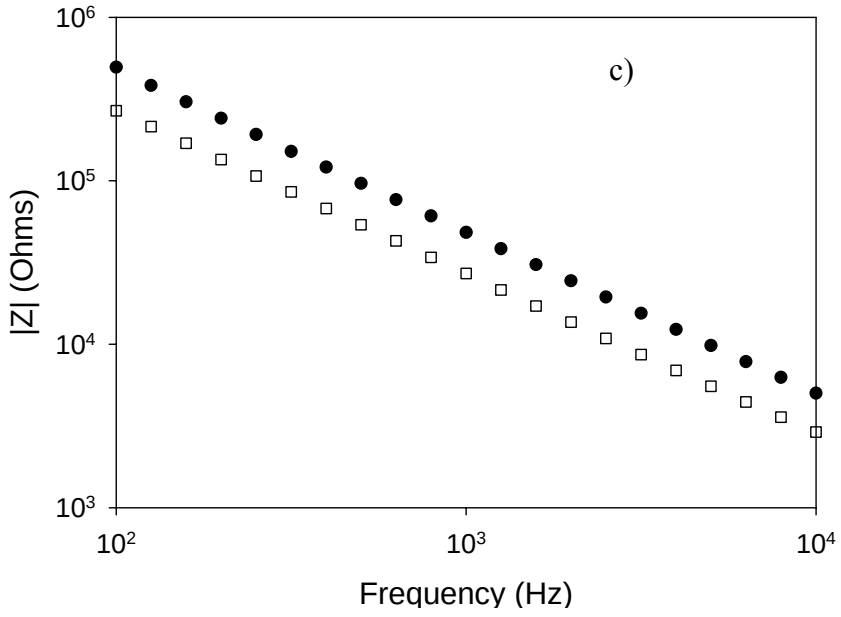

Figure 1.4 Bode plots of the magnitude of the impedance vs. frequency for **I** (a), **II** (b), and **VII** (c) biased at 0.8 V vs. SCE (filled circles) and 0.2 V vs. SCE (open squares).

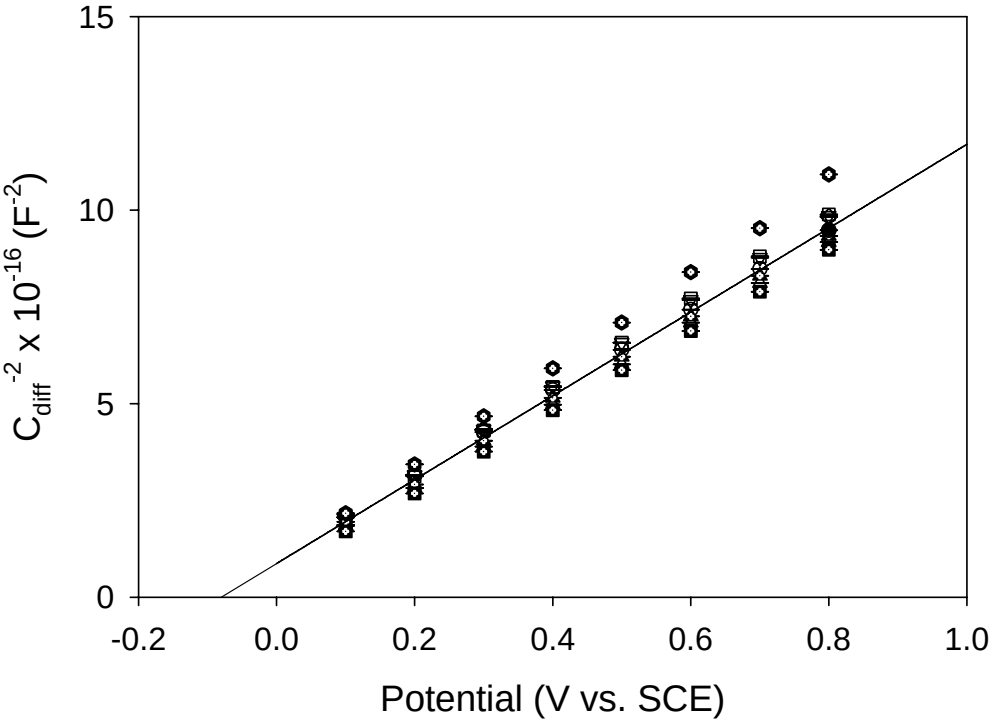

Figure 1.5 Mott-Schottky plots of compounds **I** (hexagon w/cross), **II** (open circle), **III** (open square), **IV** (open triangle up), **V** (open triangle down), **VI** (open diamond), **VII** (triangle w/cross up), and **VIII** (square w/cross). The line indicates the least-squares fit of all of the data.

C_{diff}^{-2} vs. E measurements were also performed in solutions that had varying concentrations of oxidized and reduced species of the same redox couple. For all of the junctions studied, the band-edge positions remained constant, to within 15 mV, after a 10-fold reduction in acceptor concentration.

ii. Current Density vs. Applied Potential Measurements

All of the junctions showed rectifying behavior, producing a limiting anodic current density and an exponentially increasing cathodic current density, in accord with the diode equation:

$$J = -J_0\left(e^{\frac{-qE_{corr}}{\gamma k_B T}} - 1\right) \tag{9}$$

where J_o is the exchange current density, γ is the diode quality factor, and E_{corr} is the applied potential corrected for both concentration overpotential and for series resistance losses in the electrochemical cell (eq (7)).

Figure 1.6 displays plots of ln (-J) vs. E_{corr} for all of the compounds investigated in this work. The diode quality factors were close to 1.0, in accord with expectations for a process that is kinetically first-order in the concentration of electrons at the surface of the semiconductor. The dependence of the rate on the concentration of acceptor species in the solution was determined by reducing [A], which produced shifts of the J vs. E_{corr} data, $\Delta E = (k_B T/q)\ln([A]_{high}/[A]_{low})$, as expected for a first-order process in [A]. The magnitude of the change in [A] was verified by measuring the limiting cathodic current densities at both acceptor concentrations, $J_{l,c,high}$ and $J_{l,c,low}$, with a Pt microelectrode, and the theoretical shift of the J vs. E_{corr} data was calculated by $\Delta E(\text{theor}) = (k_B T/q)\ln(J_{l,c,high}/J_{l,c,low})$. Values of γ, ΔE, and ΔE(theor) are given in Table 3 for the systems of interest in this work.

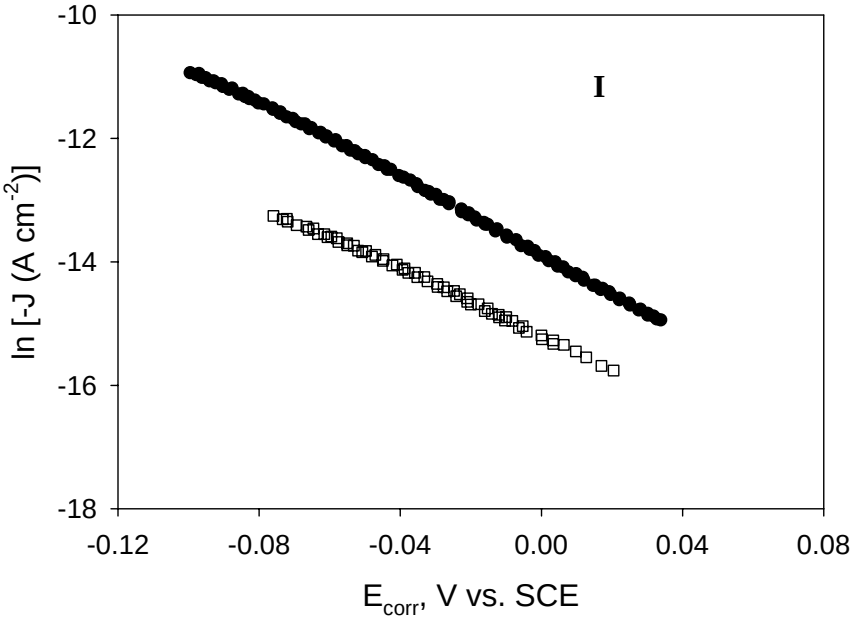
I
-10
-12
-14
-16
-18
-0.12
-0.08
-0.04
0.00
0.04
0.08
ln [-J (A cm-2)]
Ecorr, V vs. SCE

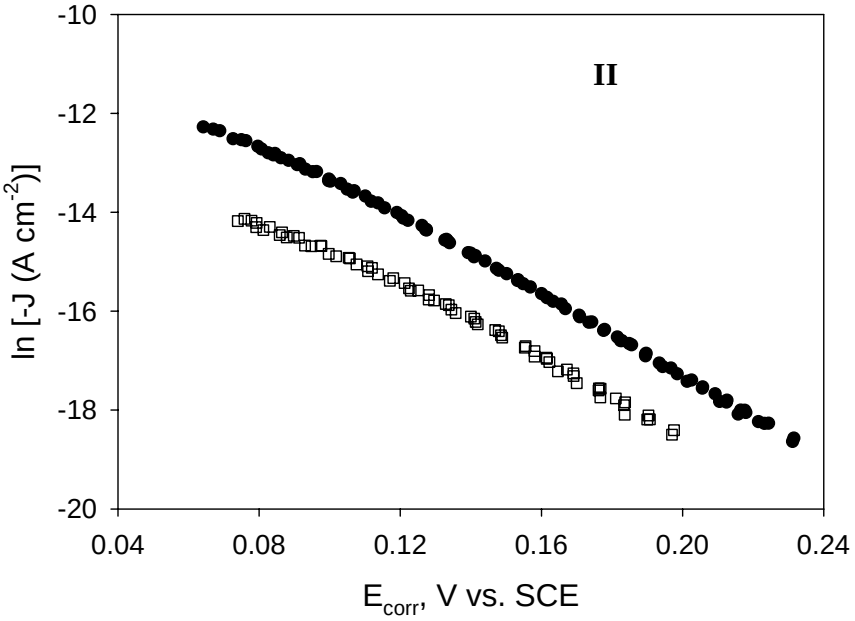
II
-10
-12
-14
-16
-18
-20
0.04
0.08
0.12
0.16
0.20
0.24
ln [-J (A cm-2)]
Ecorr, V vs. SCE

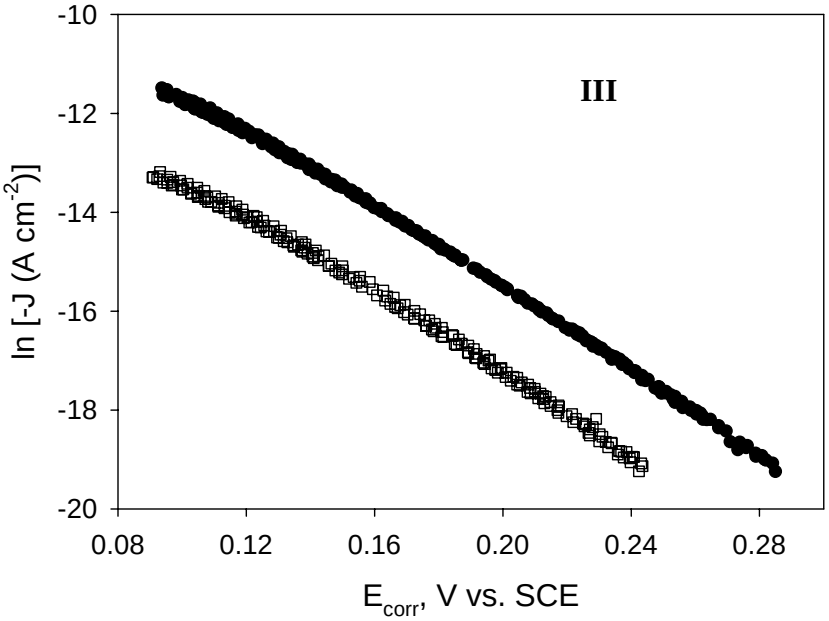
III
-10
-12
-14
-16
-18
-20
0.08
0.12
0.16
0.20
0.24
0.28
ln [-J (A cm-2)]
Ecorr, V vs. SCE

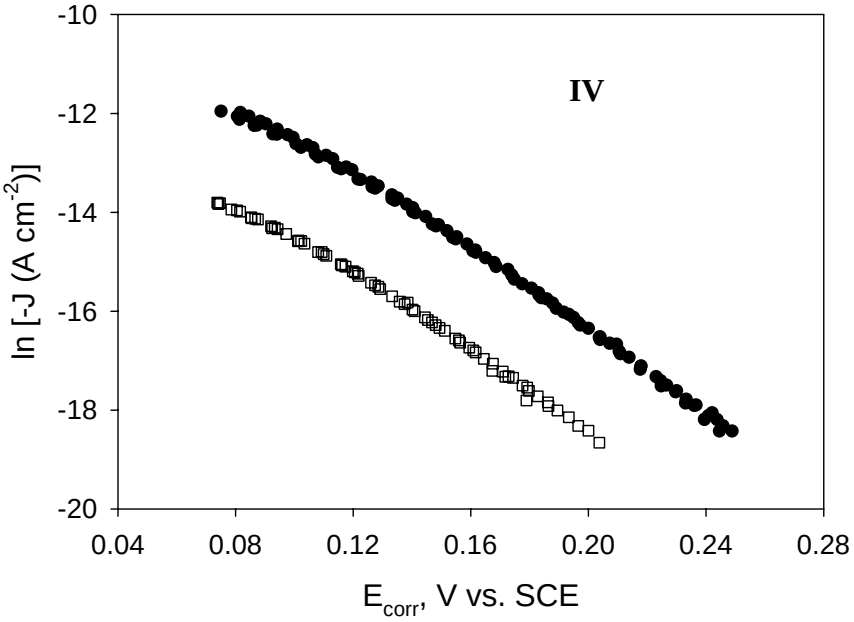
IV
-10
-12
-14
-16
-18
-20
0.04
0.08
0.12
0.16
0.20
0.24
0.28
ln [-J (A cm-2)]
Ecorr, V vs. SCE

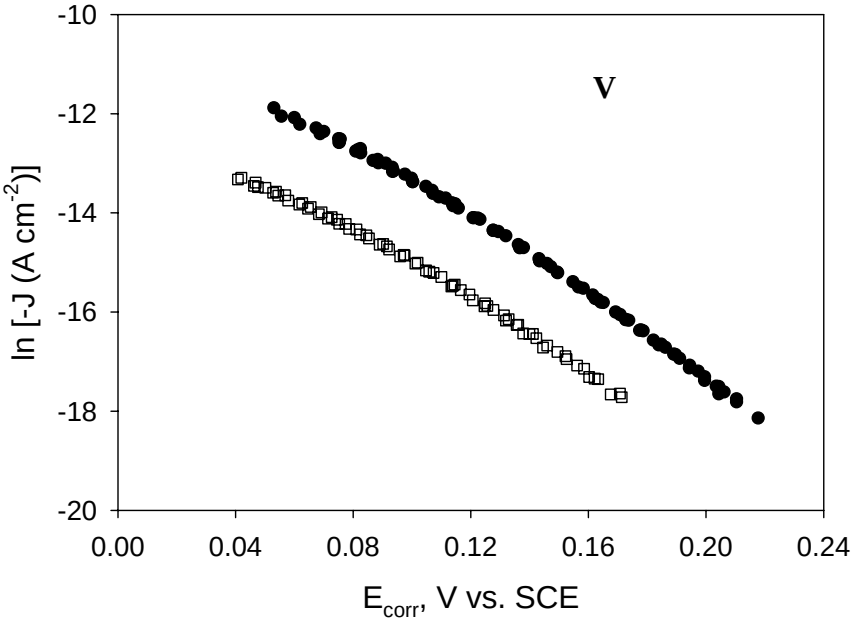
V
-10
-12
-14
-16
-18
-20
0.00
0.04
0.08
0.12
0.16
0.20
0.24
ln [-J (A cm-2)]
Ecorr, V vs. SCE

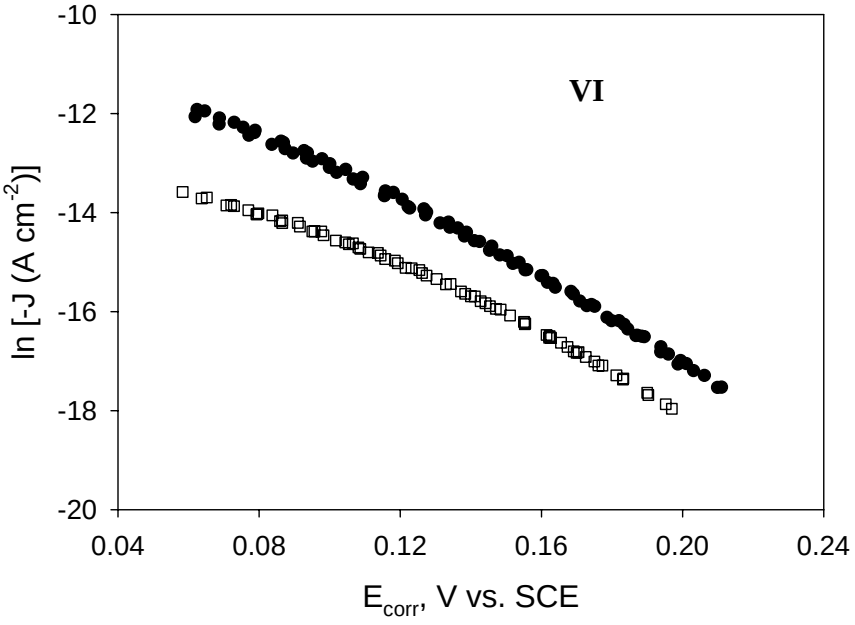
VI
-10
-12
-14
-16
-18
-20
0.04
0.08
0.12
0.16
0.20
0.24
ln [-J (A cm-2)]
Ecorr, V vs. SCE

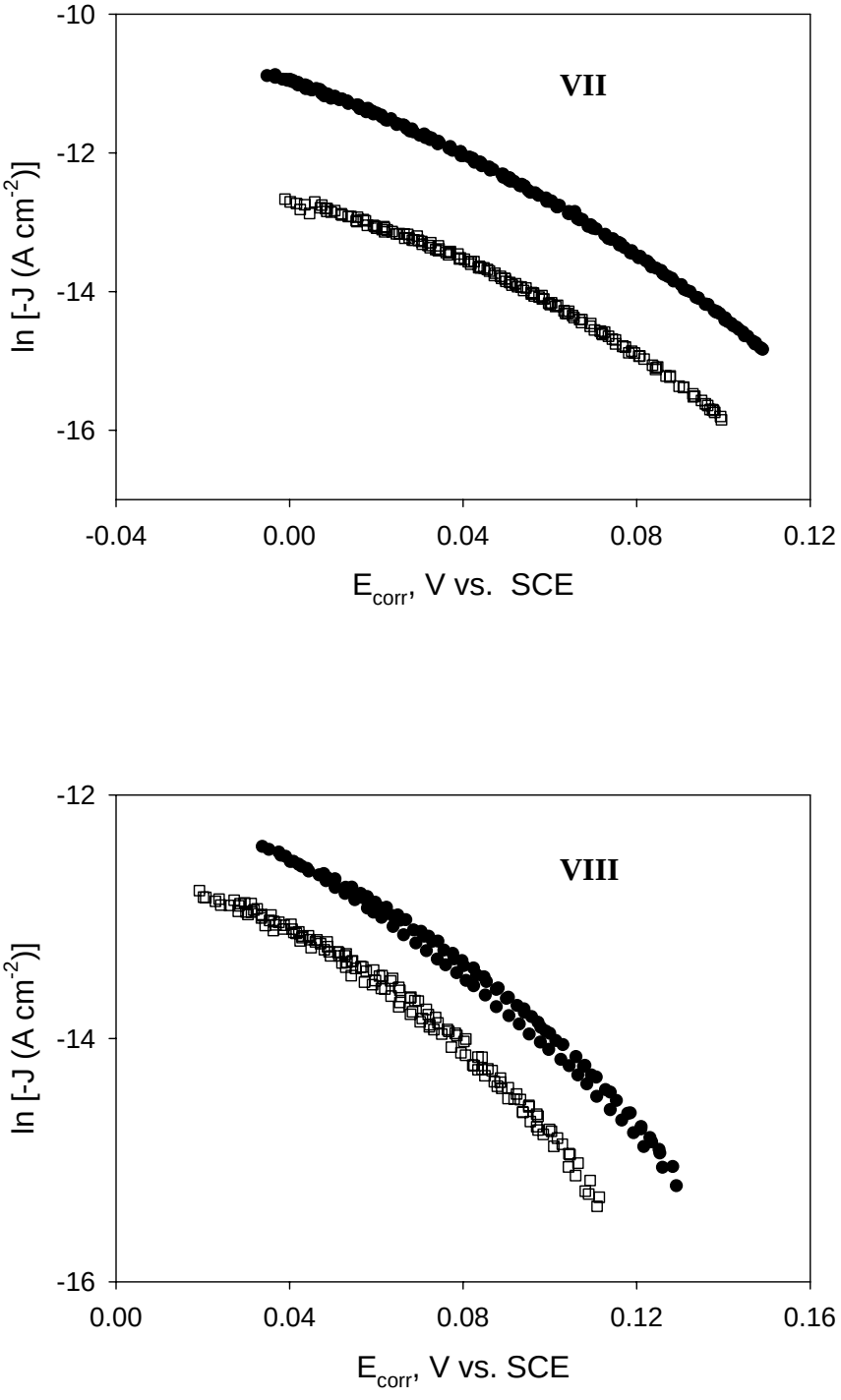

Figure 1.6 Plots of dark current density vs. E_{corr} for compounds **I**-**VIII** at high concentration ([A] = 5 mM; filled circles) and low concentration ([A] ≈ 0.5 mM; open squares). As noted in the text, a decrease in [A] should result in a shift of the J-E_{corr} curve according to $(k_BT/q)\ln([A]_{high}/[A]_{low})$. Potentials are referenced to SCE.

Table 1.3 Results of current density vs. applied potential measurements, barrier height and rate constant determinations. The quantities λ_{high} and λ_{low} are the diode quality factors at high acceptor concentration, $[A]_{high}$, and low acceptor concentration, $[A]_{low}$, respectively. The value of $[A]_{high}$ was always 5 mM, and $[A]_{low} \approx 0.5$ mM. The theoretical shift of the J vs. E_{corr} data was calculated by $\Delta E(\text{theor}) = (k_B T/q)\ln(J_{l,c,high}/J_{l,c,low})$. The quantity $qE(A/A^-) - \mathbf{E}_{cb}$ was calculated using the high acceptor concentration data. As noted in the text, k_{et} was calculated using the high acceptor concentration data for all redox systems investigated.

Compound	γ_{high}	γ_{low}	ΔE (theor) (mV)	$qE(A/A^-) - \mathbf{E}_{cb}$ (eV)	k_{et} ($cm^4\ s^{-1}$)
I	1.33	1.53	55 (60)	1.30 ± 0.01	$(1.4 \pm 0.6) \times 10^{-19}$
II	1.05	1.15	44 (54)	0.96 ± 0.01	$(2 \pm 1) \times 10^{-17}$
III	1.03	1.02	42 (51)	0.86 ± 0.01	$(1.6 \pm 0.7) \times 10^{-16}$
IV	1.04	1.06	50 (54)	0.67 ± 0.01	$(6 \pm 2) \times 10^{-17}$
V	1.06	1.14	46 (48)	0.54 ± 0.01	$(2 \pm 1) \times 10^{-17}$
VI	1.02	1.19	35 (45)	0.54 ± 0.01	$(3 \pm 1) \times 10^{-17}$
VII	1.06	1.19	50 (54)	0.40 ± 0.01	$(5 \pm 2) \times 10^{-18}$
VIII	1.19	1.29	25 (34)	0.40 ± 0.01	$(6 \pm 2) \times 10^{-18}$

iii. Rate Constants for Interfacial Charge-Transfer, k_{et}

Since non-degenerately-doped semiconductor electrodes have relatively little Frumkin correction associated with the liquid part of the solid/liquid double layer,[8] the acceptor concentration can be assumed to be equal to the bulk value. The surface electron concentration at each applied potential, $n_s(E)$, was computed according to eq (2) using the conduction band-edge energy extracted from the flat-band potential determinations (eq (5)). The value of k_{et} was then readily calculated in accordance with the rate law given in eq (1), by dividing J by the quantity $\{-qn_s[A]\}$ at a given potential. The J vs. E data collected at the largest acceptor concentration were used both to minimize the error in the concentration and because the diode quality factors were close to 1 (typically $1< \lambda <1.1$) under such conditions. The quoted k_{et} for each contact represents the average of values calculated using the same high cathodic current density portion of the J vs. E curve ($-(1 - 2) \times 10^{-6}$ A cm^{-2}) for each redox couple. A standard error analysis was performed in conjunction with calculation of the rate constants by propagating the errors of all the measured parameters used in the calculation of k_{et}. The error in $\mathbf{E}_{cb}$ dominated the error in k_{et}, due to the exponential dependence of n_s on ($\mathbf{E}_{cb}$ - qE). Table 1.3 summarizes the values of k_{et} determined for each of the ZnO/H_2O-redox couple junctions evaluated in this study.

1.4 DISCUSSION

A. Reorganization Energies

Self-exchange rate constants of $k_{ex} = 2 \times 10^7$ M^{-1} s^{-1} for **III** and **IV** and $k_{ex} = 1 \times 10^7$ M^{-1} s^{-1} for **I** have been measured in CH_3CN at 31°C with PF_6^- as the counter ion and at an ionic strength of ~ 0.1 M.[20] Rate constants were found to be larger in water and to increase with ionic strength, with a value of $k_{ex} \approx 2 \times 10^9$ M^{-1} s^{-1} estimated for the ClO_4^- salt of **I** at 25 ºC in a 1 M $HClO_4$ solution.[26] Comparison of these results highlights the

effects that solvent, counter ion, and ionic strength have on k_{ex}. Thus, in our study, the self-exchange rate constants were measured under conditions (buffered D_2O with Cl^- counter ion and 1 M KCl at 3 °C) that were as close as feasible to those used in the electrochemical measurements on ZnO.

The self-exchange rate constants for the redox couples employed were all very similar, with a mean value of $(8.6 \pm 0.7) \times 10^7$ M^{-1} s^{-1} (D_2O, 1 M KCl, 3 ºC). The self-exchange rate constants of a series of osmium tetramethyl, dimethyl, and unsubstituted phenanthroline complexes have been previously observed to vary only by a factor of 2.[27] Therefore k_{ex} is assumed to be similar for **I**, **III,** and **IV** under our conditions. In addition, k_{ex} for **II** is also assumed to be similar to **III**-**IV** since **II** has the same metal center and nominally identical ligands. The rate constants for **V** and **VIII** were taken to be representative of values for compounds **V**-**VIII**. No diffusion corrections were made to the measured self-exchange rate constants since the values are significantly below the diffusion limited value of $\approx 3 \times 10^9$ M^{-1} s^{-1}.[28]

The reorganization energy, λ_{ex}, for a given species in a self-exchange electron-transfer process can be related to the self-exchange rate constant by the expression[1,28-31]

$$k_{ex} = K_A \kappa_{el} \nu_n \Gamma e^{\frac{-\lambda_{ex}}{4k_B T}} \qquad (10)$$

where K_A is the equilibrium constant for the formation of the precursor complex of the reactants, κ_{el} is the electronic transmission coefficient, ν_n is the effective nuclear vibration frequency of the activated complex, and Γ is a correction for nuclear tunneling. For an ionic strength of 1 M, the work to bring two positively charged species together is less than $k_B T$, which implies that $K_A \approx 1$.[32,33] Given the similarity of the complexes studied, they are assumed to have similar values of $\kappa_{el} \approx 1$ (i.e., the reactions are adiabatic).[31]

The total reorganization energy in self-exchange reactions is comprised of changes in the bond lengths and angles in the inner-coordination sphere of the complexes,

$\lambda_{ex,in}$, and changes in the polarization of the solvent in the outer-coordination sphere, $\lambda_{ex,out}$ ($\lambda_{ex} = \lambda_{ex,in} + \lambda_{ex,out}$). For Os and Ru complexes that involve bipyridyl ligands, the inner-sphere does not undergo significant changes upon electron transfer.[34] The reorganization energy is therefore dominated by the solvent reorganization energy, which has a significant effect on ν_n.[31] For these reactions, ν_n was taken to be 10^{11} s^{-1}.[29,35] The values of λ_{ex} obtained using eq (9) with the measured values of k_{ex} are 0.67 ± 0.04 eV (Table 1.2).

The outer-sphere reorganization energy for two identical spherical reactants in solution can be calculated as[1]

$$\lambda_{out} = \frac{q^2}{4\pi\varepsilon_0}\left[\left(\frac{1}{a} - \frac{1}{R}\right)\left(\frac{1}{n^2} - \frac{1}{\varepsilon}\right)\right] \qquad (11)$$

where a is the radius of the reactant, R is the reactant center-to-center separation, n is the refractive index of the solvent (1.3438 for 0.98 M KCl in H_2O at 20 ºC, with a very small temperature dependence[36]), and ε is the static dielectric constant of the solvent (86.5 for H_2O at 3 ºC[36]). Using a = 0.60 nm and R = 1.2 nm produces a value of λ_{out} = 0.65 eV, in excellent agreement with the value derived from the self-exchange rate constant measurements (Table 1.2).

B. Differential Capacitance vs. Applied Potential Measurements

The nearly ideal behavior of the Mott-Schottky plots allowed accurate determination of the flat-band potentials for the ZnO/H_2O interfaces of interest. The E_{fb} values for a given ZnO/liquid contact did not vary significantly as the measurement frequency was changed. Furthermore, E_{fb} values were essentially constant vs. SCE as the Nernstian potential of the cell was changed by ≈ 0.9 V by varying the redox species in the homologous series of compounds investigated in this work (Figure 1.5).

In prior work on ZnO, the pH dependence of E_{fb} was studied and the predicted $2.3k_BT/q$ shift of E_{fb} per pH unit was verified.[37] A value for E_{fb} ≈ -0.26 V vs. SCE was determined at 25 ºC at pH 5 with $N_d = 5 \times 10^{16}$ cm^{-3}, which corresponds to a value of

$\mathbf{E}_{cb}/q \approx$ -0.37 V vs. SCE. In another report, a value for E_{fb} of ≈ -0.33 V vs. SCE was found for $N_d = 7 \times 10^{14}$ cm^{-3} at 25 ºC at pH 8.5,[14] which corresponds to a value of $\mathbf{E}_{cb}/q \approx$ -0.34 V vs. SCE at pH 5. Our experimental value of $\mathbf{E}_{cb}/q$ = -0.31 ± 0.01 V vs. SCE (calculated using eq (5) with E_{fb} = -0.10 ± 0.01 V vs. SCE, $N_d = (5.8 \pm 0.6) \times 10^{14}$ cm^{-3}, and T = 276 K) at pH = 5 is therefore in good agreement with prior results on ZnO in H_2O.

C. Current Density vs. Applied Potential Measurements

A notable feature of the ZnO/H_2O contacts reported herein is their nearly ideal *J* vs. *E* behavior.[11] Diode quality factors for data collected at high acceptor concentrations were generally found to be between 1 and 1.1, and the *J* vs. *E* curves shifted by the theoretically expected amounts as the acceptor concentration was varied. These observations imply that the interfacial kinetics follow the rate law of eq (1) and indicate that surface state effects do not dominate the charge-transfer processes of the systems investigated.[11]

D. Dependence of Interfacial Charge-Transfer Rate Constants on Driving Force: Comparison Between Theory and Experiment

One of the most interesting predictions of Marcus theory is that of the inverted region, in which the electron-transfer rate constant decreases with increasing driving force. The maximal rate for a molecular donor-acceptor system is observed when the standard free energy change for the reaction, $\Delta G°'$, exactly cancels the reorganization energy, λ. When the driving force is either increased or decreased relative to this point, an energy barrier is present for the reaction and the rate decreases.[4,5,38-40]

The Marcus description of electron transfer has been generalized for interfacial electron-transfer reactions for both metal and semiconductor electrodes.[17] Metal electrodes, in contrast with molecules, have many closely spaced electronic levels. The rate of electron transfer from a metal electrode to a redox molecule in solution consists of a summation of rates from each of the occupied metal levels, with each level having a

rate that is characterized by the Marcus free energy relationship. Thus, when the driving force for the reaction is made high enough (the electrode potential is made negative enough), an inverted region barrier, and a decreased rate of electron transfer, will be produced from the highest occupied energy levels. Since there are many closely spaced levels of lower energy, however, there will always be occupied electronic states at optimal exoergicity that dominate the interfacial current. Thus, for metal electrodes the total rate will not decrease with driving force, which precludes the direct observation of the inverted region.

An ideal semiconductor has no electronic levels in the band gap region, so only electrons with energies near the conduction band, for an n-type material, can contribute to the current flow. This situation is then analogous to a donor-acceptor system. Thus, as the driving force of the reaction increases, the electron-transfer rate of the conduction band electrons should increase, reach a maximal value, and then decrease. It should therefore be possible to observe directly the inverted region for semiconductor/liquid contacts.

Several different levels of theory have been used to derive an expression for the rate constant at optimal exoergicity of interfacial electron transfer for a semiconductor electrode in contact with acceptor species in solution. These approaches include a simple collisional model[17,41] and an electronic coupling model based on Marcus' treatment of electron transfer at the interface of two immiscible liquids.[42-44] An electronic coupling model based on the Fermi Golden Rule applied to the case of a semiconductor electrode in contact with a random distribution of acceptor species in solution, has produced the following expression for the rate constant:[45]

$$k_{et} = \frac{2\pi}{\hbar}\frac{1}{(4\pi k_B T\lambda_{sc})^{1/2}}\left(H_{AB,sc}^{2}\right)\beta_{sc}^{-1}\left\{\frac{l_{sc}}{d_{sc}^{2/3}(6/\pi)^{1/3}}\right\}\left[\exp\left\{\frac{-[(\overbrace{\mathbf{E}_{CB}-qE^{o'}}^{\Delta G^{0'}})+\lambda_{sc}]^2}{(4k_B T\lambda_{sc})}\right\}\right] \qquad (12)$$

where β_{sc} is the coupling attenuation factor, l_{sc} is the effective coupling length in the semiconductor, λ_{sc} is the reorganization energy of the acceptor species near the semiconductor electrode and d_{sc} is the atomic density of the solid. The quantity $\overline{H^2_{AB,sc}}$ represents the square of the matrix element that couples reactant and product states at energy **E**, averaged over all degenerate states in the semiconductor in a plane parallel to the electrode surface. This value is assumed to be independent of energy over the range of interest.[45] The subscript "sc" indicates parameters for a semiconductor electrode. Eq (12) can be rewritten as

$$k_{et} = k_{et,max} \exp\left\{\frac{-(\Delta G^{o\prime} + \lambda_{sc})^2}{4\lambda_{sc} k_B T}\right\} \qquad (13)$$

where the prefactor has been combined into $k_{et,max}$, which is the rate constant at optimal exoergicity. While $k_{et,max}$ is not independent of the reorganization energy, and thus will vary for different redox couples, this variation is modest.

The similarity in the values of the self-exchange rate constants for the complexes studied indicates that both the electronic coupling in homogenous solution and the reorganization energies are essentially constant. For the electrode reactions, since all compounds are coupling to the same electrode, the electronic coupling coefficient, H_{AB}, is also likely to be similar for the redox species of concern.

Figure 1.7 shows a semi-logarithmic plot of k_{et} vs. the standard driving force for interfacial electron transfer, $-\Delta G^{o\prime} = qE^{o\prime}(A/A^-) - \mathbf{E}_{cb}$. The rate constant at optimal exoergicity, $k_{et,max}$, is obtained when $\Delta G^{\circ\prime} = -\lambda_{sc}$, and has a value of $\approx 10^{-16}$ cm^4 s^{-1}.[45] A k_{et} vs. $\Delta G^{o\prime}$ curve calculated according to eq (13) with $k_{et,max} = 10^{-16}$ cm^4 s^{-1} and $\lambda_{sc} = 0.67$ eV (the value derived from self-exchange measurements, see discussion of the reorganization energy below) has been superimposed on the plot of Figure 1.7a (solid line). The agreement between our experimental data and theory is very good.

An uncertainty in the absolute value of E_{fb} would introduce a constant offset in the standard driving force and resulting rate constants for all compounds, but such an

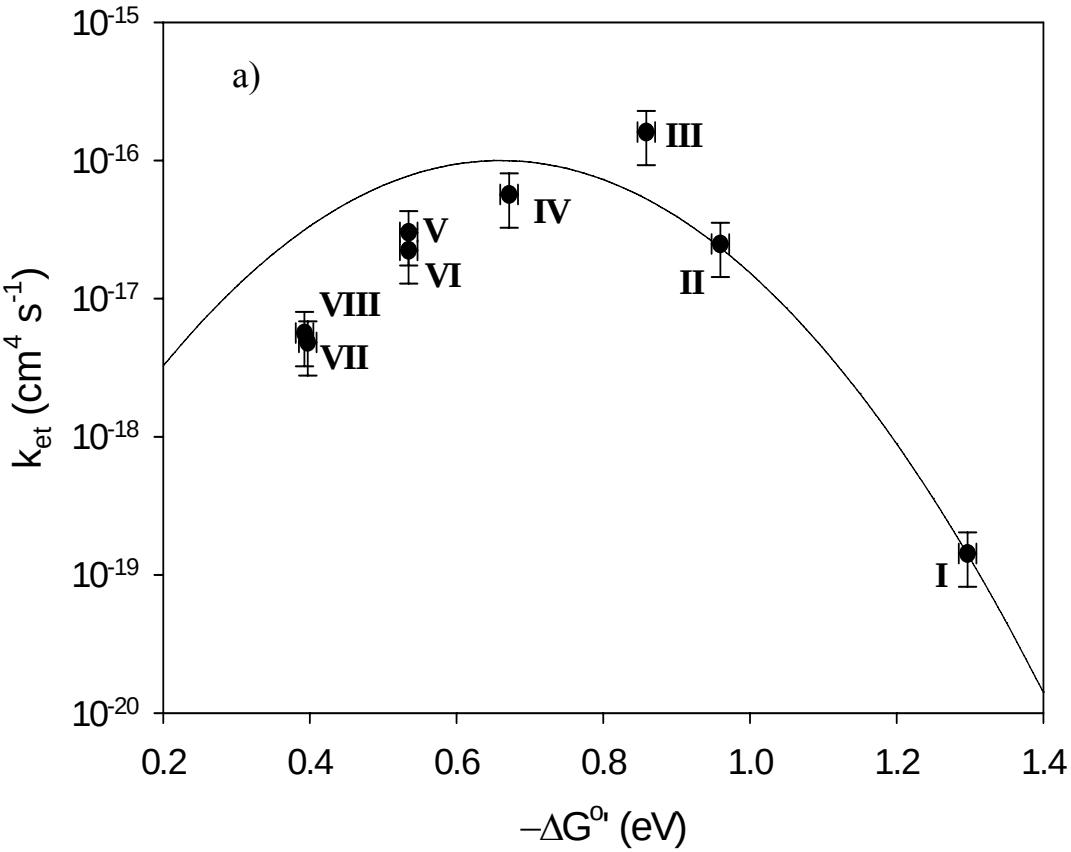
a)
III
IV
V
VI
II
VIII
VII
I
10^{-15}
10^{-16}
10^{-17}
10^{-18}
10^{-19}
10^{-20}
k_{et} (cm^4 s^{-1})
0.2
0.4
0.6
0.8
1.0
1.2
1.4
$-\Delta G^{o\prime}$ (eV)

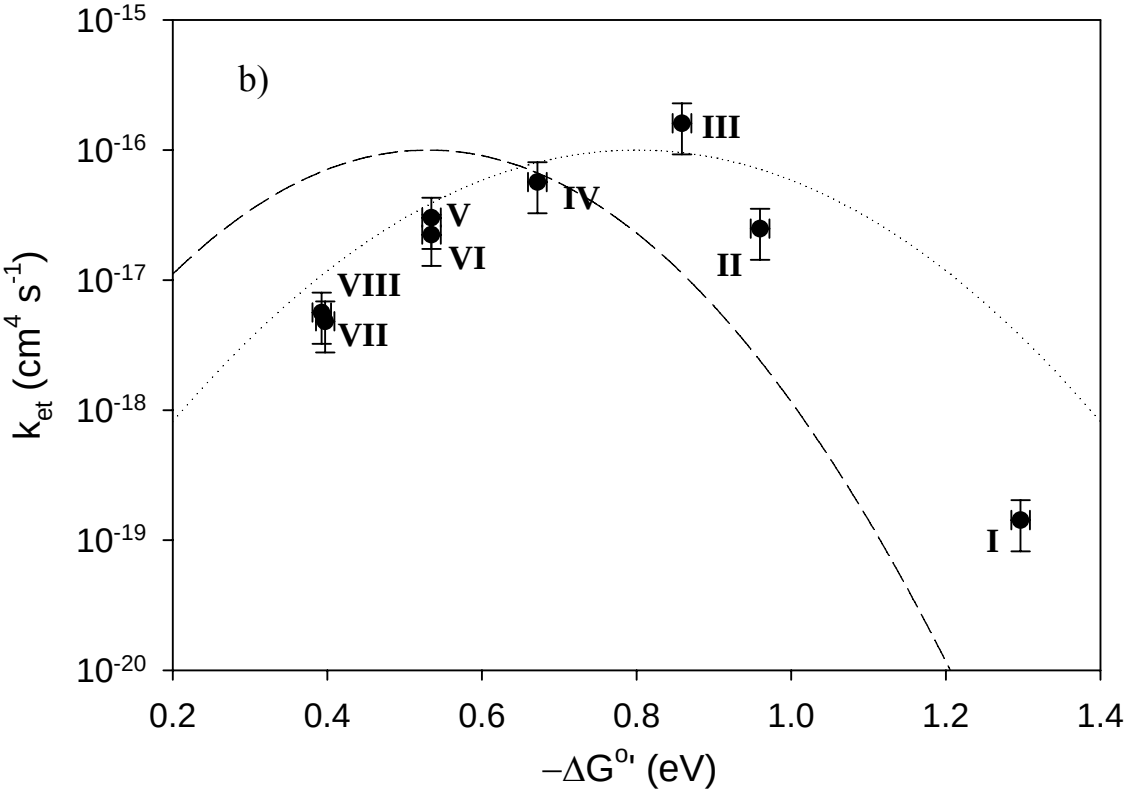

Figure 1.7 Plots of the electron transfer rate constant for compounds **I-VIII** as a function of the standard driving force, $-\Delta G^{o\prime} = qE^{o\prime}(A/A^-) - \mathbf{E}_{cb}$, for the redox systems investigated. a) The solid line represents the predicted k_{et} vs. $\Delta G^{o\prime}$ behavior for $k_{et,max} = 1\times10^{-16}$ cm^4 s^{-1} and $\lambda_{sc} = 0.67$ eV. b) The dotted line represents the predicted k_{et} vs. $\Delta G^{o\prime}$ behavior for $k_{et,max} = 1\times10^{-16}$ cm^4 s^{-1} and $\lambda_{sc} = 0.8$ eV, and the dashed line the predicted k_{et} vs. $\Delta G^{o\prime}$ behavior for $k_{et,max} = 1\times10^{-16}$ cm^4 s^{-1} and $\lambda_{sc} = 0.53$ eV.

error in E_{fb} and/or N_d would not change the observed trend of the rate constant with increasing driving force. This is in fact what we observed; other electrodes, not reported here, had variations in E_{fb} that resulted in the same trends reported here, but with a slight constant offset.

The interfacial rate constant for **I** is two orders of magnitude smaller than that for **II,** measured under the same conditions, despite > 300 mV greater driving force. It is important to point out that while **I** has a different metal center than **II**-**VIII**, this should not account for the lower k_{et} since self-exchange rate constants have been shown not to differ significantly between similar Os and Ru complexes.[20] We attribute this large decease in k_{et} for **I** primarily to the large increase in driving force. These results support the theoretical expectation of the Marcus inverted region for these interfacial electron-transfer processes.

The value of the reorganization energy for an electron-transfer reaction between a redox couple and a ZnO electrode, where both the redox couple in solution and the image charge in the semiconductor contribute to the total reorganization energy, is expected to be smaller than or equal to that for the self-exchange reaction of the couple in homogeneous solution. A theoretical value for the reorganization energy of a redox couple at a ZnO electrode can be calculated by[46,47]

$$\lambda_{sc} = \frac{q^2}{8\pi\varepsilon_0}\left[\frac{1}{a}\left(\frac{1}{n_{Sol}^2}-\frac{1}{\varepsilon_{Sol}}\right)-\frac{1}{2R_e}\left(\left(\frac{n_{ZnO}^2-n_{Sol}^2}{n_{ZnO}^2+n_{Sol}^2}\right)\frac{1}{n_{Sol}^2}-\left(\frac{\varepsilon_{ZnO}-\varepsilon_{Sol}}{\varepsilon_{ZnO}+\varepsilon_{Sol}}\right)\frac{1}{\varepsilon_{Sol}}\right)\right] \qquad (14)$$

where n_{ZnO} and n_{Sol} are the refractive index of ZnO (1.9[23,48]) and the aqueous solution, respectively, Σ_{ZnO} and Σ_{Sol} are the static dielectric constants of ZnO (8.65[23]) and the solution, respectively, and R_e is the distance from the acceptor to the electrode. Using a = 0.60 nm and R_e = 0.60 nm produces a value of λ_{sc} = 0.53 eV, which is approximately 80% of the self-exchange value.

A k_{et} vs. $\Delta G^{o\prime}$ curve calculated according to eq (13) with $k_{et,max} = 10^{-16}$ cm^4 s^{-1} and λ_{sc} = 0.53 eV is superimposed on the plot of Figure 1.7b (dashed line). Such a curve

yields a poor fit to the experimental data, with a λ_{sc} that is too low. Inspection of the plot indicates that the maximum rate constant occurs at $-\Delta G^{o'} \approx 0.8$ eV, which implies a λ_{sc} for our series of ≈ 0.8 eV. A k_{et} vs. $\Delta G^{o'}$ curve calculated according to eq (13) with $k_{et,max} = 10^{-16}$ cm^4 s^{-1} and $\lambda_{sc} = 0.8$ eV is superimposed on the plot of Figure 7b (dotted line). This theoretical curve fits the low driving force regime well, however, it deviates significantly for the high driving force compounds. The reorganization energy derived from the self-exchange reactions, and calculated according to eq (11), appears to be the best estimate for the reorganization energy of the redox compounds investigated herein at the ZnO/water interface.

1.5 CONCLUSIONS

The ZnO/H_2O junctions displayed nearly ideal energetic and kinetics behavior in contact with a homologous series of osmium polypyridyl redox couples. Differential capacitance measurements showed that the band edges of ZnO were fixed to within 10 mV with respect to SCE when the solution potential was changed by ≈ 900 mV. Current density vs. potential measurements displayed a first-order dependence on acceptor and surface electron concentrations. This behavior allowed for the experimental determination of interfacial electron-transfer rate constants for such systems. The driving force was changed by varying the formal reduction potential of the redox couple in solution. The reaction with the highest driving force had the smallest rate constant. This observation of decreasing rate constant with increasing driving force provides direct proof that semiconductor/liquid contacts can operate in the inverted regime.

1.6 ACKNOWLEDGMENTS

We acknowledge the Department of Energy, Office of Basic Energy Sciences, for support of this work. Dr. Mona Shahgholi provided helpful assistance in acquiring mass spectroscopic data, and Drs. Nagarajan Srivatsan and Norman Sutin are acknowledged for helpful conversations.

1.7 REFERENCES

(1) Marcus, R. A.; Sutin, N. *Biochim. Biophys. Acta* **1985**, *811*, 265-322.

(2) Chou, M.; Creutz, C.; Sutin, N. *J. Am. Chem. Soc.* **1977**, *99*, 5615-5623.

(3) Gray, H. B.; Winkler, J. R. *Annu. Rev. Biochem.* **1996**, *65*, 537-561.

(4) Fox, L. S.; Kozik, M.; Winkler, J. R.; Gray, H. B. *Science* **1990**, *247*, 1069-1071.

(5) Closs, G. L.; Miller, J. R. *Science* **1988**, *240*, 440-447.

(6) Nakabayashi, S.; Itoh, K.; Fujishima, A.; Honda, K. *J. Phys. Chem.* **1983**, *87*, 5301-5303.

(7) Lu, H.; Prieskorn, J. N.; Hupp, J. T. *J. Am. Chem. Soc.* **1993**, *115*, 4927-4928.

(8) Lewis, N. S. *J. Phys. Chem. B* **1998**, *102*, 4843-4855.

(9) Lewis, N. S. *Ann. Rev. Phys. Chem.* **1991**, *42*, 543-580.

(10) Fajardo, A. M.; Lewis, N. S. *Science* **1996**, *274*, 969-972.

(11) Fajardo, A. M.; Lewis, N. S. *J. Phys. Chem. B* **1997**, *101*, 11136-11151.

(12) Pomykal, K. E.; Lewis, N. S. *J. Phys. Chem. B* **1997**, *101*, 2476-2484.

(13) Dewald, J. F. *Bell Tech. J.* **1960**, *39*, 615-639.

(14) Dewald, J. F. *J. Phys. Chem. Solids* **1960**, *14*, 155-161.

(15) Morrison, S. R. *Surf. Sci.* **1969**, *15*, 363-379.

(16) Morrison, S. R.; Freund, T. *J. Chem. Phys.* **1967**, *47*, 1543-1551.

(17) Morrison, S. R. *Electrochemistry at Semiconductor and Oxidized Metal Electrodes*; Plenum: New York, 1980.

(18) Nakabayashi, Y.; Omayu, A.; Yagi, S.; Nakamura, K. *Anal. Sci.* **2001**, *17*, 945-950.

(19) Nakabayashi, Y.; Nakamura, K.; Kawachi, M.; Motoyama, T.; Yamauchi, O. *J. Bio. Inorg. Chem.* **2003**, *8*, 45-52.

(20) Chan, M. S.; Wahl, A. C. *J. Phys. Chem.* **1978**, *82*, 2542-2549.

(21) Jameson, D. L.; Anand, R. *J. Chem. Educ.* **2000**, *77*, 88-89.

(22) Gerischer, H.; Sorg, N. *Electrochim. Acta* **1992**, *37*, 827-835.

(23) Bhargava, R. *Properties of Wide Bandgap II-VI Semiconductors*; Inspec: London, 1997; Series No. 17.

(24) Sze, S. M. *The Physics of Semiconductor Devices*; 2nd ed.; Wiley: New York, 1981.

(25) Bard, A. J.; Faulkner, L. R. *Electrochemical Methods: Fundamentals and Applications*; John Wiley & Sons: New York, 2001.

(26) Young, R. C.; Keene, F. R.; Meyer, T. J. *J. Am. Chem. Soc.* **1977**, *99*, 2468-2473.

(27) Triegaardt, D. M.; Wahl, A. C. *J. Phys. Chem.* **1986**, *90*, 1957-1963.

(28) Sutin, N. *Acc. Chem. Res.* **1982**, *15*, 275-282.

(29) Meyer, T. J.; Taube, H. In *Comprehensive Coordination Chemistry*; Wilkinson, S. G., Gilliard, R. D., McCleverty, J. A., Eds.; Pergamon Press: New York, 1987; Vol. 1, p 331.

(30) Sutin, N. *Prog. Inorg. Chem.* **1983**, *30*, 441-498.

(31) Brunschwig, B. S.; Logan, J.; Newton, M. D.; Sutin, N. *J. Am. Chem. Soc.* **1980**, *102*, 5798-5809.

(32) Sutin, N.; Brunschwig, B. S. *ACS Symp. Ser.* **1982**, *198*, 105-135.

(33) Sutin, N. In *Tuneling in Biological Systems*; B. Chance, R. Marcus, D. C. DeVault, J. R. Schrieffer, H. Frauenfelder, N. Sutin, Eds.; Academic Press: New York, 1979, pp 201-228.

(34) Biner, M.; Burgi, H.-B.; Ludi, A.; Rohr, C. *J. Am. Chem. Soc.* **1992**, *114*, 5197-5203.

(35) Marcus, R. A. *J. Phys. Chem.* **1963**, *67*, 853-857.

(36) Lide, D. R., Ed. *CRC Handbook of Chemistry and Physics*; 81 ed.; CRC Press, 2001.

(37) Lohmann, F. *Ber. Bunsenges. Phys. Chem.* **1966**, *70*, 428-434.

(38) McCleskey, T. M.; Winkler, J. R.; Gray, H. B. *Inorg. Chim. Acta* **1994**, *225*, 319-322.

(39) Creutz, C.; Sutin, N. *J. Am. Chem. Soc.* **1977**, *99*, 241-243.

(40) Closs, G. L.; Calcaterra, L. T.; Green, N. J.; Penfield, K. W.; Miller, J. R. *J. Phys. Chem.* **1986**, *90*, 3673-3683.

(41) Gerischer, H. *J. Phys. Chem.* **1991**, *95*, 1356-1359.

(42) Marcus, R. A. *J. Phys. Chem.* **1990**, *94*, 1050-1055.

(43) Pomykal, K. E.; Fajardo, A. M.; Lewis, N. S. *J. Phys. Chem.* **1996**, *100*, 3652-3664.

(44) Gao, Y. Q.; Georgievskii, Y.; Marcus, R. A. *J. Chem. Phys.* **2000**, *112*, 3358-3369.

(45) Royea, W. J.; Fajardo, A. M.; Lewis, N. S. *J. Phys. Chem. B* **1997**, *101*, 11152-11159.

(46) Kuciauskas, D.; Freund, M. S.; Gray, H. B.; Winkler, J. R.; Lewis, N. S. *J. Phys. Chem. B* **2001**, *105*, 392-403.

(47) Marcus, R. A. *J. Phys. Chem.* **1991**, *95*, 2010-2013.

(48) Ashkenov, N.; Mbenkum, B. N.; Bundesmann, C.; Riede, V.; Lorenz, M.; Spemann, D.; Kaidashev, E. M.; Kasic, A.; Schubert, M.; Grundmann, M.; Wagner, G.; Neumann, H.; Darakchieva, V.; Arwin, H.; Monemar, B. *J. Appl. Phys.* **2003**, *93*, 126-133.

CHAPTER 2

Measurement of the Dependence of Interfacial Charge-Transfer Rate Constants on the Reorganization Energy of Redox Species at n-ZnO/H_2O Interfaces

2.1 INTRODUCTION

Electron transfer across the semiconductor/liquid interface is one of the most fundamental processes in the operation of a photoelectrochemical energy conversion system. Control of the interfacial electron-transfer rate is required to optimize the solar energy conversion efficiency of such devices. Some of the factors that govern these interfacial electron-transfer rate constants, however, remain relatively poorly understood. While in principle semiconductor electrodes have advantages over metal electrodes in addressing some of the basic predictions of interfacial electron-transfer theories, such measurements are difficult because extraordinarily low defect densities at the semiconductor/liquid interface are required to prevent adsorption and surface-state related reactions from dominating the observed interfacial kinetics processes.[1,2]

Carefully prepared n-type ZnO/H_2O contacts with a series of $Os^{3+/2+}$ redox couples have recently been reported to exhibit the predicted dependence of interfacial charge-transfer rate constants, k_{et}, on changes in standard interfacial free energies, $\Delta G°'$, for driving forces up to and beyond that of optimum exoergicity.[3] The rate constants were observed to decrease for high driving force contacts, indicating, by a straightforward application of Marcus theory,[4] that interfacial charge-transfer processes of some electrodes can operate in the inverted region.

This work addresses another basic prediction of the Marcus model for interfacial electron-transfer reactions at semiconductor electrodes. The interfacial electron-transfer rate constant should be strongly dependant on the reorganization energy, λ, of the acceptor species in solution. At constant driving force, in the normal region, k_{et} should

decrease as λ increases. Previous measurements in our laboratory of the stability of n-Si/CH_3OH contacts as a function of the reorganization energy of the electron donor in the electrolyte provided indirect evidence of this prediction.[5] To verify this basic theoretical prediction, we have synthesized a series of one-electron redox couples having relatively constant potentials in the band-gap region of ZnO and having reorganization energies that span approximately 1 eV. Charge-transfer rate constants have been measured for these systems in contact with n-type ZnO electrodes. This investigation has provided a detailed comparison of interfacial electron-transfer reactions at an "ideally" behaving semiconductor/electrode interface with the predictions of Marcus theory for such systems.

2.2 EXPERIMENTAL

A. Electrodes

The preparation of the ZnO electrodes has been described previously.[3] Electrochemical experiments reported in this work were confined to the Zn-rich surface. An area of 0.46 cm^2 was determined for the electrode reported here, with an estimated error of 0.03 cm^2.

Due to the limited number of high-quality ZnO single crystals available, a statistical approach was not feasible. At least two additional electrodes displayed similar energetic and kinetics features in measurements of all of the compounds reported here, and produced nominally identical trends in the measured rate constants. All of the data

reported herein were collected using a single electrode to minimize variation due to slight shifts in the flat-band potential of different electrode surfaces.

B. Electrolyte Solutions

Electrochemical experiments were carried out in an imidazole buffer prepared by adding 1 M HCl(aq) drop-wise to 2.72 g of imidazole in 100 mL H_2O until the desired pH was reached. The solution was then diluted to a volume of 500 mL (80 mM, pH = 6.5). The ionic strength, *I*, was adjusted to 1 M by addition of 37.4 g KCl (Aldrich, 99+%) to provide the supporting electrolyte for electrochemical measurements.

C. Redox Compounds

Cobalt(II) chloride hexahydrate, cobalt(II) tetrafluoroborate hexahydrate, ammonium hexachloroosmate(IV), 1,4,7-trithiacyclononae (TTCN), pyridine (py), 2,2'-bipyridine (bpy), 4,4'-dimethyl 2,2'-bipyridine (Me_2bpy), imidazole (Im), ammonium hexafluorophosphate, and tetrabutylammonium chloride (TBACl) were purchased from Aldrich and used as received. All solvents were reagent grade and were used as received. All compounds were prepared by modified literature procedures. The synthesis of $[Os(Me_2bpy)_2(Im)_2]Cl_2$ has been described previously.[3]

$[Co(bpy)_3](PF_6)_2$ was prepared by adding 1.7 g of $CoCl_2 \cdot 6H_2O$ in 50 mL of methanol to 6.4 g (3 equivalents) of bpy dissolved in 100 mL of methanol.[5] The solution was stirred for 1 hr. A stoichiometric amount of ammonium hexafluorophosphate was used to precipitate a yellow compound that was filtered and washed with ethanol, methanol, and ether. Elemental analysis yielded (calculated): C 43.91 (44.08), H 3.06 (2.96), N 10.23 (10.28). The chloride salt was made by dissolving $[Co(bpy)_3](PF_6)_2$ in acetone followed by addition of a stoichiometric amount of TBACl dissolved in acetone.

The chloride salt precipitated out of solution, was filtered, washed with acetone and ether, and then dried under vacuum. Elemental analysis for $[Co(bpy)_3]Cl_2 \cdot 4H_2O$ yielded (calculated): C 53.68 (53.74), H 4.03 (5.11), N 12.11 (12.53). Since chloride salts can adsorb water, water was added to the molecular formula to obtain agreement with the elemental analysis data. The compound composition was confirmed by NMR data on $Co(bpy)_3Cl_3$ that was prepared by oxidizing the parent compound with $Cl_2(g)$ in D_2O.

$[Ru(NH_3)_5py](PF_6)_2$ was prepared by adding 9 mL of pyridine to 0.7 g of $[Ru^{III}(NH_3)_5Cl]Cl_2$ dissolved in 50 ml of 18 MΩ cm resistivity H_2O (Barnstead NANOpure) that had been purged with Ar(g) over approximately 10 g of Zn-amalgam.[6] The Ru(II) compound was precipitated by adding excess aqueous ammonium hexafluorophosphate, and was collected by filtration, washed with ice-cold water and then with diethylether, and dried under vacuum. Elemental analysis yielded (calculated): C 11.27 (10.81), H 3.36 (3.63), N 14.64 (15.13). The chloride salt was made by dissolving $[Ru(NH_3)_5py](PF_6)_2$ in acetone followed by addition of a stoichiometric amount of TBACl dissolved in acetone. The chloride salt immediately precipitated out of solution, was filtered, washed with acetone and ether, and was then dried under vacuum. The compound was further investigated using UV-VIS spectroscopy and exhibited an absorption maximum at 407 nm.[6]

$[Co(TTCN)_2](BF_4)_2$ was prepared by adding two equivalents, 0.36 g, of TTCN dissolved in 50 mL of ethanol to 0.34 g of $CoBF_4 \cdot 6H_2O$ dissolved in 50 mL of ethanol.[7] A purple precipitate was filtered, washed with ethanol and ether, and then dried under vacuum. Elemental analysis yielded (calculated): C 24.12 (24.29), H 3.62 (4.08). The

compound composition was also confirmed by NMR data on $Co(TTCN)_2Cl_3$ that was prepared by oxidizing the parent compound with $Cl_2(g)$ in D_2O.

The formal reduction potential of each compound, $E^{o'}$, (Table 2.2) was determined using cyclic voltammetry in buffered H_2O with 1 M KCl as the electrolyte. A glassy carbon disc electrode was used as the working electrode, a platinum mesh was employed as the counter electrode, and a standard calomel electrode (SCE) in a separate cell was used as the reference electrode. Scans were taken from -0.4 V to 0.8 V vs. SCE at a scan rate of 75 mV s^{-1}.

D. Electrochemical Measurements

Details of the electrochemical experiments have been described previously.[3] All experiments were carried out at room temperature. All potentials are referenced to SCE. The oxidized, acceptor form, A, of each compound was created in situ via bulk electrolysis using a carbon mesh working electrode ([A] = 10 mM for $Co(bpy)_3^{3+}$, $Ru(NH_3)_5py^{3+}$, and $Co(TTCN)_2^{3+}$ and [A] = 5 mM for $Os(Me_2bpy)_2(Im)_2^{3+}$); a 5% error in [A] was estimated. The concentration of acceptor was varied by diluting a 1 mL aliquot of the redox solution with 9 mL of buffer. The Nernstian potential of the solution changed by less than 3 mV during each measurement and by less than 7 mV following dilution.

To deduce the space-charge capacitance at the ZnO electrode, impedance spectra were fitted to an equivalent circuit that consisted of the cell resistance, R_s, in series with two parallel components: the resistance to charge transfer, R_{sc}, and the space-charge capacitance, C_{sc}. Because C_{sc} is much less than the differential capacitance, C_{diff}, of either the Helmholtz layer or the double layer, C_{diff} was set equal to C_{sc}.[8] A linear

regression was used to fit the A_s^2/C_{sc}^2 vs. E data in accordance with the Mott-Schottky equation:[9]

$$\frac{A_s^2}{C_{sc}^2} = \frac{2}{q\varepsilon_{ZnO}\varepsilon_o N_d}\left(E - E_{fb} - \frac{k_B T}{q}\right) \quad (1)$$

where A_s is the surface area of the semiconductor electrode, k_B is Boltzmann's constant, T is the temperature, q is the charge of an electron (1.6022×10^{-19} C), ε_{ZnO} is the static dielectric constant of ZnO (8.65),[10] ε_o is the permittivity of free space, N_d is the dopant density of the semiconductor, and E_{fb} is the flat-band potential of the semiconductor/liquid contact. Values for N_D and E_{fb} were obtained from the slope, and from the x-intercept adjusted by $k_B T/q$, respectively.

With knowledge of N_d and E_{fb}, the energy of the conduction band edge, $\mathbf{E}_{cb}$, was determined using the expression

$$\mathbf{E}_{cb} = qE_{fb} + k_B T \ln\left(\frac{N_d}{N_c}\right) \quad (2)$$

where N_c is the effective density of states in the conduction band of the semiconductor ($N_c = 3.5 \times 10^{18}$ cm^{-3} for ZnO).[11] Given $\mathbf{E}_{cb}$, the electron concentration in the conduction band at the surface of the semiconductor, n_s, can be calculated at a given potential through the Boltzmann-type relationship:[1]

$$n_s = N_c e^{\frac{(\mathbf{E}_{cb} - qE)}{k_B T}} \quad (3)$$

Thus, application of a potential to an ideally behaving semiconductor electrode interface effects a change in n_s, as opposed to changing the energetics of the interfacial charge-transfer process.

The J vs. E data were obtained with a Schlumberger Instruments Electrochemical Interface Model SI1287 potentiostat. Two scans at a rate of 20 mV s^{-1} were measured for each system. At forward bias, the net flux of electrons from the conduction band to randomly dissolved acceptors in solution is given by[9]

$$J(E) = -qk_{et}[A]n_s \tag{4}$$

where k_{et} is the electron-transfer rate constant (cm^4 s^{-1}), and [A] is the acceptor concentration (cm^{-3}). The concentrations of the acceptor, [A], and n_s appear explicitly in the expression for the current density, thus yielding a second-order rate law for the charge-transfer process. Therefore, if J is shown to follow eq (4) and [A] is known, the value of k_{et} is be readily calculated from the observed steady-state J vs. E data.

2.3 RESULTS AND DISCUSSION

A. Differential Capacitance vs. Applied Potential Measurements

For each interface studied, Bode plots of the impedance magnitude, |Z|, vs. the ac signal frequency, f, were linear over at least two orders of magnitude variation in frequency, with slopes ≈ -1 and phase angles of the current vs. ac voltage ≈ -90º. The observed impedance of these systems was thus dominated by a single capacitive circuit element, with $Z_{im} \approx (2\pi f C_{diff})^{-1}$.[8] The impedance spectra were fitted over the frequency range of 10^2 to 10^4 Hz to the equivalent circuit described above. The capacitance, C_{diff}, was independent of frequency, resulting in very small errors (< 1%) for each fit. The series resistance of the system, R_s, was essentially constant for all measurements, with a value of 35 Ω.

Figure 2.1 displays Mott-Schottky plots in the form of A_s^2/C_{diff}^2 vs. E data for all contacts with varying concentrations of oxidized and reduced species grouped together. All of the Mott-Schottky plots were linear, as predicted by eq (1). Values for N_d and E_{fb} were obtained from the slope and intercept, respectively. The standard errors resulting from the fit were used to calculate the errors in N_d and E_{fb}, producing values of E_{fb} = -0.35 ± 0.01 V vs. SCE and $N_d = (5.5 \pm 0.6) \times 10^{16}$ cm^{-3}. Equation (2) was then used to calculate a value for $\mathbf{E}_{cb}/q$ = -0.46 ± 0.01 V vs. SCE. The invariance of the capacitance data at a fixed electrode potential for all of the compounds is in accord with the "ideal" model of a semiconductor/liquid interface.

The nearly ideal behavior of the Mott-Schottky plots allowed accurate determination of the flat-band potentials for the ZnO/H_2O interfaces of interest. The E_{fb} values for a given ZnO/liquid contact did not vary significantly as the measurement frequency was changed. Our experimental value of $\mathbf{E}_{cb}/q$ = -0.46 ± 0.01 V vs. SCE at pH = 6.5 is in very good agreement with prior results from our laboratory and from the work of others on ZnO in H_2O.[3,12,13]

B. Current Density vs. Applied Potential Measurements

A notable feature of the ZnO/H_2O contacts reported herein is their excellent J vs. E behavior. All of the junctions showed rectifying behavior, producing a limiting anodic current density and an exponentially increasing cathodic current density, in accord with the diode equation:

$$J = -J_0\left(e^{\frac{-qE}{\gamma k_B T}} - 1\right) \tag{5}$$

where J_o is the exchange current density and γ is the diode quality factor.

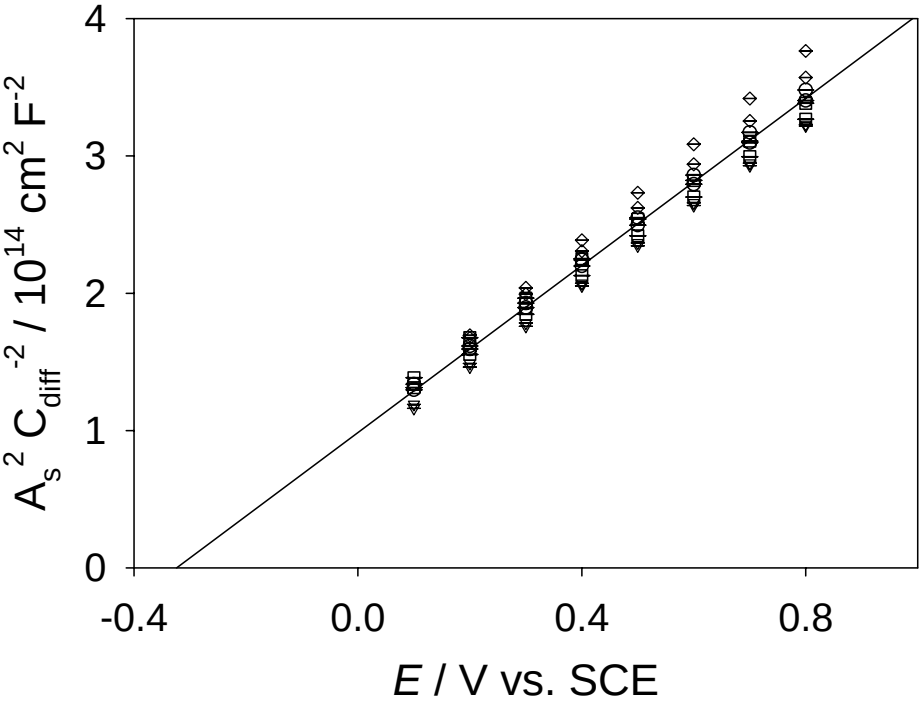

Figure 2.1 Mott-Schottky plots of ZnO in contact with $Co(bpy)_3^{3+/2+}$ (open circles), $Ru(NH_3)_5py^{3+/2+}$ (open squares), $Co(TTCN)_2^{3+/2+}$ (open diamonds), and $Os(Me_2bpy)_2(Im)_2^{3+/2+}$ (open triangles) at high and low concentrations. The line indicates the least-squares fit of all of the data.

Figure 2.2 displays plots of ln (-J) vs. E for all of the compounds investigated in this work. The diode quality factors were 1.2-1.3 at low concentrations of acceptors, indicating some relatively small but observable contribution from the presence of non-ideal recombination pathways. Large acceptor concentrations, however, favor direct electron transfer. Diode quality factors were ≈ 1.1 at high acceptor concentrations, in accord with the expectation of $\gamma = 1$ for a process that is kinetically first-order in the concentration of electrons at the surface of the semiconductor. The dependence of the rate on the concentration of acceptor species in the solution was determined by decreasing [A] by a factor of 10. This decrease in acceptor concentration produced shifts of the J vs. E data, ΔE, at a given current according to $\Delta E = (k_B T/q)\ln([A]_{low}/[A]_{high})$. The magnitude of the change in [A] was verified by measuring the limiting cathodic current densities at both acceptor concentrations, $J_{l,c,high}$ and $J_{l,c,low}$, with a Pt microelectrode. Values of γ and ΔE are given in Table 2.1 for the systems of interest in this work. In the series of measurements reported herein, the J-E behavior for $Ru(NH_3)_5py^{3+/2+}$ shifted by less than the predicted -59 mV, however larger shifts were generally observed in other measurements with this couple, so the rate law was still taken to be a first-order process. The observed first-order dependence of J on n_s and [A] validates the rate law of eq (4) and indicates that surface state effects do not dominate the charge-transfer processes of the systems investigated.[8]

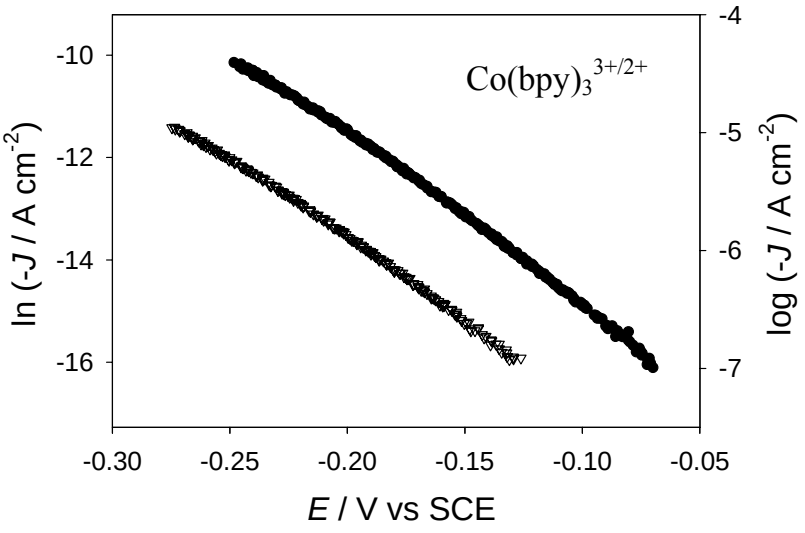
Co(bpy)3 3+/2+
ln (-J / A cm-2)
log (-J / A cm-2)
E / V vs SCE
-10
-12
-14
-16
-4
-5
-6
-7
-0.30
-0.25
-0.20
-0.15
-0.10
-0.05

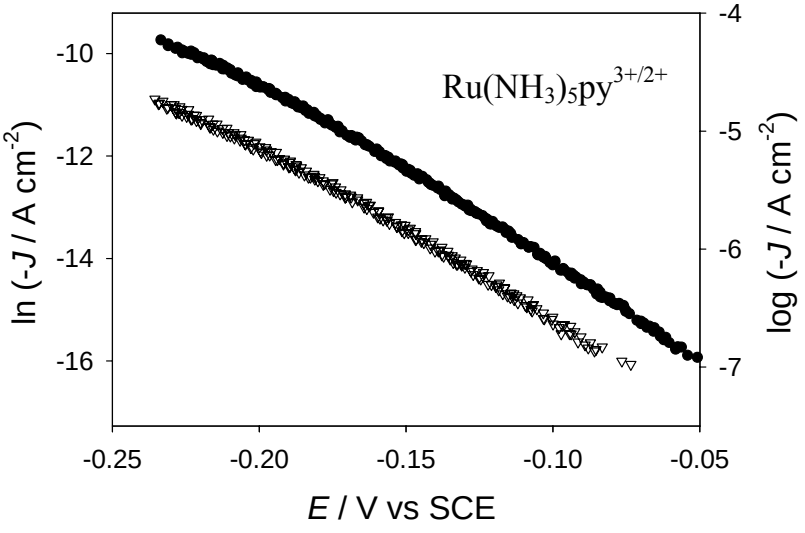
Ru(NH3)5py 3+/2+
ln (-J / A cm-2)
log (-J / A cm-2)
E / V vs SCE
-10
-12
-14
-16
-4
-5
-6
-7
-0.25
-0.20
-0.15
-0.10
-0.05

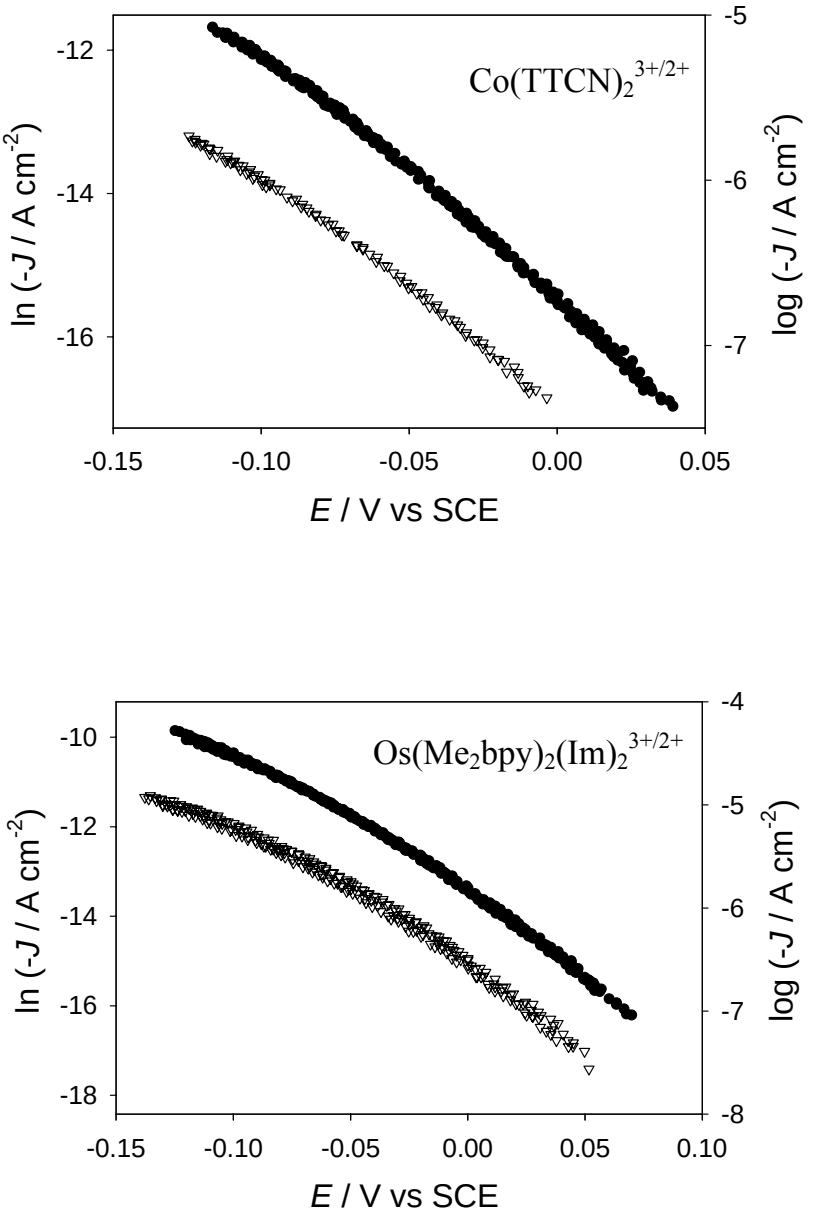

Figure 2.2 Plots of the dark current density, *J*, vs. applied potential, *E*, for compounds at high concentration ([*A*] = 10 mM for $Co(bpy)_3^{3+/2+}$, $Ru(NH_3)_5py^{3+/2+}$, and $Co(TTCN)_2^{3+/2+}$ and [*A*] = 5 mM for $Os(Me_2bpy)_2(Im)_2^{3+/2+}$; filled circles) and low concentration ([*A*] ≈ 1 mM for $Co(bpy)_3^{3+/2+}$, $Ru(NH_3)_5py^{3+/2+}$, and $Co(TTCN)_2^{3+/2+}$, and [*A*] ≈ 0.5 mM for $Os(Me_2bpy)_2(Im)_2^{3+/2+}$; open triangles). As noted in the text, a ten-fold decrease in [*A*] should result in a -59 mV shift of the *J*-*E* curve. All potentials are referenced to SCE.

C. Rate Constants for Interfacial Charge-Transfer, k_{et}

Because non-degenerately-doped semiconductor electrodes show relatively little Frumkin effect associated with the liquid part of the solid/liquid double layer,[1] the acceptor concentration can be assumed to be equal to the bulk value. The surface electron concentration at each applied potential, $n_s(E)$, was computed according to eq (3) using the conduction band-edge energy extracted from the flat-band potential determinations (eq (2)). The value of k_{et} was then calculated in accordance with the rate law given in eq (4), by dividing J by the quantity $\{-qn_s[A]\}$ at a given potential. The J vs. E data collected at the largest acceptor concentration were used both to minimize the error in the concentration and because the diode quality factors were close to 1 under such conditions. The quoted k_{et} value for each contact represents the average of values calculated using potentials from the high cathodic current density portion of the J vs. E curve ((-2 to -5) $\times 10^{-6}$ A cm^{-2}), and therefore includes any effects of the deviation of the diode quality factor (typically 1.1 at the high redox species concentrations) from the ideal value of 1.0. A standard Gaussian error analysis was performed in conjunction with calculation of the rate constants by propagating the errors of all the measured parameters used in the calculation of k_{et}. The error in $\mathbf{E}_{cb}$ dominated the error in k_{et}, due to the exponential dependence of n_s on ($\mathbf{E}_{cb}$ - qE). Table 2.1 summarizes the values of k_{et} determined for each of the ZnO/H_2O-redox couple junctions evaluated in this study.

Table 2.1 Results from current density vs. applied potential measurements and rate constant determinations. The quantities γ_{high} and γ_{low} are the diode quality factors at high and low acceptor concentration, respectively.

Compound	γ_{high}	γ_{low}	ΔE	$-\Delta G^{o\prime}$ (eV)	k_{et} ($cm^4\ s^{-1}$)	k_{et}^{calc} ($cm^4\ s^{-1}$)
$Co(bpy)_3^{3+/2+}$	1.1	1.2	-62	0.50 ± 0.01	$(1 \pm 0.6) \times 10^{-19}$	6.1×10^{-20}
$Ru(NH_3)_5py^{3+/2+}$	1.1	1.2	-38	0.49 ± 0.01	$(4 \pm 2) \times 10^{-19}$	2.5×10^{-18}
$Co(TTCN)_2^{3+/2+}$	1.1	1.3	-58	0.61 ± 0.01	$(5 \pm 3) \times 10^{-18}$	6.4×10^{-18}
$Os(Me_2bpy)_2(Im)_2^{3+/2+}$	1.1	1.3	-50	0.57 ± 0.01	$(6 \pm 4) \times 10^{-17}$	4.9×10^{-17}

D. Reorganization Energies

The total reorganization energy in self-exchange reactions is comprised of changes in electronic configuration and in the bond lengths and angles in the inner-coordination sphere of the complexes, $\lambda_{se,in}$, and of changes in the polarization of the solvent in the outer-coordination sphere, $\lambda_{se,out}$. The total reorganization energy, λ_{se} (with $\lambda_{se} = \lambda_{se,in} + \lambda_{se,out}$), for a given species in a self-exchange electron-transfer process can be related to the self-exchange rate constant, k_{ex}, by the expression[14-18]

$$k_{ex} = K_A \kappa_{el} \nu_n \Gamma e^{\frac{-\lambda_{se}}{4k_B T}} \tag{6}$$

where K_A is the equilibrium constant for the formation of the precursor complex of the reactants, κ_{el} is the electronic transmission coefficient, ν_n is the effective nuclear vibration frequency of the activated complex, and Γ is a correction for nuclear tunneling. The precursor formation equilibrium constant for reactant pairs separated by the distance between r and $r + \delta r$ (cm) can be calculated as[16]

$$K_A(r) = \frac{4\pi N_A r^2 \delta r}{1000} e^{-\frac{w(r)}{k_B T}} \tag{7}$$

where N_A is Avogadro's number and $w(r)$ is the work required to bring the reactants to the separation distance, r. With the assumptions that the work is primarily Coulombic, the reactants are spherical, and the radii of the ions are equal ($r = 2a$, where a is the reactant radius), $w(r)$ is given by[16]

$$w(r) = \frac{z_1 z_2 q^2}{4\pi\varepsilon_0 \varepsilon r\left(1 + \beta r I^{1/2}\right)} \tag{8}$$

where z_1 and z_2 are the charges on the ions (2 and 3 for the redox couples of interest here), ε is the static dielectric constant of the medium (80.2 for H_2O at 20 °C[19]), and $\beta = (2N_A q^2/1000\varepsilon_0 \varepsilon k_B T)^{1/2}$. The Debye-Hückel model is not expected to give quantitatively correct results as the ionic strength increases, particularly at the higher values of the ionic strength normally used in electrochemical experiments. However, $w(r)$ decreases as the ionic strength increases, so although the absolute value of the work calculated may be in error by a factor of 2 or more, the error in $K_A(r)$ is much smaller.

The frequency factor is given by[16]

$$\nu_n^{\,2} = \frac{\nu_{out}^{\,2}\lambda_{out} + \nu_{in}^{\,2}\lambda_{in}}{\lambda_{out} + \lambda_{in}} \tag{9}$$

where ν_{out} and ν_{in} are the solvent and ligand stretching frequencies, respectively. For Os polypyridyl complexes, the inner sphere does not undergo significant changes upon electron transfer,[20] and the reorganization energy is dominated by the solvent reorganization energy, so $\nu_n \approx \nu_{out} = 10^{11}$ s^{-1}.[3,15,21] The other compounds of interest in this work have a significant inner-sphere contribution to the reorganization energy, hence $\nu_n \approx \nu_{in} = 10^{13}$ s^{-1}.[16] All of the complexes studied are assumed to have similar values of $\kappa_{el} \approx 1$ (i.e., the reactions are adiabatic), and $\Gamma \approx 1$ (no significant tunneling contribution).[18] Values for k_{ex} are available from prior work, and the resulting values calculated for K_A, ν_n, and λ_{se} are given in Table 2.2.

The outer-sphere reorganization energy for two spherical reactants in solution can be calculated by[14]

$$\lambda_{se,out} = \frac{(\Delta z q)^2}{4\pi\varepsilon_0}\left[\left(\frac{1}{a} - \frac{1}{R}\right)\left(\frac{1}{n^2} - \frac{1}{\varepsilon}\right)\right] \tag{10}$$

where Δz is the difference in the charge of the ions, R is the reactant center-to-center separation ($R = 2a$), and n is the refractive index of the solvent (1.3438 for 0.98 M KCl in H_2O at 20 °C[19]). The inner-sphere reorganization energy can be deduced by subtracting the outer-sphere reorganization energy from the total ($\lambda_{se,in} = \lambda_{se} - \lambda_{se,out}$). Values of a, $\lambda_{se,out}$, and $\lambda_{se,in}$ are given in Table 2.2.

The outer-sphere reorganization energy of a redox couple at a ZnO electrode, $\lambda_{sc,out}$, where both the redox couple in solution and the image charge in the semiconductor contribute to the total reorganization energy, is expected to be less than that for the self-exchange reaction of the couple in homogeneous solution. A theoretical value for the outer-sphere reorganization energy of a redox couple at a ZnO electrode can be calculated by[22-24]

$$\lambda_{sc,out} = \frac{(\Delta zq)^2}{8\pi\varepsilon_0}\left[\frac{1}{a}\left(\frac{1}{n^2}-\frac{1}{\varepsilon}\right)-\frac{1}{2R_e}\left(\left(\frac{n_{ZnO}^2-n^2}{n_{ZnO}^2+n^2}\right)\frac{1}{n^2}-\left(\frac{\varepsilon_{ZnO}-\varepsilon}{\varepsilon_{ZnO}+\varepsilon}\right)\frac{1}{\varepsilon}\right)\right] \qquad (11)$$

where n_{ZnO} is refractive index of ZnO (1.9[10,25]) and R_e is the distance from the acceptor to the electrode ($R_e = a$).

The inner-sphere reorganization energy at a ZnO electrode is half of the value of $\lambda_{se,in}$, since half as many molecules participate in each electron-transfer event. The total reorganization energy for a redox couple at a ZnO electrode is therefore given by $\lambda_{sc} = (\lambda_{se} - \lambda_{se,out})/2 + \lambda_{sc,out}$. Values of $\lambda_{sc,out}$ and λ_{sc} for each of the redox couples are given in Table 2.2.

Table 2.2 Formal potentials, $E^{o\prime}$, self-exchange rate constants, k_{ex}, and reorganization energies, λ, for the redox couples of interest in this work.

	$E^{o\prime}$ (mV) [a]	k_{ex} (M^{-1} s^{-1})	I (M)	a (A)	K_A (M^{-1})	ν_n (s^{-1})	λ_{se} (eV)	$\lambda_{se,out}$ (eV)	$\lambda_{se,in}$ (eV)	$\lambda_{sc,out}$ (eV)	λ_{sc} (eV)
$Co(bpy)_3^{3+/2+}$	40	20 [b]	0.1	6.5	0.28	10^{13}	2.64	0.60	2.04	0.49	1.51
$Ru(NH_3)_5py^{3+/2+}$	35	4.7×10^5 [c]	1	4.2	0.12	10^{13}	1.52	0.93	0.59	0.76	1.06
$Co(TTCN)_2^{3+/2+}$	150	1.3×10^5 [d]	0.2	5	0.14	10^{13}	1.67	0.75	0.92	0.62	1.08
$Os(Me_2bpy)_2(Im)_2^{3+/2+}$	110	8.7×10^7 [e]	1	6.5	0.57	10^{11}	0.67	0.60	0.07	0.49	0.53

[a] referenced to SCE [b] Weaver, M. J.; Yee, E. L. *Inorg. Chem.* **1980**, *19*, 1936-1945. [c] Brown, G. M.; Krentzien, H. J.; Abe, M.; Taube, H. *Inorg. Chem.* **1979**, *18*, 3374-3379. [d] Chandrasekhar, S.; McAuley, A. *Inorg. Chem.* **1992**, *31*, 480-487. [e] ref (3).

E. Dependence of Interfacial Charge-Transfer Rate Constants on Reorganization Energy: Comparison Between Theory and Experiment

A non-adiabatic electronic coupling model, based on the Fermi golden rule applied to the case of a semiconductor electrode in contact with a random distribution of acceptor species in solution, has produced the following expression for the electron-transfer rate constant at a semiconductor/liquid interface:[26]

$$k_{et} = \frac{4\pi^2}{h}\frac{1}{(4\pi\lambda_{sc}k_BT)^{1/2}}\left\{\overline{H^2_{AB,sc}}\right\}\left\{\beta_{sc}^{-1}\right\}\left\{\frac{l_{sc}}{d_{sc}^{2/3}(6/\pi)^{1/3}}\right\}e^{\frac{-[(\overbrace{E_{CB}-qE^{o'}}^{\Delta G^{0'}})+\lambda_{sc}]^2}{(4\lambda_{sc}k_BT)}} \qquad (12)$$

where β_{sc} is the attenuation factor of the electronic coupling between the semiconductor and the redox species in the electrolyte, l_{sc} is the effective coupling length in the semiconductor, and d_{sc} is the atomic density of the solid. The quantity $\overline{H^2_{AB,sc}}$ represents the square of the matrix element that couples reactant and product states at energy **E**, averaged over all degenerate states in the semiconductor in a plane parallel to the electrode surface. This value is assumed to be independent of energy over the range of interest.[26] The interfacial free energy for charge transfer under standard conditions, $\Delta G^{o\prime}$, is computed by subtracting $qE^{o\prime}(A/A^-)$ from $\mathbf{E}_{cb}$. The subscript "sc" indicates parameters for a semiconductor electrode. Eq (12) can be rewritten as

$$k_{et} = k_{et,max}e^{\frac{-(\Delta G^{o\prime}+\lambda_{sc})^2}{4\lambda_{sc}k_BT}} \qquad (13)$$

where the prefactor has been combined into $k_{et,max}$, the rate constant at optimum exoergicity, obtained when $-\Delta G^{o\prime} = \lambda_{sc}$, with $k_{et,max} \approx 10^{-17}$ - 10^{-16} cm^4 s^{-1}.[3,8,26] The value of $k_{et,max}$ is expected to be a weak function of the reorganization energy ($k_{et,max} \propto \lambda_{sc}^{-1/2}$) for non-adiabatic reactions and is independent of λ for adiabatic reactions. Any

dependence of $k_{et,max}$ on $\lambda_{sc}^{-1/2}$ is therefore too small to be observed reliably in our experiments, and is not included in this expression. Because all of the compounds are coupling to the same electrode, the electronic coupling coefficient, H_{AB}, for the interfacial electron-transfer reactions is likely to be similar for the various redox species of concern.

The expression for k_{et} in eq (13) can conveniently be written as

$$\ln k_{et} = \ln k_{et,max} - \frac{(\Delta G^{o}{}' + \lambda_{sc})^2}{4\lambda_{sc} k_B T} \qquad (14)$$

As shown in Figure 2.3, a plot of ln k_{et} vs. $\frac{(\Delta G^{o}{}' + \lambda_{sc})^2}{4\lambda_{sc} k_B T}$ is linear, with a linear least-squares fit yielding a slope of -0.94 and an intercept of -38. The slope of -0.94 indicates adherence of the data to the Marcus model's prediction of the dependence of the interfacial electron-transfer rate constants on the reorganization energy and driving force of the reaction. A value for $k_{et,max}$ can be derived from the intercept, yielding $k_{et,max} = 3 \times 10^{-17}$ cm^4 s^{-1}. This result is in reasonable agreement with the value of $k_{et} = 6 \times 10^{-17}$ cm^4 s^{-1} for $Os(Me_2bpy)_2(Im)_2^{3+/2+}$, which is essentially at maximal exoergicity, and with the theoretically predicted and experimentally determined value of $k_{et,max} = 10^{-17}$ - 10^{-16} cm^4 s^{-1}.[3,8,26] Although both the $\Delta G°'$ and λ_{sc} terms are included in eq (14) and Figure 2.3, for the redox couples investigated in this work $\Delta G°'$ only varies by 0.1 eV while λ_{sc} varies by 1.0 eV. Prior work on ZnO electrodes has clearly elucidated the dependence of k_{et} on driving force at essentially constant reorganization energy of the redox species,[3] and the results described herein indicate satisfying agreement between theory and experiment for the dependence of k_{et} on the reorganization energy of the redox species involved in the interfacial charge-transfer process.

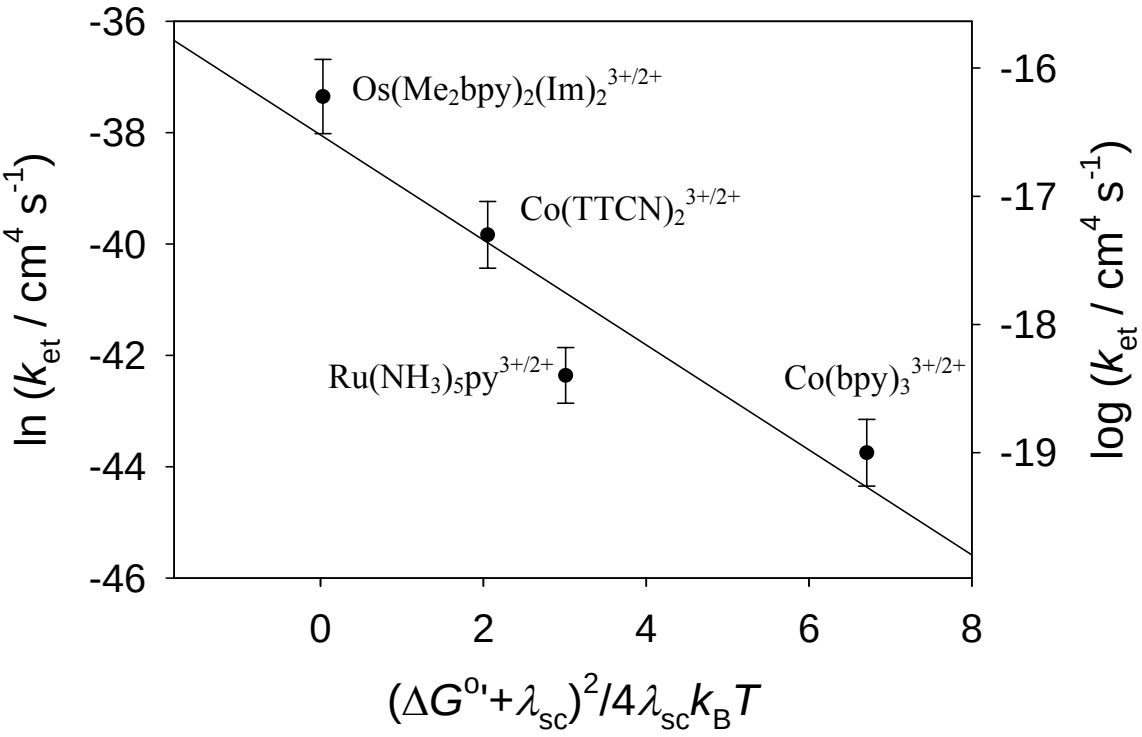

Figure 2.3 Plot of ln k_{et} as a function of the quantity $\frac{(\Delta G^{o\prime}+\lambda_{sc})^2}{4\lambda_{sc}k_BT}$ for the redox systems investigated. The solid line represents a linear least-squares fit of the data.

Another method to compare the data with Marcus theory is to calculate the interfacial rate constant expected at a given driving force and reorganization energy, assuming $k_{et,max} = 5 \times 10^{-17}$ cm^4 s^{-1}, according to eq (13). Values of the calculated rate constants, k_{et}^{calc}, corresponding to the $\Delta G^{o'}$ and λ_{sc} for each of the contacts in this study are given in Table 2.2. The calculated rate constant is within the error of values determined for k_{et} for the complexes $Co(bpy)_3^{3+/2+}$, $Os(Me_2bpy)_2(Im)_2^{3+/2+}$, and $Co(TTCN)_2^{3+/2+}$ and is approximately a factor of 6 larger than the measured k_{et} value for $Ru(NH_3)_5py^{3+/2+}$. In general, the agreement between theory and experiment within an order of magnitude is considered good, and in this context the agreement observed herein is excellent.

2.4 CONCLUSIONS

The ZnO/H_2O junctions displayed nearly ideal energetic and kinetics behavior in contact with different redox couples. Current density vs. potential measurements displayed a first-order dependence on the acceptor and surface electron concentrations. This behavior allowed for the straightforward experimental determination of the interfacial electron-transfer rate constants for such systems. The reorganization energy of the redox couples varied by approximately 1 eV, and resulted in a change in k_{et} by a factor of 600. The data are thus in excellent agreement with the reorganization energy dependence of interfacial electron-transfer reactions predicted by the Marcus model of interfacial electron transfer at semiconductor electrode surfaces.

3.5 ACKNOWLEDGMENTS

We acknowledge the Department of Energy, Office of Basic Energy Sciences, for support of this work.

3.6 REFERENCES

(1) Lewis, N. S. *J. Phys. Chem. B* **1998**, *102*, 4843-4850.

(2) Lewis, N. S. *Ann. Rev. Phys. Chem.* **1991**, *42*, 543-580.

(3) Hamann, T.; Gstrein, F.; Brunschwig, B. S.; Lewis, N. S. *J. Am. Chem. Soc.* **2005**, *127*, 7815-7824.

(4) Marcus, R. A. *Ann. Rev. Phys. Chem.* **1964**, *15*, 155-196.

(5) Pomykal, K. E.; Fajardo, A. M.; Lewis, N. S. *J. Phys. Chem.* **1995**, *99*, 8302-8310.

(6) Lavallee, D. K.; Lavallee, C.; Sullivan, J. C.; Deutsch, E. *Inorg. Chem.* **1973**, *12*, 570-574.

(7) Setzer, W. N.; Ogle, C. A.; Wilson, G. S.; Glass, R. S. *Inorg. Chem.* **1983**, *22*, 266-271.

(8) Fajardo, A. M.; Lewis, N. S. *J. Phys. Chem. B* **1997**, *101*, 11136-11151.

(9) Morrison, S. R. *Electrochemistry at Semiconductor and Oxidized Metal Electrodes*; Plenum: New York, 1980.

(10) Bhargava, R. *Properties of Wide Bandgap II-VI Semiconductors*; Inspec: London, 1997; Vol. Series No. 17.

(11) Sze, S. M. *The Physics of Semiconductor Devices*; 2nd ed.; Wiley: New York, 1981.

(12) Dewald, J. F. *J. Phys. Chem. Solids* **1960**, *14*, 155-161.

(13) Lohmann, F. *Ber. Bunsenges. Phys. Chem.* **1966**, *70*, 428-434.

(14) Marcus, R. A.; Sutin, N. *Biochem. Biophys. Acta* **1985**, *811*, 265-322.

(15) Meyer, T. J.; Taube, H. In *Comprehensive Coordination Chemistry*; Wilkinson, S. G., Gilliard, R. D., McCleverty, J. A., Eds.; Pergamon Press: New York, 1987; Vol. 1, p 331.

(16) Sutin, N. *Acc. Chem. Res.* **1982**, *15*, 275-282.

(17) Sutin, N. *Prog. Inorg. Chem.* **1983**, *30*, 441-498.

(18) Brunschwig, B. S.; Logan, J.; Newton, M. D.; Sutin, N. *J. Am. Chem. Soc.* **1980**, *102*, 5798-5809.

(19) Lide, D. R., Ed. *CRC Handbook of Chemistry and Physics*; 81 ed.; CRC Press, 2001.

(20) Biner, M.; Burgi, H. B.; Ludi, A.; Rohr, C. *J. Am. Chem. Soc.* **1992**, *114*, 5197-5203.

(21) Marcus, R. A. *J. Phys. Chem.* **1963**, *67*, 853-857.

(22) Marcus, R. A. *J. Phys. Chem.* **1990**, *94*, 1050-1055.

(23) Marcus, R. A. *J. Phys. Chem.* **1990**, *94*, 4152-4155.

(24) Kuciauskas, D.; Freund, M. S.; Gray, H. B.; Winkler, J. R.; Lewis, N. S. *J. Phys. Chem. B* **2001**, *105*, 392-403.

(25) Ashkenov, N.; Mbenkum, B. N.; Bundesmann, C.; Riede, V.; Lorenz, M.; Spemann, D.; Kaidashev, E. M.; Kasic, A.; Schubert, M.; Grundmann, M.;

Wagner, G.; Neumann, H.; Darakchieva, V.; Arwin, H.; Monemar, B. *J. Appl. Phys.* **2003**, *93*, 126-133.

(26) Royea, W. J.; Fajardo, A. M.; Lewis, N. S. *J. Phys. Chem. B* **1997**, *101*, 11152-11159.

CHAPTER 3

Measurement of the Driving Force Dependence of Interfacial Charge-Transfer Rate Constants in Response to pH Changes at n-ZnO/H_2O Interfaces

3.1 INTRODUCTION

A. Background

One of the most interesting predictions of the electron-transfer theory developed by Hush[1] and Marcus[2] is that of the inverted region, in which an increase in driving force produces a decrease in the electron-transfer rate constant. The inverted region has been observed experimentally for both intermolecular and intramolecular donor-acceptor (D-A) systems.[3-5] For electrochemical systems, the electron-transfer rate constant from an individual electronic level in an electrode should show both normal and inverted region behavior, in close analogy to the behavior of molecular D-A systems. However, the observed rate of electron transfer from a metal electrode to an acceptor in solution is a summation of the individual electron-transfer rates from the collection of closely spaced occupied electronic levels in the metal. The observed interfacial current will therefore be dominated by the electronic states that transfer electrons at optimum exoergicity, so for metal electrodes the total rate will not decrease with driving force, and the inverted region cannot be directly observed.[6,7]

In contrast to metal electrodes, semiconductor electrodes are well-suited to address some of the fundamental predictions of interfacial electron-transfer theories.[8] An ideal semiconductor has no electronic levels in the band gap region, so only electrons with energies near the conduction band, for an n-type material, can contribute to the cathodic interfacial current flow. As is the case for a molecular D-A system, the interfacial electron-transfer rate constant of conduction-band electrons to an acceptor in

solution should therefore increase, reach a maximal value, and then decrease as the driving force of the interfacial charge-transfer reaction is increased.

Unlike a metal electrode, the driving force at a semiconductor electrode cannot be changed by varying the potential of the electrode. This situation occurs because the differential capacitance of a non-degenerately-doped semiconductor electrode is much smaller than the differential capacitance of the electrolyte, so essentially all of the applied potential drops across the electrode and not the electrolyte. Hence, the only two methods of changing the driving force are to vary the energetics of the redox species in the solution or to vary the identity or chemical state of the semiconductor surface.

Comparisons of current vs. potential data for electron transfer from ZnO to deutero- vs. protio-thianthrene acceptors[9] as well as potential-step data for 9,10-diphenylanthracene and its cation radical at ZnO electrodes[10,11] have been cited as evidence for the inverted region of interfacial charge-transfer reactions. The charge-transfer kinetics have been measured for a series of redox species in contact with ZnO electrodes, and some of the systems, notably $Fe(CN)_6^{3-/4-}$, showed ideal behavior that allowed for the determination of interfacial electron-transfer rate constants.[12-15] Most of the simple metal-ion-based redox systems investigated, however, such as Ce^{4+} (in HNO_3 and H_2SO_4), $IrCl_6^{2-}$, V^{3+} (in HCl), and $Ag(NH_3)_2^{+}$, are known to adsorb onto hydroxylated surfaces or to involve inner-sphere electron-transfer pathways that precluded the analysis of the kinetics as a function of driving force.[15] Recently, the dependence of the interfacial charge-transfer rate constant, k_{et}, on the standard interfacial driving force for charge transfer, $-\Delta G^{o'}$, has been investigated using a homologous series of one-electron, outer-sphere redox systems at n-type ZnO electrodes.[16] Variation in the driving force by

> 1 eV through changes in the energetics of the acceptor species has yielded evidence for both the normal and inverted regions of interfacial electron transfer, with a maximum rate constant of approximately 10^{-16} cm^4 s^{-1} (ch 1).[16] Excellent agreement between theory and experiment has additionally been observed in response to a change in the reorganization energy of the redox species at nearly constant driving force (ch 2).[17]

The other method of changing the driving force is to hold the energetics of the redox couple constant and to change the chemical state of the semiconductor surface. A pH-dependent variation of the conduction band edge energy is expected for metal oxide electrodes due to the protonation/deprotonation equilibrium of –OH sites on the oxide surface.[15] Prior work on ZnO has, however, revealed an unexpected lack of sensitivity of the flat-band potential to variation of the solution pH.[18] Various other complications of the systems investigated thwarted a full analysis of the interfacial kinetics within the framework of the ideal model of electron transfer at a semiconductor electrode. In a separate study, Hupp and co-workers observed that the rate constant for recombination between absorbed $[Ru(bpy)_3]^{3+}$ (bpy = 2,2'-bipyridyl) and electrons photoinjected into nanocrystalline TiO_2 was independent of pH over a variation of 14 pH units.[19,20]

In this work, we have evaluated the pH dependence of the rate constants for interfacial charge transfer at single crystal ZnO electrodes in contact with the dissolved, outer-sphere redox species $[Co(bpy)_3]^{3+/2+}$ and $[Ru(bpy)_2(MeIm)_2]^{3+/2+}$ (where MeIm = 1-methyl imidazole). For a series of one-electron outer-sphere redox species, n-type, (0001)-oriented ZnO electrodes have been shown to exhibit charge-transfer rates that are first-order in the concentration of electrons at the semiconductor surface and first-order in redox acceptor species in the electrolyte solution.[16,17] The pH-dependent shift in the

band-edge positions of ZnO and other metal oxides is well-known,[15,21] and therefore should afford a method to investigate the driving force dependence of the rate constant to a given redox species. The redox couples $[Co(bpy)_3]^{3+/2+}$ and $[Ru(bpy)_2(MeIm)_2]^{3+/2+}$ are of specific interest because prior measurements of the band-edge positions at n-type ZnO electrodes indicate that $[Co(bpy)_3]^{3+/2+}$ should be in the normal region, whereas $[Ru(bpy)_2(MeIm)_2]^{3+/2+}$ should be in the inverted region.[6] The charge-transfer rate constant for $[Co(bpy)_3]^{3+/2+}$ is therefore expected to increase, while the rate constant for $[Ru(bpy)_2(MeIm)_2]^{3+/2+}$ is expected to decrease, as the band-edge position is made more negative, and therefore the interfacial driving force is increased, by increasing the pH of the solution.[16,17]

B. Rate Laws and Models for Charge-Transfer Processes

The flat-band potential, E_{fb}, in the absence of an electric field in a semiconductor is related to the Fermi level of the semiconductor, $\mathbf{E}_F$, by $\mathbf{E}_f = qE_{fb}$, where q is the charge of an electron. The difference between $\mathbf{E}_f$ and the energy of the bottom of the conduction band, $\mathbf{E}_{cb}$, in the bulk of the semiconductor is

$$\mathbf{E}_f - \mathbf{E}_{cb} = -qV_n = k_B T \ln\left(N_c / N_d\right) \quad (1)$$

where N_d is the doping density, N_c is the effective density of states in the conduction band of the solid, k_B is Boltzmann's constant, T is the temperature, and the potential difference between the Fermi level and the conduction band is defined as $-V_n$.

When the n-type semiconductor is brought into contact with a liquid containing a redox couple having an electrochemical potential $qE(A/A^-)$, where $E(A/A^-)$ is the Nernstian potential of the redox couple consisting of the acceptor, A, and the donor, A^-, charge will flow between the semiconductor and the solution (as depicted in Scheme 1a)

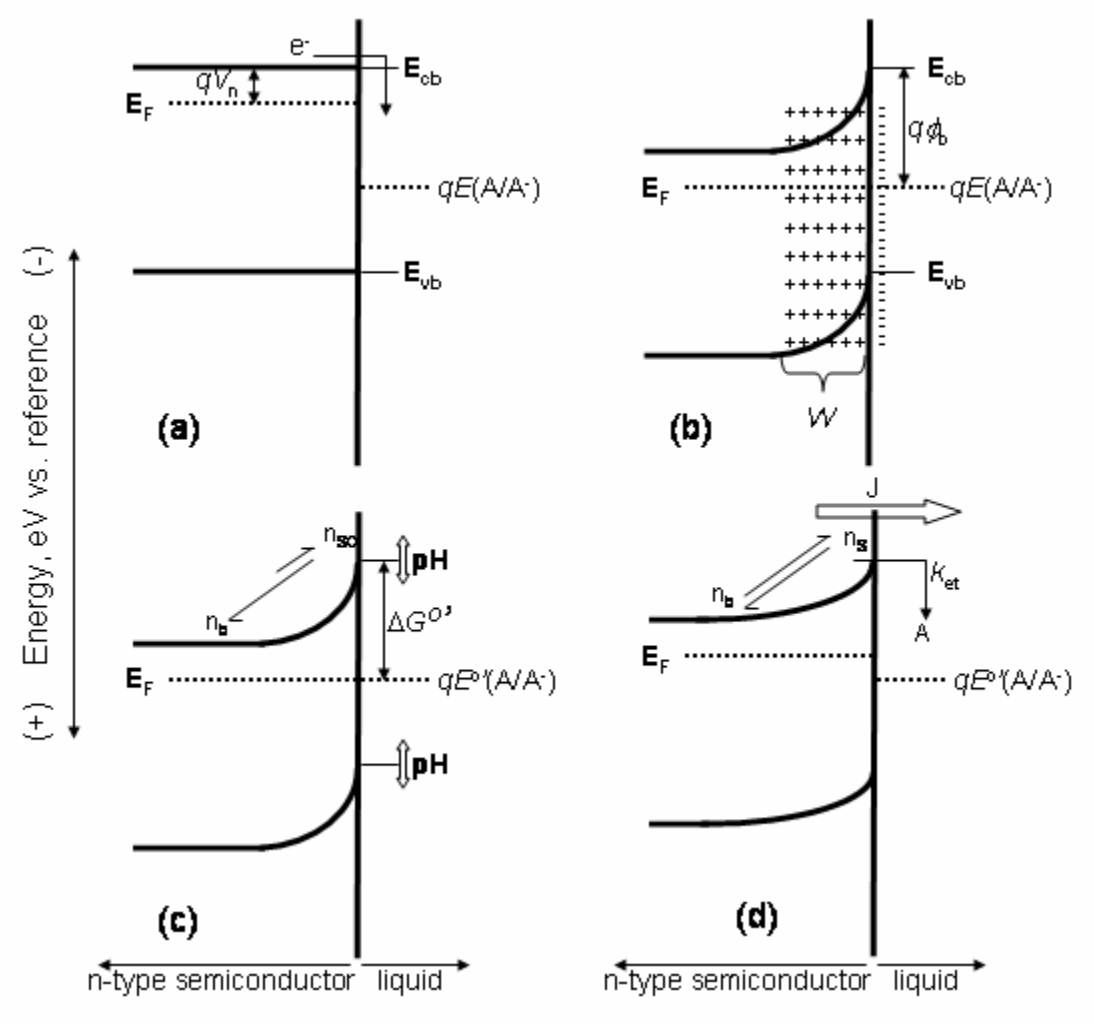

Scheme 3.1 Energy vs. distance for an n-type semiconductor in contact with a redox species (A/A^-). (a-b) Equilibration of the semiconductor Fermi level, $\mathbf{E}_F$, with the solution Nernstian potential, $E(A/A^-)$, results in a space-charge region with width W, which produces a spatially dependent electric potential drop in the solid. (c) The value of $\Delta G^{o'}$, the standard free energy change for interfacial charge transfer, is given by $\Delta G^{o'} = \mathbf{E}_{cb} - qE^{o'}(A/A^-)$, where $E^{o'}(A/A^-)$ is the formal reduction potential of the (A/A^-) redox system. The surface and bulk electron concentrations are denoted as n_s and n_b, respectively. At equilibrium, the electode potential, E, is such that the Fermi level of the semiconductor, $\mathbf{E}_F$, equals $qE(A/A^-)$, and $n_s = n_{so}$, where n_{so} is the surface electron concentration at equilibrium of the solid/liquid interface. (d) If a potential is applied such that the junction is biased away from equilibrium, n_s is not equal to n_{so}, and a non-zero net current, J, flows across the semiconductor/liquid interface.

until equilibrium is established. The value of $\mathbf{E}_F$ in the semiconductor will change much more than the value $qE(A/A^-)$ because for even a dilute concentration of redox species, the solution has far more states per unit energy than the semiconductor in its band gap region. As a consequence of this interfacial charge flow, at equilibrium (Scheme 1b) the semiconductor has excess positive charge, arising from the ionized dopant atoms in the semiconductor, and the solution has excess negative charge. The positive charge is spread out over the depletion width, W,[22] while the negative charge is spread over a much narrower region close to the electrode.

The energy barrier that must be surmounted to transfer charge from solution to the semiconductor, the barrier height, $q\phi_b$, is equal to the difference between $qE(A/A^-)$ and the energy of the bottom of the conduction band edge at the semiconductor surface, $\mathbf{E}_{cb}$.[22] Since E_{fb} is an experimentally measurable quantity, the value of $\mathbf{E}_{cb}$ can thus be deduced by adding qV_n to qE_{fb} and referencing the value to $E(A/A^-)$:

$$q\phi_b = qE\left(A/A^-\right) - qE_{fb} - qV_n \tag{2}$$

When $E(A/A^-)$ is equal to the formal potential of the redox system, $E^{o\prime}(A/A^-)$, the value of $-q\phi_b$ is equal to the standard free energy change for the interfacial electron transfer process, $\Delta G^{o\prime}$. Hence, $\Delta G^{o\prime}$ is

$$-\Delta G^{\circ\prime} = qE^{\circ\prime}\left(A/A^-\right) - qE_{fb} - k_B T \ln\left(N_d / N_c\right) \tag{3}$$

with $N_c = 3.5 \times 10^{18}$ cm^{-3} for ZnO.[23]

The electron concentration at the surface of the semiconductor, n_s, is related to the difference between the potential applied to the electrode, E, and E_{fb} through a Boltzmann-type relationship:[12,24]

$$n_s = N_d e^{\frac{q(E_{fb} - E)}{k_B T}} \quad (4)$$

with n_{so} defined as the value of n_s at $E = E(A/A^-)$. At forward bias, n_s increases exponentially with $-E$, which results in a net current across the semiconductor/liquid interface. The net flux of electrons from the conduction band to randomly dissolved acceptors in solution is given by the rate law[15]

$$J(E) = -qk_{et}[A]n_s \quad (5)$$

where J is the current density (A cm^{-2}), k_{et} is the electron-transfer rate constant (cm^4 s^{-1}), and $[A]$ is the acceptor concentration (cm^{-3}). Unlike the case for metallic electrodes, the surface electron concentration is explicit in the rate law for electron transfer at semiconductor electrodes, yielding a second-order rate expression. Hence, application of a potential to an ideally behaving semiconductor electrode interface effects a change in the observed current density (i.e., the charge-transfer rate) by changing the value of the electron concentration at the surface of the solid, as opposed to changing the rate constant, or the energetics, of the interfacial charge-transfer process.

If J is shown to follow eq (5), with knowledge of n_s and $[A]$, the value of k_{et} can be calculated from the observed steady-state J vs. E data. Unlike the situation for metallic electrodes, the relatively small, and controllable, value of the electron concentration at the semiconductor surface affords the ability to avoid redox coupled mass-transport limitations on the charge-transfer flux even for reactions at optimal exoergicity. Hence, rate measurements at semiconductor electrodes can be performed using simple steady-state methods with dissolved redox species, even for relatively large values of the interfacial charge-transfer rate constant.

If $E^{o'}(A/A^-)$ is independent of pH, $\Delta G^{o'}$ can be varied with pH due to the dependence of E_{fb} (eq 3), and therefore $\mathbf{E}_{cb}$, on a change in pH, ΔpH (Scheme 1c):[15]

$$\Delta\mathbf{E}_{cb} = -(2.3k_BT)\Delta(pH); \qquad \Delta E_{fb} = -(2.3k_BT)\Delta(pH) \tag{6}$$

3.2 EXPERIMENTAL

A. Electrodes

The preparation of the ZnO electrodes has been described previously.[16] Electrochemical experiments reported in this work were confined to the Zn-rich (0001)-oriented surface. The electrodes used in this work were prepared from three separate ZnO single crystals having varying dopant densities. Due to the limited number of high-quality ZnO single crystals available, a statistical approach to the assessment of random errors over several electrodes was not feasible, but at least three different electrodes showed the same trends as those reported herein.

B. Electrolyte Solutions

Electrochemical experiments were carried out in a 50 mM imidazole (pH 6-8) or phthalate (pH 4-6) buffer. The pH was adjusted by addition of KOH or HCl and the pH was measured using a VWR Scientific model 8010 pH meter. The ionic strength, *I*, was adjusted to 1 M by addition of KCl (Aldrich, 99+%) to provide the supporting electrolyte for the electrochemical measurements.

C. Redox Compounds

The preparation of $[Co(bpy)_3]Cl_2$ has been described previously.[17] $[Ru(bpy)_2(MeIm)_2]Cl_2$ was prepared by a modified literature procedure, as follows.[25]

Excess 1-methyl imidazole (MeIm, Aldrich, 1 mL) was added to $Ru(bpy)_2Cl_2$ (Aldrich, 500 mg) that had been dissolved in 50 mL of a 1:1 (vol) methanol/water mixture. The solution was refluxed under Ar for 3 hr. After cooling to room temperature, NH_4PF_6 was added to the solution and the dark red precipitate was filtered. The precipitate was recrystalized from acetone by the slow addition of diethyl ether. The product, $[Ru(bpy)_2(MeIm)_2](PF_6)_2$, was then filtered and dried under vacuum. Elemental analysis yielded (calculated): C 38.64 (38.76), H 3.51(3.25), N 12.58 (12.92). The compound was converted to the chloride salt by dissolving in acetone followed by the addition, while stirring, of a concentrated solution of tetra(n-butyl)ammonium chloride (TBACl, Aldrich) in acetone. All solvents were reagent grade and were used as received.

D. Electrochemical Measurements

Details of the electrochemical experiments have been described previously.[16] The formal reduction potentials, $E^{o\prime}(A/A^-)$, were determined in each electrolyte solution using cyclic voltammetry employing a glassy carbon electrode as the working electrode, a platinum mesh counter electrode, and a saturated calomel electrode, SCE, in a separate cell, as the reference electrode. Scans were taken from -0.4 V to 1.0 V vs. SCE at a scan rate of 50-75 mV s^{-1}. An error of ± 5 mV was estimated for $E^{o\prime}(A/A^-)$ of each redox couple, as determined from the cyclic voltammetry data.

All solutions were aerated with Ar prior to measurement. Measurements of k_{et} for $[Co(bpy)_3]^{3+/2+}$ were performed at room temperature. To minimize any deleterious side reactions, measurements with $[Ru(bpy)_2(MeIm)_2]^{3+/2+}$ were carried out in an ice bath at ≈ 3 ºC. The oxidized, acceptor form, A, of each compound was created in situ via bulk electrolysis using a carbon mesh working electrode. The acceptor concentration was

determined from the number of coulombs passed (for $[Co(bpy)_3]^{3+/2+}$, $[A]_{low}$ = 1 mM, $[A]_{high}$ = 10 mM and for $[Ru(bpy)_2(MeIm)_2]^{3+/2+}$, $[A]_{low}$ = 0.5 mM, $[A]_{high}$ = 5 mM); a 5% error in [*A*] was estimated. The variation in [*A*] was verified by monitoring the cell potential, $E(A/A^-)$, and by measuring the limiting cathodic current densities at both acceptor concentrations, $J_{l,c,high}$ and $J_{l,c,low}$. All potentials are referenced to SCE.

The data for the lowest barrier height system, $[Co(bpy)_3]^{3+/2+}$ at pH 4, were corrected for the concentration overpotential, η_{conc}.[26] The value of η_{conc} was calculated according to eqs (7) and (8):

$$\eta_{conc} = \left(\frac{k_B T}{nq}\right)\left\{\ln\left(\frac{J_{l,a}}{-J_{l,c}}\right) - \ln\left(\frac{J_{l,a} - J}{J - J_{l,c}}\right)\right\} \tag{7}$$

$$E_{corr} = E - \eta_{conc} \tag{8}$$

where $J_{l,c}$ and $J_{l,a}$, are the mass-transport-limited cathodic and anodic current densities, respectively, that were measured with a one-sided Pt-foil electrode of known area.

3.3 RESULTS AND DISCUSSION

A. Differential Capacitance vs. Applied Potential Measurements

For all electrodes reported herein, Bode plots of the impedance magnitude, |Z|, vs. ac signal frequency, *f*, were linear over at least two orders of magnitude variation in *f*, with slopes of ≈ -1. In addition, the phase angles of the current vs. ac voltage of ≈ -90° indicated that the impedance of these systems was dominated by a single capacitive circuit element, with $Z_{im} \approx (2\pi f C_{diff})^{-1}$.[27] To deduce the space-charge capacitance at the ZnO electrode, the impedance spectra were fitted over the frequency range 10 to 10^3 Hz

or 10^2 to 10^4 Hz to an equivalent circuit that consisted of the cell resistance, R_s, in series with two parallel components: the resistance to charge transfer, R_{sc}, and the space-charge capacitance, C_{sc}. No frequency dependence of the capacitance was observed, resulting in very small errors (<1 %) for each fit. Because C_{sc} is much less than the differential capacitance of either the Helmholtz layer or the double layer, the measured differential capacitance, C_{diff}, was set equal to C_{sc}.[27] A linear regression was used to fit the A_s^2/C_{sc}^2 vs. E data in accordance with the Mott-Schottky equation:[15]

$$\frac{A_s^2}{C_{sc}^2} = \frac{2}{q\varepsilon_{ZnO}\varepsilon_o N_d}\left(E - E_{fb} - \frac{k_B T}{q}\right) \tag{9}$$

where A_s is the surface area of the semiconductor electrode, ε_{ZnO} is the static dielectric constant of ZnO (8.65),[28] and ε_o is the permittivity of free space. Representative values of N_d and E_{fb} for electrodes prepared from three different ZnO crystals obtained from the slope, and from the x-intercept adjusted by k_BT/q, respectively, are given in Table 3.1.

The interfacial energetics were investigated at different pH values of the buffer solutions. The value of $-E_{fb}$, and therefore ϕ_B, of ZnO should shift by $2.3k_BT/q$ for a unit change in pH of the solution (eq (2)).[15,21] This allows for variation of the driving force of interfacial electron-transfer reactions without changing the redox couple of concern. Figure 3.1 shows plots of A_s^2/C_{sc}^2 vs. E data for a ZnO electrode (A_s = 0.145 cm^2) in contact with $[Co(bpy)_3]^{3+/2+}$ and $[Ru(bpy)_2(MeIm)_2]^{3+/2+}$ in pH 4 and pH 6 phthalate buffer solutions, respectively. The data were fitted in accordance with eq (9) with the constraint that the slope was fixed to be the same for the different systems, since the slope should be independent of pH. The standard errors resulting from the fits were used to calculate the errors in N_d and E_{fb}, producing values of $N_d = (2.0 \pm 0.1) \times 10^{15}$ cm^{-3}, E_{fb}

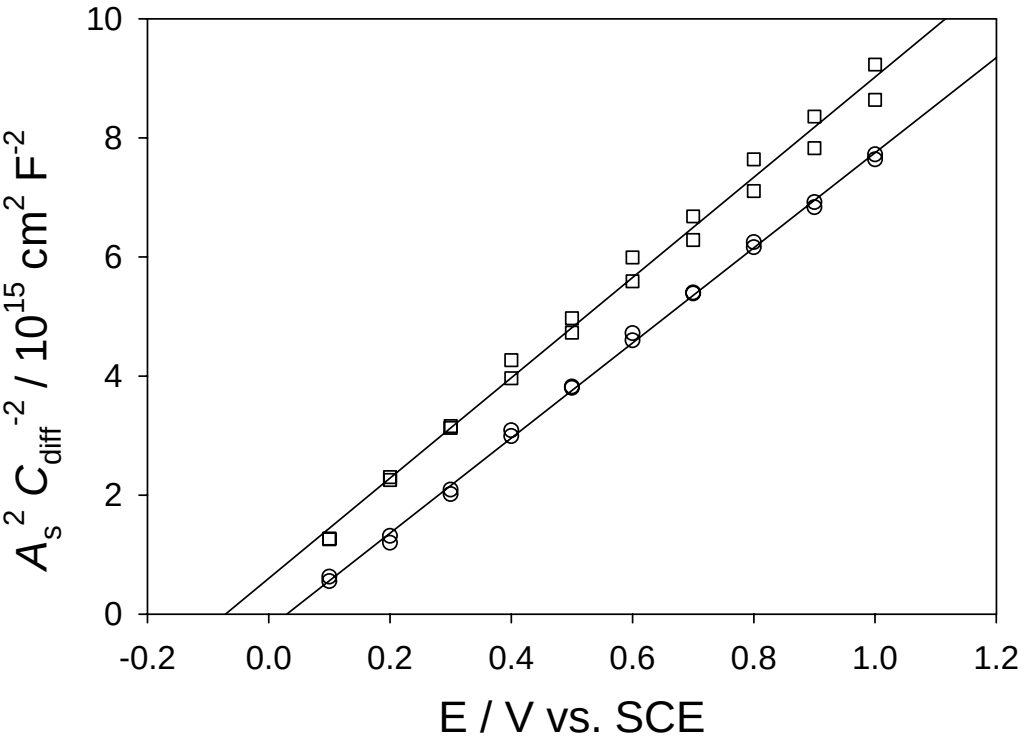

Figure 3.1 Mott-Schottky plots for ZnO in contact with $[Co(bpy)_3]^{3+/2+}$ and $[Ru(bpy)_2(MeIm)_2)]^{3+/2+}$ in pH 4 (circles) and pH 6 (squares) phthalate buffer solutions.

Table 3.1 Results of J vs. E and C_{diff} vs. E measurements of ZnO electrodes, and rate constant determinations. The quantity γ is the diode quality factor at the high acceptor concentration used in the calculation of k_{et}. As noted in the text, ΔE, the shift in potential to maintain a constant current density for a 10-fold increase in [A], should be approximately 59 mV for $[Co(bpy)_3]^{3+/2+}$ and 54 mV for $[Ru(bpy)_2(MeIm)_2]^{3+/2+}$. The superscripts [a-c] designate the ZnO crystal used for each measurement.

pH	Redox Couple	γ	ΔE (mV)	N_d (cm^{-3})	E_{fb} (V vs. SCE)	$\mathbf{E}_{cb}/q$ (V vs SCE)	$-\Delta G^{o'}$ (eV)	k_{et} ($cm^4\ s^{-1}$)
4 [a]	$Co(bpy)_3$	1.3	82	$(2.0 \pm 0.1) \times 10^{15}$	0.020 ± 0.008	-0.17	0.21	$(5 \pm 2) \times 10^{-22}$
6 [a]	$Co(bpy)_3$	1.1	62	$(2.0 \pm 0.1) \times 10^{15}$	-0.111 ± 0.008	-0.30	0.34	$(9 \pm 3) \times 10^{-21}$
6 [b]	$Co(bpy)_3$	1.2	75	$(8.9 \pm 0.5) \times 10^{14}$	-0.105 ± 0.009	-0.32	0.40	$(1.7 \pm 0.5) \times 10^{-20}$
8 [b]	$Co(bpy)_3$	1.2	70	$(8.9 \pm 0.5) \times 10^{14}$	-0.189 ± 0.009	-0.40	0.54	$(7 \pm 2) \times 10^{-20}$
4 [a]	$Ru(bpy)_2(MeIm)_2$	1.1	30	$(2.0 \pm 0.1) \times 10^{15}$	0.020 ± 0.008	-0.17	0.87	$(2.1 \pm 0.8) \times 10^{-18}$
6 [a]	$Ru(bpy)_2(MeIm)_2$	1.2	50	$(2.0 \pm 0.1) \times 10^{15}$	-0.111 ± 0.008	-0.30	1.01	$(8 \pm 3) \times 10^{-19}$
6 [c]	$Ru(bpy)_2(MeIm)_2$	1.0	30	$(4.3 \pm 0.2) \times 10^{16}$	-0.256 ± 0.006	-0.37	1.02	$(1.0 \pm 0.5) \times 10^{-18}$
8 [c]	$Ru(bpy)_2(MeIm)_2$	1.1	51	$(4.3 \pm 0.2) \times 10^{16}$	-0.393 ± 0.006	-0.51	1.10	$(3 \pm 1) \times 10^{-20}$

= 0.020 ± 0.008 V vs. SCE at pH 4 and E_{fb} = -0.111 ± 0.008 V vs. SCE at pH 6. The measured shift of E_{fb} was therefore -131 mV, in good agreement with the theoretical expectation of -118 mV for a 2 pH unit change at 25 ºC. Other electrodes exhibited behavior similar to those reported in Table 3.1.

The slope, and therefore N_d, remained essentially constant for all C_{diff}^{-2} vs. E measurements in the different buffer systems reported herein. This internal consistency between the various C_{diff}^{-2} vs. E measurements indicates that the driving force can be probed over 200 mV through shifts in the band edge position with a 4 pH unit variation, allowing investigation of interfacial reactions over a significant range of interfacial charge-transfer exoergicities.

Some unaccounted for discrepancy was observed in the measured values of E_{fb} and/or N_d for different electrodes. At a given pH, every electrode should have the same value of $\mathbf{E}_{cb}$, and therefore the same value of $\Delta G^{o\prime}$. The observed values, however, had variations in $\mathbf{E}_{cb}$ of up to 110 mV at a given pH for different electrodes (see Table 3.1). Errors of this magnitude in the absolute value of E_{fb} and N_d, however, do not significantly affect the interpretation of the results reported herein, as described in more detail below.

B. Current Density vs. Applied Potential Measurements

All of the junctions reported herein showed an asymptotically limiting anodic current density at positive potentials and an exponentially increasing cathodic current density at negative potentials, in accord with the diode equation:

$$J = -J_0\left(e^{\frac{-qE}{\gamma k_B T}} - 1\right) \tag{10}$$

where J_o is the exchange current density and γ is the diode quality factor. Figure 3.2 displays plots of ln (-J) vs. E in both pH = 4 and pH = 6 phthalate buffer solutions at two concentrations of either $[Co(bpy)_3]^{3+/2+}$ or $[Ru(bpy)_2(MeIm)_2]^{3+/2+}$. The diode quality factors were 1.1-1.4 at low concentrations of acceptor, indicating some relatively small but observable contribution from the presence of non-ideal recombination pathways. Large acceptor concentrations, however, favor direct electron transfer. Diode quality factors were generally 1.1-1.2 at high acceptor concentrations, in accord with the expectation of $\gamma = 1$ for a process that is kinetically first-order in the concentration of electrons at the surface of the semiconductor.

The dependence of the rate on the concentration of acceptor species in the solution was determined by increasing [A] by a factor of 10. If the rate law of eq (5) is obeyed, the 10-fold increase in [A] should shift the potential, ΔE, producing a given current density by the quantity $(k_B T/q)\ln(10)$. Thus, values of ΔE = 59 mV at room temperature ($[Co(bpy)_3]^{3+/2+}$) and ΔE = 54 mV at 3 ºC ($[Ru(bpy)_2(MeIm)_2]^{3+/2+}$) are expected. Values of γ and ΔE are given in Table 3.1 for the systems of interest in this work. The observed first-order dependences of J on n_s and of J on [A] validate the rate law of eq (5) and indicate that surface state effects do not dominate the charge-transfer processes of the systems investigated.[27]

C. Rate Constants for Interfacial Charge-Transfer, k_{et}

Because non-degenerately-doped semiconductor electrodes show relatively little Frumkin effect[26] associated with the liquid part of the solid/liquid double layer,[24] the acceptor concentration at the electrode can be assumed to be equal to the bulk value. The surface electron concentration at each applied potential, $n_s(E)$, was computed according

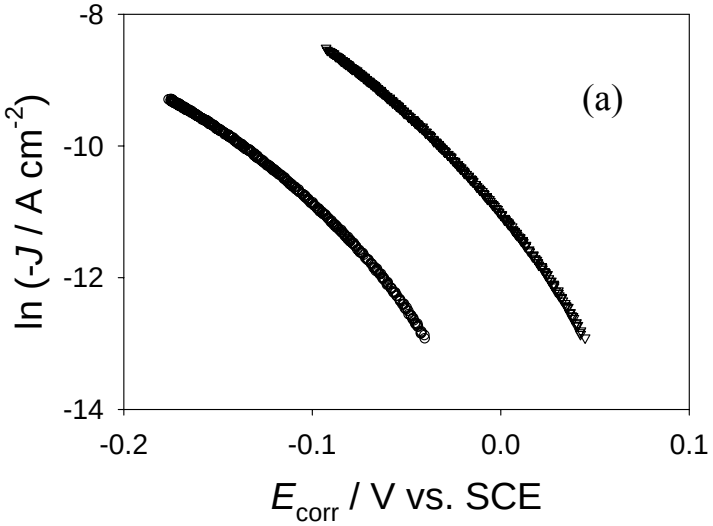
-8
-10
-12
-14
-0.2
-0.1
0.0
0.1
(a)
ln (-J / A cm-2)
Ecorr / V vs. SCE

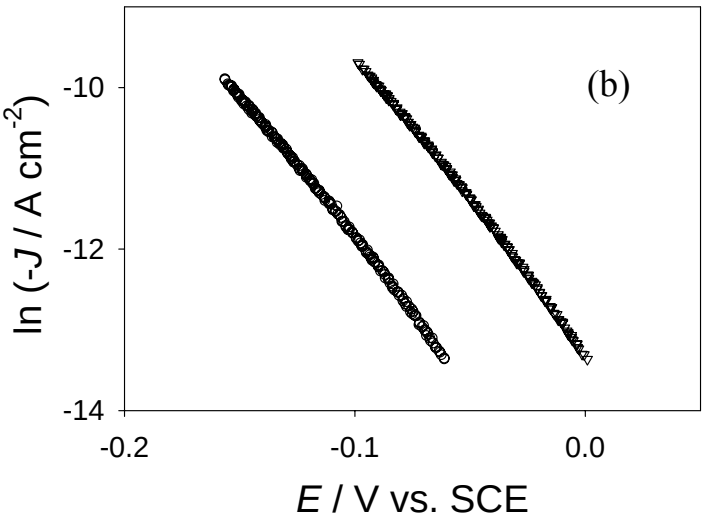
-10
-12
-14
-0.2
-0.1
0.0
(b)
ln (-J / A cm-2)
E / V vs. SCE

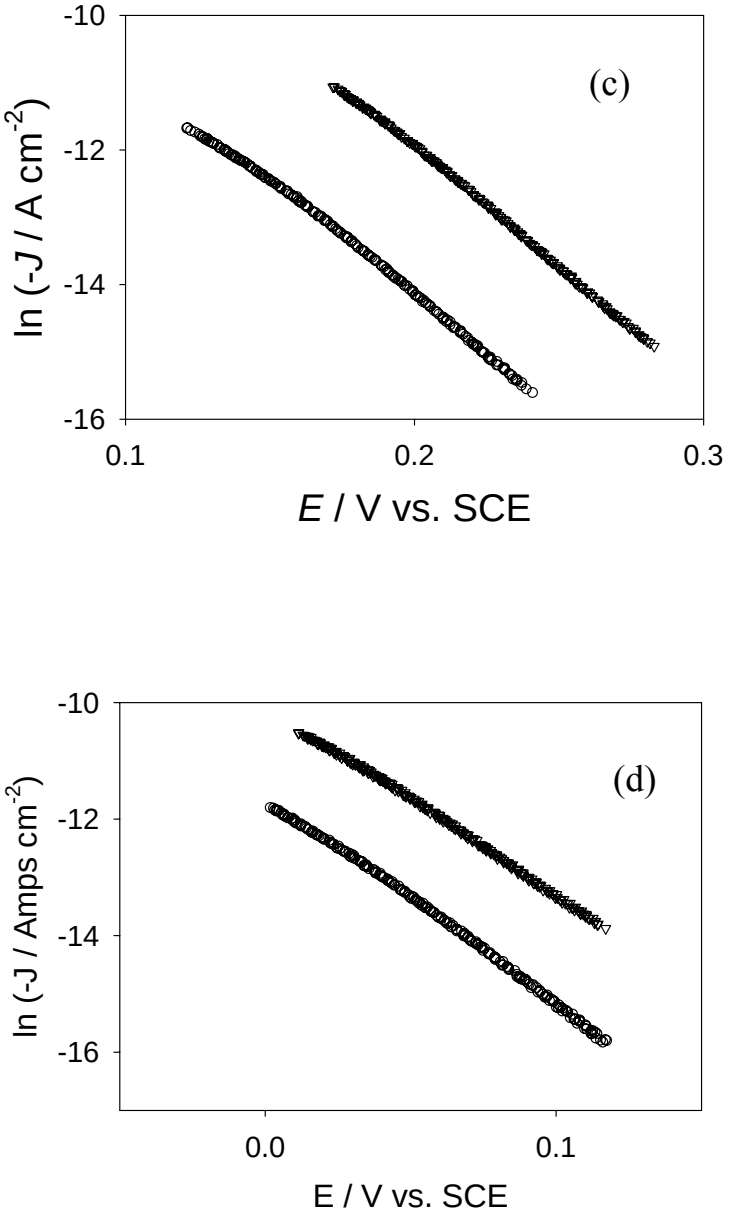

Figure 3.2 Logarithmic plots of dark current density vs. *E* for (a) $[Co(bpy)_3]^{3+/2+}$ in pH 4; (b) $[Co(bpy)_3]^{3+/2+}$ in pH 6; (c) $[Ru(bpy)_2(MeIm)_2)]^{3+/2+}$ in pH 4; and (d) $[Ru(bpy)_2(MeIm)_2)]^{3+/2+}$ in pH 6 phthalate buffer solutions at high (triangles) and low (circles) concentrations. As noted in the text, an increase in [*A*] should result in a shift of the *J*-*E* curve by approximately $\Delta E = 59$ mV for $[Co(bpy)_3]^{3+/2+}$ and $\Delta E = 54$ mV for $[Ru(bpy)_2(MeIm)_2]^{3+/2+}$. Potentials are referenced to SCE.

to eq (4) using the N_d and E_{fb} values extracted from the differential capacitance vs. applied potential measurements (eq (9)).

The value of k_{et} was calculated by dividing J by the quantity $\{-qn_s[A]\}$ at a given potential, in accord with the rate law of eq (5). The J vs. E data collected at the largest acceptor concentration were used to calculate k_{et} because direct electron transfer should be favored under this condition as indicated by the diode quality factors being closer to the ideal value of 1. The quoted k_{et} value for each contact represents the average of values calculated using potentials from the same high cathodic current density portion of the J vs. E curve ((-1 to -2) $\times 10^{-5}$ A cm^{-2}), and therefore includes any effects of the deviation of the diode quality factor from the ideal value of 1. A standard Gaussian error analysis was performed in conjunction with calculation of the rate constants by propagating the errors of all the measured parameters used in the calculation of k_{et}. The error in E_{fb} dominated the error in k_{et}, due to the exponential dependence of n_s on (E_{fb} - qE). Table 3.1 summarizes the values of k_{et} determined for representative ZnO/H_2O-redox couple junctions evaluated in this study.

D. Dependence of Interfacial Charge-Transfer Rate Constants on pH-Induced Changes in Driving Force: Comparison Between Theory and Experiment

A rapid method of evaluating the change in rate constant with a pH-induced change in driving force is to compare the shift in the J vs. E curves, ΔE_{pH}, with the shift in E_{fb}, ΔE_{fb}, as the pH is varied. An increase in pH of 1 unit should shift E_{fb} by -59 mV at 25 ºC (eq (8)). In turn, this shift should result in a 10-fold decrease in n_s (eq (4)) at a constant value of E, and therefore should produce a ΔE_{pH} = -59 mV shift in the potential required to produce a given current density. Any deviation from this expected shift of the

J vs. *E* curve with a change in pH can then be attributed to a change in the rate constant due to the pH change. At a constant current density, this change in rate constant can be described according to

$$\frac{k_{et}^{high}}{k_{et}^{low}} = e^{\frac{q}{k_B T}\left[\left(E_{fb}^{low} - E_{fb}^{high}\right) + \left(E^{high} - E^{low}\right)\right]} \tag{11}$$

where the superscripts high and low refer to higher and lower pH values respectively. Thus, when the *J* vs. *E* curve shifts negatively along the potential axis by less than $-\Delta E_{fb}$ (i.e., $-\Delta E_{pH} < -\Delta E_{fb}$) k_{et}^{high} is larger than k_{et}^{low} (normal region behavior), and when the *J* vs. *E* curve shifts negatively by more than $-\Delta E_{fb}$ (i.e., $-\Delta E_{pH} > -\Delta E_{fb}$), k_{et}^{high} is smaller than k_{et}^{low} (inverted region behavior).

Figure 3.3 displays *J* vs. *E* curves in pH 6 and pH 8 imidazole buffer solutions for $[Co(bpy)_3]^{3+/2+}$ with [*A*] = 10 mM and for $[Ru(bpy)_2(MeIm)_2]^{3+/2+}$ with [*A*] = 5 mM. The *J* vs. *E* curves for $[Co(bpy)_3]^{3+/2+}$ exhibited $-\Delta E_{pH}$ = 110 mV, less than the $-\Delta E_{fb}$ = 137 mV shift of E_{fb}, indicating that k_{et} is in the normal region. The *J* vs. *E* curves for $[Ru(bpy)_2(MeIm)_2]^{3+/2+}$ exhibited $-\Delta E_{pH}$ = 172 mV, more than the $-\Delta E_{fb}$ = 84 mV shift of E_{fb}, indicating that for this system k_{et} is in the inverted region. While the E_{fb} shifts deviated somewhat from the expected -118 mV shift at the temperature of the measurement, the trend of the *J* vs. *E* curves showing $-\Delta E_{pH} < -\Delta E_{fb}$ for $[Co(bpy)_3]^{3+/2+}$ and $-\Delta E_{pH} > -\Delta E_{fb}$ for $[Ru(bpy)_2(MeIm)_2]^{3+/2+}$ appears to be robust.

An expression for the rate constant of interfacial charge-transfer reactions for a semiconductor electrode in contact with a random distribution of acceptor species in solution is[29]

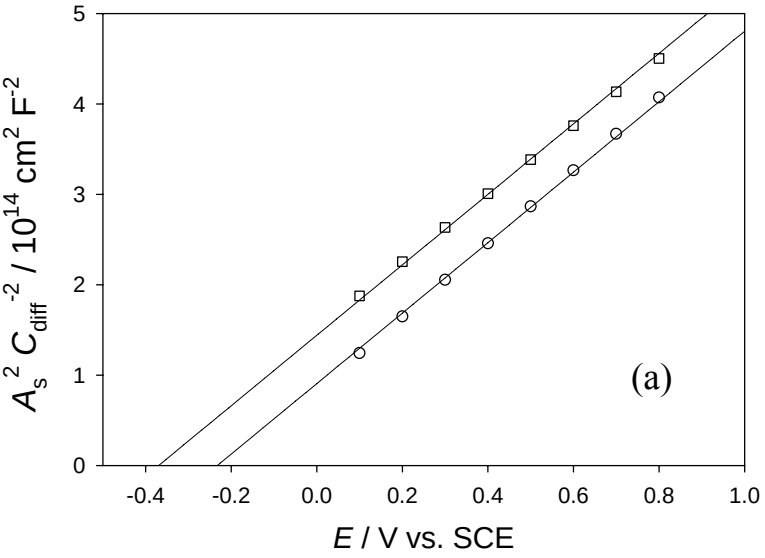
5
4
3
2
1
0
-0.4
-0.2
0.0
0.2
0.4
0.6
0.8
1.0
$A_s^2 C_{diff}^{-2}$ / 10^{14} cm^2 F^{-2}
(a)
E / V vs. SCE

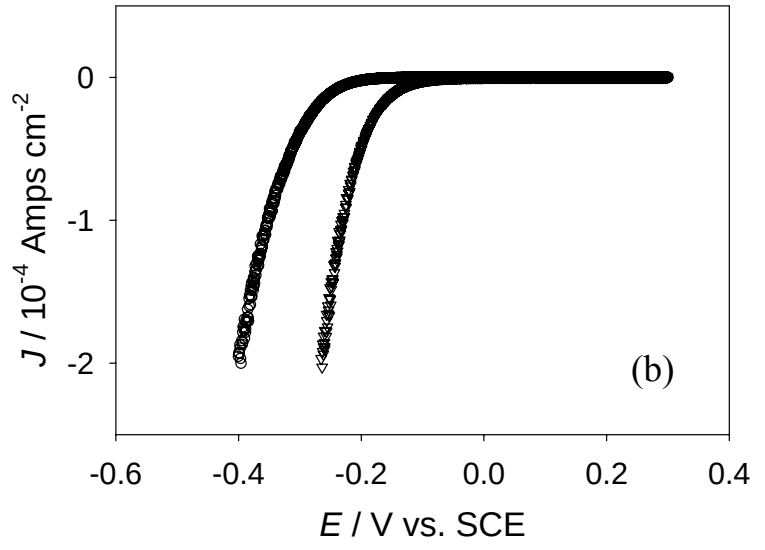
0
-1
-2
-0.6
-0.4
-0.2
0.0
0.2
0.4
J / 10^{-4} Amps cm^{-2}
(b)
E / V vs. SCE

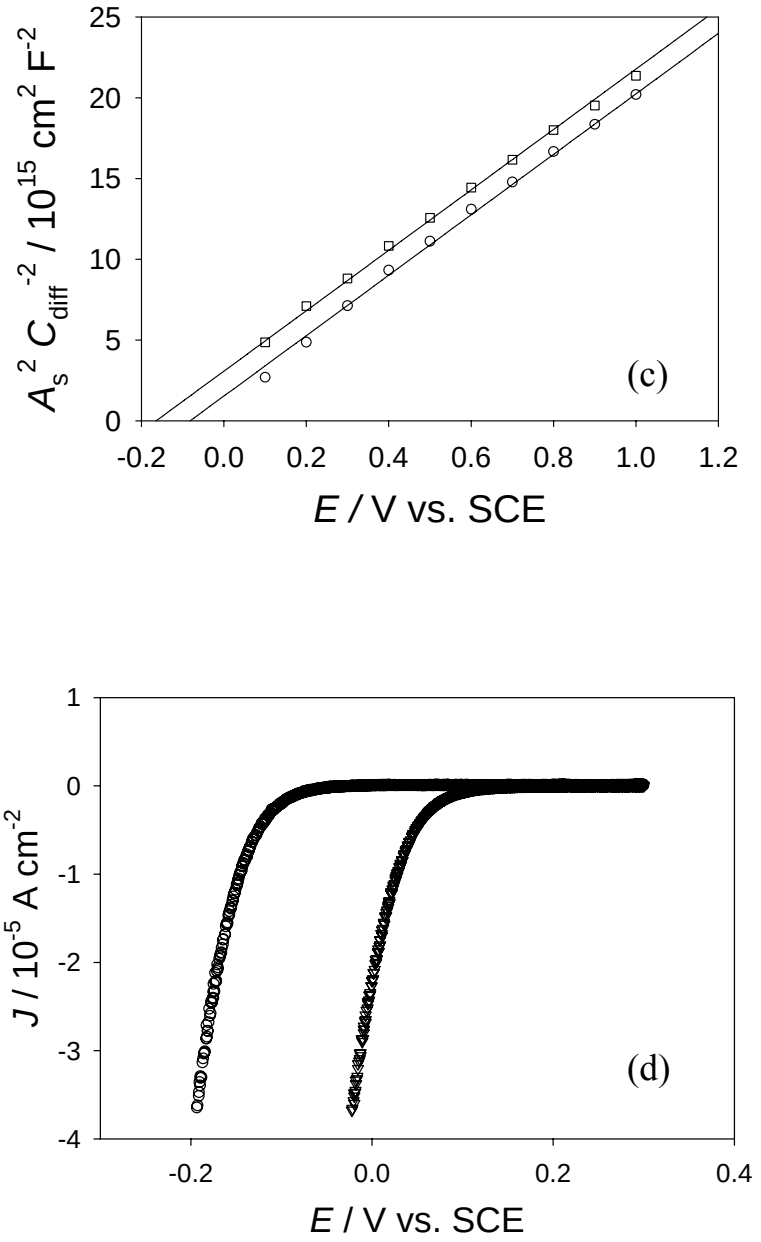

Figure 3.3 Mott-Schottky plots for ZnO in contact with (a) $[Co(bpy)_3]^{3+/2+}$ and (c) $[Ru(bpy)_2(MeIm)_2)]^{3+/2+}$ in pH 6 (circles) and pH 8 (squares) imidazole buffer solutions and *J* vs. *E* plots for (b) $[Co(bpy)_3]^{3+/2+}$ and (d) $[Ru(bpy)_2(MeIm)_2)]^{3+/2+}$ in pH 6 (triangles) and pH 8 (circles) imidazole buffer solutions.

$$k_{et} = k_{et,max} e^{\frac{-(\Delta G^{o'} + \lambda_{sc})^2}{4\lambda_{sc} k_B T}} \quad (12)$$

where λ_{sc} is the reorganization energy of the acceptor species near the semiconductor electrode. The prefactor, $k_{et,max}$, is the rate constant at optimum exoergicity, obtained when $-\Delta G^{o'} = \lambda_{sc}$, with $k_{et,max} \approx 10^{-17}$ - 10^{-16} cm^4 s^{-1}.[16,17,27,29] For a given redox couple, $k_{et,max}$ and λ_{sc} are constant at different values of the solution pH, so varying the driving force with pH offers a direct method to isolate the dependence of k_{et} on $\Delta G^{o'}$ (eqs (3), (6)). Values of $E^{o'}(A/A^-)$ for $[Co(bpy)_3]^{3+/2+}$ and $[Ru(bpy)_2(MeIm)_2]^{3+/2+}$ were determined to be 0.04 V and 0.72 V vs. SCE, respectively, and did not vary with the measurement conditions reported herein.

The value of the reorganization energy for an electron-transfer reaction between a redox couple and a ZnO electrode, where both the redox couple in solution and the image charge in the semiconductor contribute to the total reorganization energy, is expected to be smaller than or equal to that for the self-exchange reaction of the couple in homogeneous solution. A detailed analysis of $[Co(bpy)_3]^{3+/2+}$ has yielded a value of λ_{sc} = 1.5 eV at ZnO.[17] For Ru complexes that involve bipyridyl ligands, the inner-sphere does not undergo significant changes upon electron transfer.[30] The reorganization energy is therefore dominated by the solvent reorganization energy. A theoretical value for the outer-sphere reorganization energy of a redox couple at a ZnO electrode can be calculated by[31,32]

$$\lambda_{sc,out} = \frac{(\Delta z q)^2}{8\pi\varepsilon_0}\left[\frac{1}{a}\left(\frac{1}{n_{sol}^2} - \frac{1}{\varepsilon_{sol}}\right) - \frac{1}{2R_e}\left(\left(\frac{n_{ZnO}^2 - n_{sol}^2}{n_{ZnO}^2 + n_{sol}^2}\right)\frac{1}{n^2} - \left(\frac{\varepsilon_{ZnO} - \varepsilon_{sol}}{\varepsilon_{ZnO} + \varepsilon_{sol}}\right)\frac{1}{\varepsilon_{sol}}\right)\right] \quad (13)$$

where Δz is the difference in the charge of the ions, n_{ZnO} and n_{sol} are the refractive index of ZnO (1.9[28,33]) and the aqueous solution, respectively, ε_{ZnO} and ε_{sol} are the static dielectric constants of ZnO (8.65[28]) and the solution, respectively, and R_e is the distance from the acceptor to the electrode. Using a = 0.60 nm and R_e = 0.60 nm, as appropriate for $[Ru(bpy)_2(MeIm)_2]^{3+/2+}$, produces a value of λ_{sc} = 0.53 eV.

Figure 3.4 depicts a plot of k_{et} vs. $-\Delta G^{o'}$ for the rate constants reported above (Table 3.1). The k_{et} vs. $\Delta G^{o'}$ curves calculated according to eq (12) with $k_{et,max} = 5 \times 10^{-17}$ cm^4 s^{-1} and λ_{sc} = 1.5 eV (straight line) or λ_{sc} = 0.53 eV (dashed line) are superimposed on this plot. All data are in excellent agreement with theoretical predictions.

An uncertainty in the absolute value of E_{fb} would introduce a constant offset in the standard driving force, and resulting rate constants for all compounds, but such an error in E_{fb} and/or N_d would not change the observed trends for the redox systems investigated.

3.4 CONCLUSIONS

The ZnO/H_2O junctions displayed nearly ideal energetic and kinetics behavior in contact with $[Co(bpy)_3]^{3+/2+}$ and $[Ru(bpy)_2(MeIm)_2]^{3+/2+}$ in buffered aqueous solutions. Differential capacitance measurements showed that when the solution potential was changed by ≈ 700 mV, the band edges of ZnO were fixed to within 10 mV at a given pH with respect to SCE. The flat-band potential of the electrode was shown to vary with pH as expected, thereby allowing controlled variation of the driving force by approximately 200 mV for each redox couple. Current density vs. potential measurements displayed a

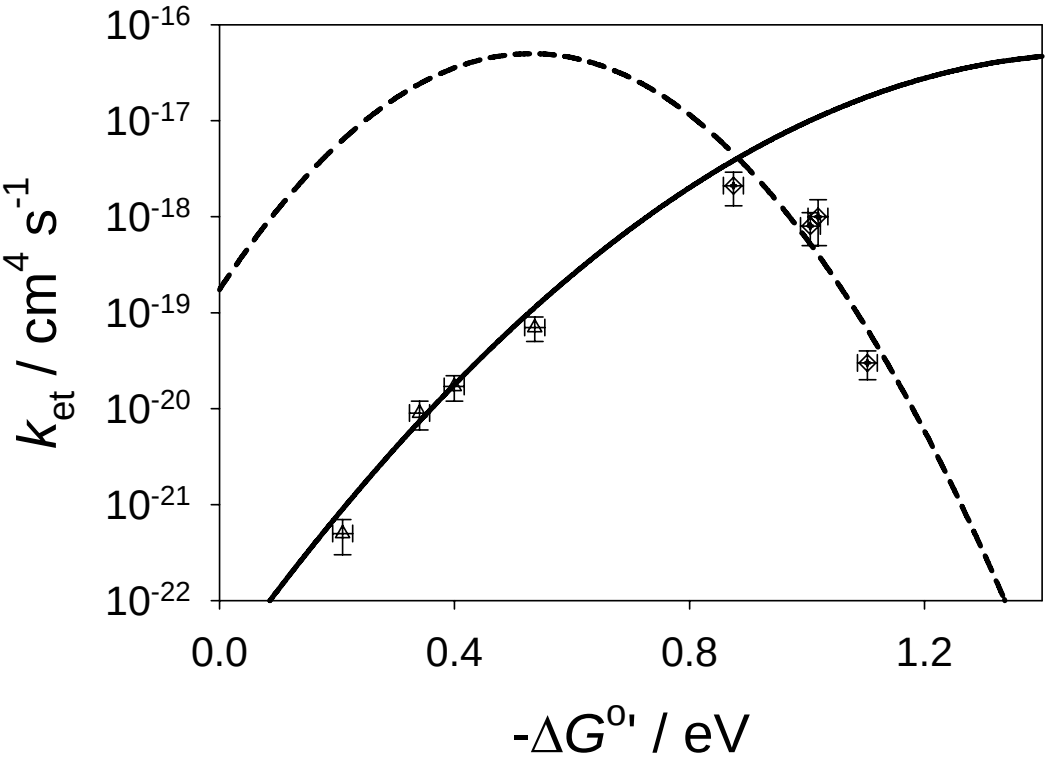

Figure 3.4 Plots of the electron-transfer rate constant as a function of the standard driving force for $[Co(bpy)_3]^{3+/2+}$ (triangles) and $[Ru(bpy)_2(MeIm)_2)]^{3+/2+}$ (diamonds). The solid line represents the predicted k_{et} vs. $\Delta G^{o'}$ behavior for $k_{et,max} = 5 \times 10^{-17}$ cm^4 s^{-1} and $\lambda_{sc} = 1.5$ eV. The dashed line represents the predicted k_{et} vs. $\Delta G^{o'}$ behavior for $k_{et,max} = 5 \times 10^{-17}$ cm^4 s^{-1} and $\lambda_{sc} = 0.53$ eV.

first-order dependence on acceptor and surface electron concentrations, respectively. This behavior allowed for the experimental determination of interfacial electron-transfer rate constants for such systems.

The interfacial charge-transfer rate constant, k_{et}, for $[Co(bpy)_3]^{3+/2+}$ was observed to increase with increasing pH while k_{et} for $[Ru(bpy)_2(MeIm)_2]^{3+/2+}$ was observed to decrease with increasing pH. Since increases in pH cause increases in the standard driving force for charge transfer, $-\Delta G^{o'}$, the redox couples $[Co(bpy)_3]^{3+/2+}$ and $[Ru(bpy)_2(MeIm)_2]^{3+/2+}$ in contact with n-ZnO are in the normal and inverted regions of electron transfer, respectively. These results are in excellent agreement with theoretical predictions of the free energy dependence of such interfacial electron-transfer reactions. Taken together with previous results of the standard driving force and reorganization energy dependence of k_{et}, the present data offer strong validation of the Hush and Marcus model of interfacial charge-transfer reactions.

3.5 ACKNOWLEDGMENTS

We acknowledge the Department of Energy, Office of Basic Energy Sciences, for support of this work.

3.6 REFERENCES

(1) Hush, N. S. *Trans. Faraday Soc* **1961**, *57*, 557-580.

(2) Marcus, R. A. *Ann. Rev. Phys. Chem.* **1964**, *15*, 155-196.

(3) McCleskey, T. M.; Winkler, J. R.; Gray, H. B. *Inorg. Chim. Acta* **1994**, *225*, 319-322.

(4) Closs, G. L.; Calcaterra, L. T.; Green, N. J.; Penfield, K. W.; Miller, J. R. *J. Phys. Chem.* **1986**, *90*, 3673-3683.

(5) Fox, L. S.; Kozik, M.; Winkler, J. R.; Gray, H. B. *Science* **1990**, *247*, 1069.

(6) Hush, N. S. *Electrochim. Acta* **1968**, *13*, 1005-1023.

(7) Marcus, R. A. *J. Chem. Phys.* **1963**, *38*, 1858-1862.

(8) Gerischer, H. *Adv. Electrochem. Electrochem. Engr.* **1961**, *1*, 139.

(9) Nakabayashi, S.; Itoh, K.; Fujishima, A.; Honda, K. *J. Phys. Chem.* **1983**, *87*, 5301-5303.

(10) Nakabayashi, S.; Fujishima, A.; Honda, K. *J. Phys. Chem.* **1983**, *87*, 3487-3492.

(11) Nakabayashi, S.; Fujishima, A.; Honda, K. *J. Electroanal. Chem.* **1982**, *140*, 223-225.

(12) Dewald, J. F. *Bell Techn. J.* **1960**, *May*, 615.

(13) Dewald, J. F. *J. Phys. Chem. Solids* **1960**, *14*, 155-161.

(14) Morrison, S. R. *Surf. Sci.* **1969**, *15*, 363.

(15) Morrison, S. R. *Electrochemistry at Semiconductor and Oxidized Metal Electrodes*; Plenum: New York, 1980.

(16) Hamann, T.; Gstrein, F.; Brunschwig, B. S.; Lewis, N. S. *J. Am. Chem. Soc.* **2005**, *127*, 7815-7824.

(17) Hamann, T.; Gstrein, F.; Brunschwig, B. S.; Lewis, N. S. *J. Am. Chem. Soc.*

(18) Li, B.; Morrison, S. R. *J. Phys. Chem.* **1985**, *89*, 1804-1809.

(19) Yan, S. G.; Hupp, J. T. *J. Phys. Chem.* **1996**, *100*, 6867-6870.

(20) Yan, S. G.; Hupp, J. T. *J. Phys. Chem. B* **1997**, *101*, 1493-1495.

(21) Lohmann, F. *Ber. Bunsenges. Phys. Chem.* **1966**, *70*, 428-434.

(22) Tan, M. X.; Laibinis, P. E.; Nguyen, S. T.; Kesselman, J. M.; Stanton, C. E.; Lewis, N. S. *Prog. Inorg. Chem.* **1994**, *41*, 21-144.

(23) Sze, S. M. *The Physics of Semiconductor Devices*; 2nd ed.; Wiley: New York, 1981.

(24) Lewis, N. S. *J. Phys. Chem. B* **1998**, *102*, 4843-4850.

(25) Caspar, J. V.; Meyer, T. J. *Inorg. Chem.* **1983**, *22*, 2444-2453.

(26) Bard, A. J.; Faulkner, L. R. *Electrochemical Methods: Fundamentals and Applications*; John Wiley & Sons: New York, 1980.

(27) Fajardo, A. M.; Lewis, N. S. *J. Phys. Chem. B* **1997**, *101*, 11136-11151.

(28) Bhargava, R. *Properties of Wide Bandgap II-VI Semiconductors*; Inspec: London, 1997; Vol. Series No. 17.

(29) Royea, W. J.; Fajardo, A. M.; Lewis, N. S. *J. Phys. Chem. B* **1997**, *101*, 11152-11159.

(30) Biner, M.; Burgi, H. B.; Ludi, A.; Rohr, C. *J. Am. Chem. Soc.* **1992**, *114*, 5197-5203.

(31) Kuciauskas, D.; Freund, M. S.; Gray, H. B.; Winkler, J. R.; Lewis, N. S. *J. Phys. Chem. B* **2001**, *105*, 392-403.

(32) Marcus, R. A. *J. Phys. Chem.* **1991**, *95*, 2010-2013.

(33) Ashkenov, N.; Mbenkum, B. N.; Bundesmann, C.; Riede, V.; Lorenz, M.; Spemann, D.; Kaidashev, E. M.; Kasic, A.; Schubert, M.; Grundmann, M.; Wagner, G.; Neumann, H.; Darakchieva, V.; Arwin, H.; Monemar, B. *J. Appl. Phys.* **2003**, *93*, 126-133.

CHAPTER 4

A Comparison of the Self-Exchange and Interfacial Charge-Transfer Rate Constants for Methyl vs. t-Butyl Substituted Osmium Polypyridyl Complexes

4.1 INTRODUCTION

Factors that affect the electronic coupling in electron-transfer processes have been of significant recent interest. Differences in electronic coupling through various bond pathways have been shown to control the rates of intramolecular electron transfer in redox-labeled metalloproteins,[1-4] in photosynthetic reaction centers,[5-9] in organic donor/acceptor systems,[10-16] and in redox species covalently linked to electrode surfaces.[17-26]

Dye-sensitized solar cells, DSSCs, based on nanocrystalline TiO_2, have exhibited solar energy conversion efficiencies of over 10%.[27-29] The most efficient DSSCs reported to date utilize the I_3^-/ I^- couple as a redox mediator. The good performance of the I_3^-/ I^- couple is generally attributed to the slow recombination kinetics involved with the electron transfer from TiO_2 and/or the F:SnO to the complicated, potentially multi-electron, I_3^-/ I^- redox system.[30-32] The I_3^-/ I^- couple, however, has some disadvantages, including the redox potential limitations on the open-circuit voltage and the absorption of visible light by the redox species.[33,34] In general, one-electron outer sphere, redox reagents such as ferrocenes do not provide useful mediators in DSSCs. Although such species often rapidly reduce the oxidized dye created by injection of an excited electron into the TiO_2, these one-electron outer-sphere redox systems also facilitate rapid recombination, due to facile reduction of their oxidized form by electrons in the conduction band of the TiO_2.[32] Interestingly, DSSCs that use cobalt(III/II) tris(4,4'-di-tert-butyl-2,2'-bipyridyl), $[Co(t\text{-}Bu_2bpy)_3]^{3+/2+}$, as a mediator have exhibited excellent efficiencies, while cobalt(III/II) tris(4,4'-di-methyl-2,2'-bipyridyl), $[Co(Me_2bpy)_3]^{3+/2+}$, systems have shown poor performance.[33-36] The authors attributed the difference in mediator behavior to the steric bulk of the tert-butyl group.[36]

The distance dependence of the back electron transfer from TiO_2 to covalently attached oxidized dyes has been examined in several studies.[37-40] In addition, electron

transfer from SnO to electrostatically bound redox complexes with varying chain length alkyl substituents have been reported to exhibit distance-dependent rate constants.[41] These studies clearly show that electron transfer from a semiconductor electrode to a redox couple can be controlled by separation distance. To the best of our knowledge, however, there are no reports of the distance dependence of strictly outer-sphere heterogeneous electron-transfer reactions at a semiconductor electrode. In addition, we present herein the first direct comparison of distance modulated outer-sphere heterogeneous and homogeneous electron-transfer reactions.

In this work, we have compared the homogeneous and interfacial electron-transfer rate constants between osmium polypyridyl complexes that are relatively unhindered and complexes that have t-Bu groups, by analogy to the $[Co(t\text{-}Bu_2bpy)_3]^{3+/2+}$ system. The self-exchange measurements in solution have been performed by conventional NMR line-broadening analysis, and yield information on the relative contributions of electronic coupling vs. outer-sphere reorganization energy on affecting the electron-transfer rate of the self-exchange process.

The interfacial charge-transfer kinetics for metal complexes using these two different ligand systems have also been investigated in our work using semiconductor electrodes. In 1961, Gerischer pointed out that semiconductor electrodes are well-suited for measuring interfacial electron-transfer processes, because the low, and experimentally controllable, electron concentration at the surface of such electrodes would eliminate the diffusion-controlled constraints on rate constant measurements that plague interfacial kinetics measurements at metallic electrodes.[42,43] However, relatively few interfacial electron-transfer measurements at semiconducting electrodes are available, because of complications due to non-ideal electrode behavior, redox species adsorption, and other issues at semiconductor electrode surfaces.[44,45] We have recently shown that carefully etched, well-controlled, n-type ZnO electrodes can exhibit ideal, second-order interfacial kinetics behavior for one-electron, outer-sphere, redox systems, thereby allowing a

straightforward determination of the interfacial rate constants for such systems.[46,47] Measurements using a series of Ru- and Os-derived redox species have elucidated the dependence of the interfacial rate constant on the driving force,[47] reorganization energy,[46] and thermodynamics[48] of such systems. The changes in the steric properties of the ligands used in the present study provides an elucidation of the potential role of the electronic coupling in affecting the interfacial electron-transfer rate constants in such systems.

4.2 EXPERIMENTAL

Ammonium hexachloroosmate(IV), 4,4'-di-tert-butyl 2,2'-bipyridine (t-Bu_2bpy), 4,4'-dimethyl 2,2'-bipyridine (Me_2bpy), imidazole, NH_4PF_6, and tetra(n-butyl)ammonium chloride (TBACl) were used as received from Aldrich Chemical Co. All solvents were reagent grade and were used as received.

The $[Os(Me_2bpy)_3]Cl_2$ compound was prepared as described previously.[47] The oxidized, acceptor form of this compound was prepared *in situ* via bulk electrolysis. To prepare $[Os(t\text{-}Bu_2bpy)_3]Cl_2$, $(NH_4)_2[OsCl_6]$ (0.25 g, 0.56 mmol) and 3.5 equivalents of t-Bu_2bpy were added to 25 mL of ethylene glycol. The solution was rapidly stirred under Ar and heated to reflux for 3 hr. An excess of NH_4PF_6(aq) was then added, and the resulting $[Os(II)(t\text{-}Bu_2bpy)_3](PF_6^-)_2$ salt precipitate was filtered, yielding a dark green product. The product was washed with cold water and diethyl ether. The precipitate was dissolved in a minimal amount of acetone, and the product was precipitated by addition of diethyl ether. The complex was then filtered, and dried under vacuum. The chloride salt was prepared by dissolving the PF_6^- salt in acetone, followed by addition, while stirring, of a concentrated solution of TBACl in acetone. The chloride salt precipitated out of solution, was filtered, washed with acetone and ether, and was then dried under

vacuum. Elemental analysis yielded (calculated): C 60.57 (60.82), H 6.69 (6.81), N 7.71 (7.88).

The NMR line-broadening measurements were performed as described previously.[47] Measurements were carried out at ≈ 20° C in CD_3CN. Self-exchange rate constants reported herein were the average of measurements on three compositionally different samples having both the oxidized and reduced forms of the redox species in the solution.

The formal reduction potential of each compound was determined using cyclic voltammetry in pH = 6 buffered H_2O with 0.1 M KCl electrolyte. A glassy carbon disc electrode was used as the working electrode, a platinum mesh was employed as the counter electrode, and a standard calomel electrode (SCE) was used as the reference electrode. Scans were performed between 10 and 500 mV s^{-1} from 0.2V to 0.9 V vs. SCE.

Hydrothermally grown, n-type, <0001>-oriented, ZnO single crystals with resistivities reported to be between 10^1 and 10^4 Ω cm were purchased from Commercial Crystal Laboratories, Inc. (Naples, FL). Details of the electrochemical experiments have been reported previously.[46,47] Electrochemical experiments were carried out at room temperature in a 50 mM pH = 6.0 imidazole buffer with 0.1 M KCl (Aldrich, 99+%) added to provide the supporting electrolyte for electrochemical measurements. Water was obtained from a Barnstead NANOPure filter (> 18 MΩ resistivity).

4.3 RESULTS

A. Electron-Transfer Self-Exchange Rate Constant for $[Os(t\text{-}Bu_2bpy)_3]^{3+/2+}$

Figure 4.1 displays the proton NMR spectra of the methyl peak of solutions that contained the diamagnetic $[Os(t\text{-}Bu_2bpy)_3]^{2+}$ complex, mixtures of the diamagnetic $[Os(t\text{-}Bu_2bpy)_3]^{2+}$ and paramagnetic $[Os(t\text{-}Bu_2bpy)_3]^{3+}$ species, and the pure paramagnetic

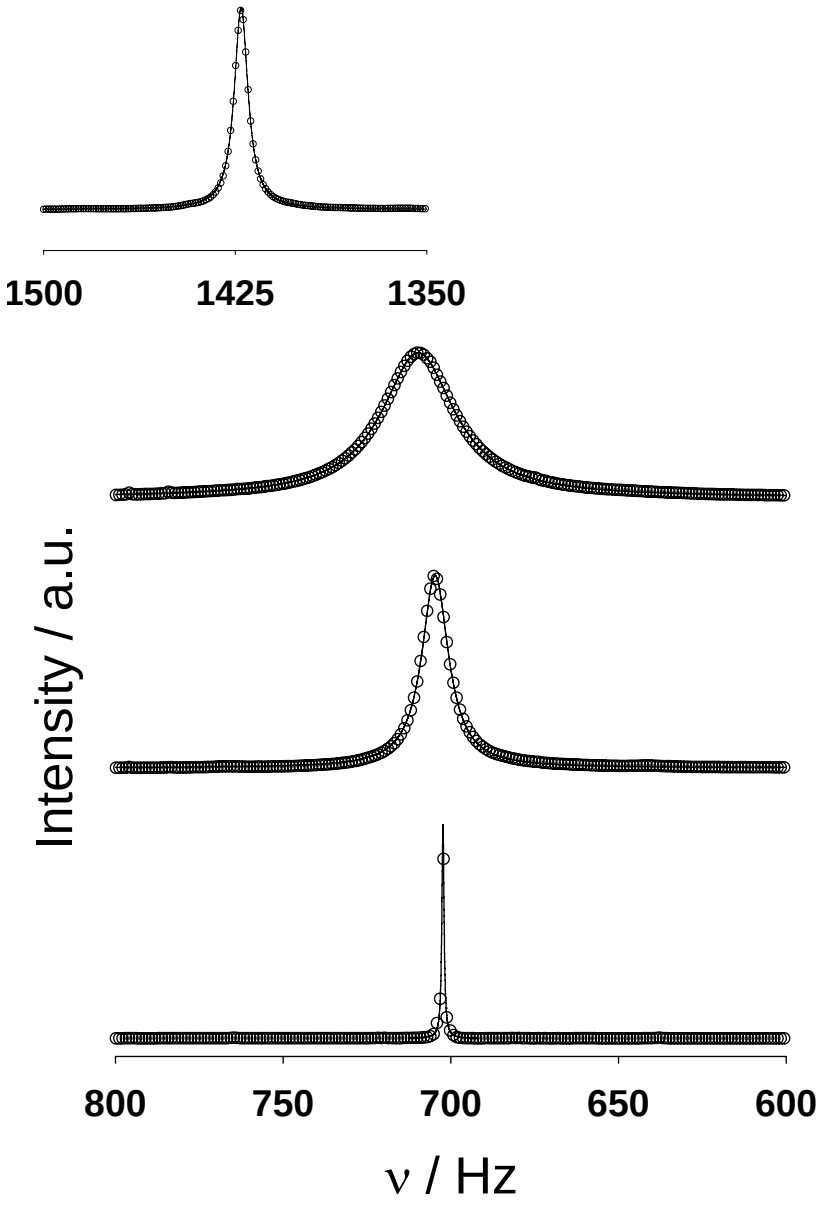

Figure 4.1 ^{1}H NMR spectra of the methyl proton peak of $Os(t\text{-}Bu_2bpy)_3^{2+}$ and of a mixture of $Os(t\text{-}Bu_2bpy)_3^{2+}$ and $Os(t\text{-}Bu_2bpy)_3^{3+}$. Above is the $Os(t\text{-}Bu_2bpy)_3^{3+}$ methyl proton spectrum. The lines indicate the results of non-linear least-squares fitting of each spectrum.

$[Os(t\text{-}Bu_2bpy)_3]^{3+}$ species, respectively. All peaks were fitted to a Lorentzian line shape. The self-exchange rate constant, k_{ex}, was calculated from[49]

$$k_{ex} = \frac{4\pi X_d X_p (\Delta\nu)^2}{(W_{dp} - X_p W_p - X_d W_d) C} \quad (1)$$

where W_{dp} is the line width (full width at half maximum) of the mixed species resonance peak, W_p and W_d are the line widths of the paramagnetic and diamagnetic peaks, respectively, and X_p and X_d are the mole fractions of the paramagnetic and diamagnetic species, C is the total concentration of the exchanging species and $\Delta\nu$ is the observed frequency shift relative to the position of the resonance for the diamagnetic species. The diamagnetic and paramagnetic line widths were observed to be 0.8 and 6.5 Hz, respectively, and $\Delta\nu$ was measured as 720.4 Hz. This analysis produced a value of k_{ex} = $(3.7 \pm 0.6) \times 10^5$ M^{-1} s^{-1} for $[Os(t\text{-}Bu_2bpy)_3]^{3+/2+}$ in CD_3CN.

B. Interfacial Electron-Transfer Rate Constant for $[Os(t\text{-}Bu_2bpy)_3]^{3+/2+}$ at n-ZnO Electrodes

1. J-E Behavior: Determination of Interfacial Kinetics

Figure 4.2 shows plots of J/[A] vs. E for reduction of $[Os(t\text{-}Bu_2bpy)_3]^{3+}$ and $[Os(t\text{-}Me_2bpy)_3]^{3+}$ at n-ZnO electrodes, where [A] is the concentration of the acceptor species in units of molecules cm^{-3}. The acceptor concentrations were determined by counting the coulombs passed during bulk electrolysis and by monitoring the absorption bands at 302 (ε = 38700 mol^{-1} cm^{-1}) and 313 nm (ε = 41500 mol^{-1} cm^{-1}).[50] All junctions showed rectifying behavior, producing a limiting anodic current density and an exponentially increasing cathodic current density as the electrode potential, E, became more negative, in accord with the diode equation:

$$J = -J_0 \left[\exp\left(\frac{-qE}{\gamma k_B T} \right) - 1 \right] \quad (2)$$

where J_o is the exchange current density, γ is the diode quality factor, q is the charge on an electron, and k_B is Boltzmann's constant. The diode quality factors were 1.2 for

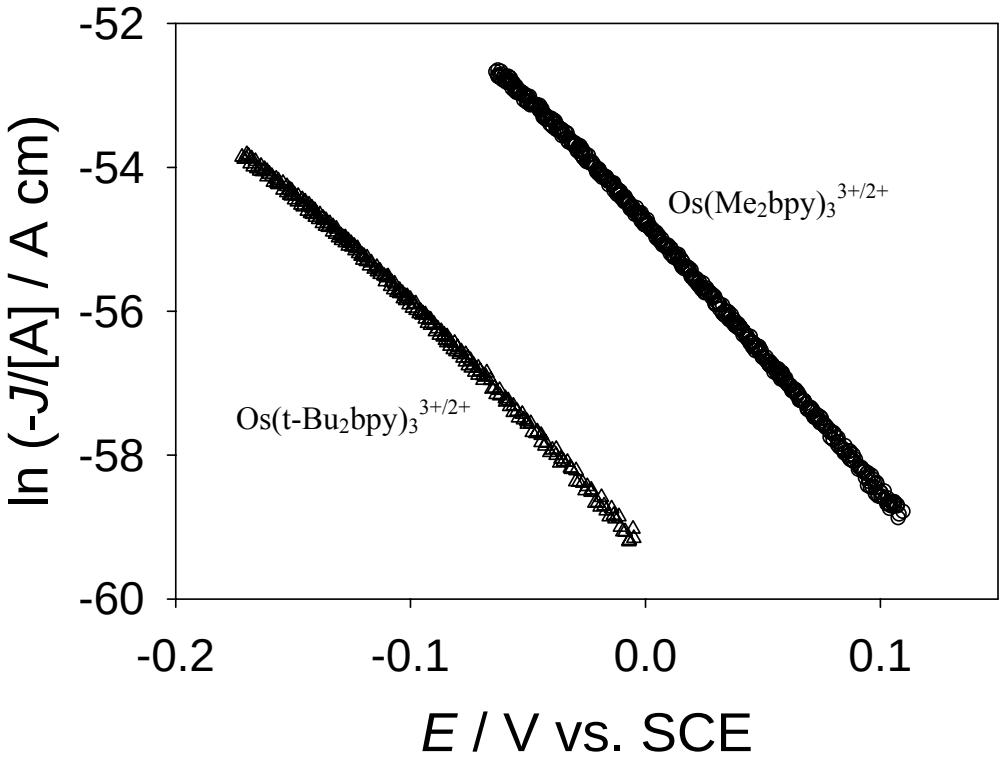

Figure 4.2 Plots of $J/[A]$ vs. E for $Os(Me_2bpy)_3^{3+/2+}$ ([A] = 4.6 mM; open circles) and $Os(t\text{-}Bu_2bpy)_3^{3+/2+}$ ([A] = 2.3 mM; open triangles).

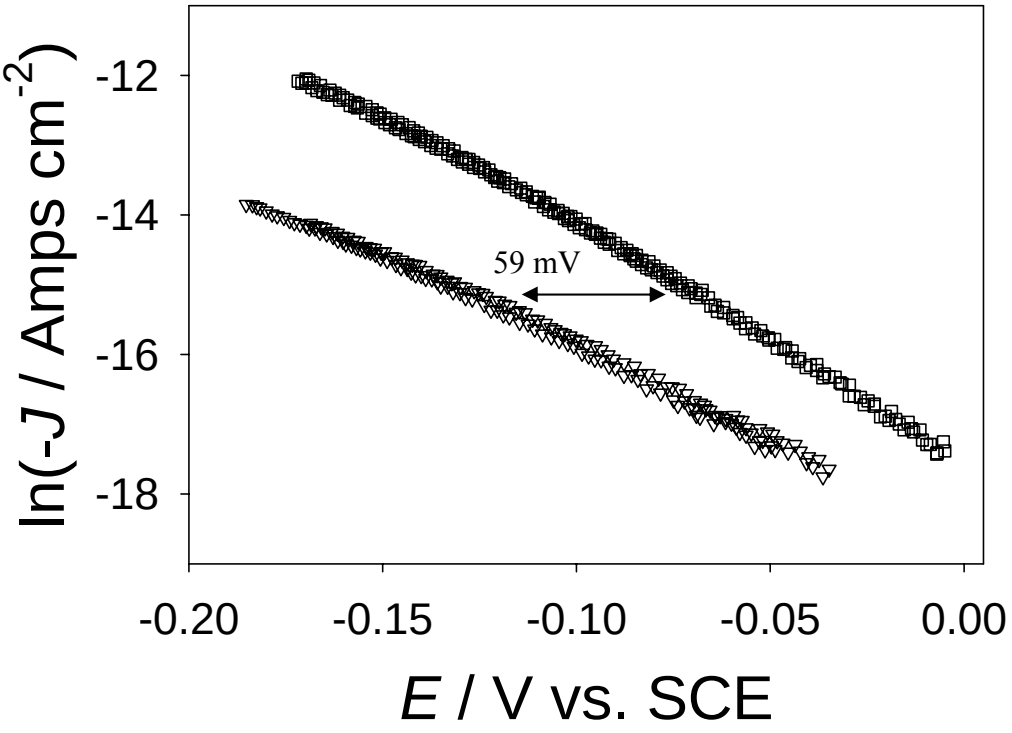

Figure 4.3 Plots of *J* vs. *E* for $Os(t\text{-}Bu_2bpy)_3^{3+/2+}$ at [A] = 2.3 mM (open squares) and [A] = 0.23 mM (open triangles). As noted in the text, a 10-fold decrease in [A] should result in a shift of the *J*-*E* curve by 59 mV.

$[Os(t\text{-}Bu_2bpy)_3]^{3+/2+}$ and 1.1 for $[Os(Me_2bpy)_3]^{2+/3+}$, respectively, in accord with theoretical expectations for a process that is kinetically first-order in the concentration of electrons at the surface of the semiconductor.[45,51,52]

At forward bias, the net flux of electrons from the conduction band of the semiconductor electrode to randomly dissolved acceptors in solution is given by[45]

$$J(E) = -qk_{et}[A]n_s \quad (3)$$

where k_{et} is the electron-transfer rate constant ($cm^4\ s^{-1}$) and n_s is the electron concentration in the conduction band at the semiconductor surface (cm^{-3}). The concentrations of the acceptor, [A], and of electrons at the semiconductor surface, n_s, appear explicitly in the expression for the current density, thus yielding a second-order rate law for the interfacial charge-transfer process at a non-degenerately-doped semiconductor electrode. Because [A] was not constant for the different experiments, the current density for each junction was normalized by dividing by [A]. The observed interfacial kinetics exhibited the theoretically expected first-order dependence on [A], shown by the ~ 59 mV shift of the *J-E* curves expected for a 10-fold decrease in [A] (Figure 4.3).

2. Differential Capacitance vs. Potential Measurements: Determination of Interfacial Thermodynamics

The interfacial thermodynamics were determined from differential capacitance vs. potential measurements.[45] The impedance spectra were fitted over the frequency range of 10^2 to 10^4 Hz to an equivalent circuit consisting of the cell resistance, R_s, in series with two parallel components: the resistance to charge transfer, R_{sc}, and the space-charge capacitance, C_{sc}.[45] No frequency dependence of the capacitance was observed. The series resistance of the system, R_s, was essentially constant for all measurements. Figure

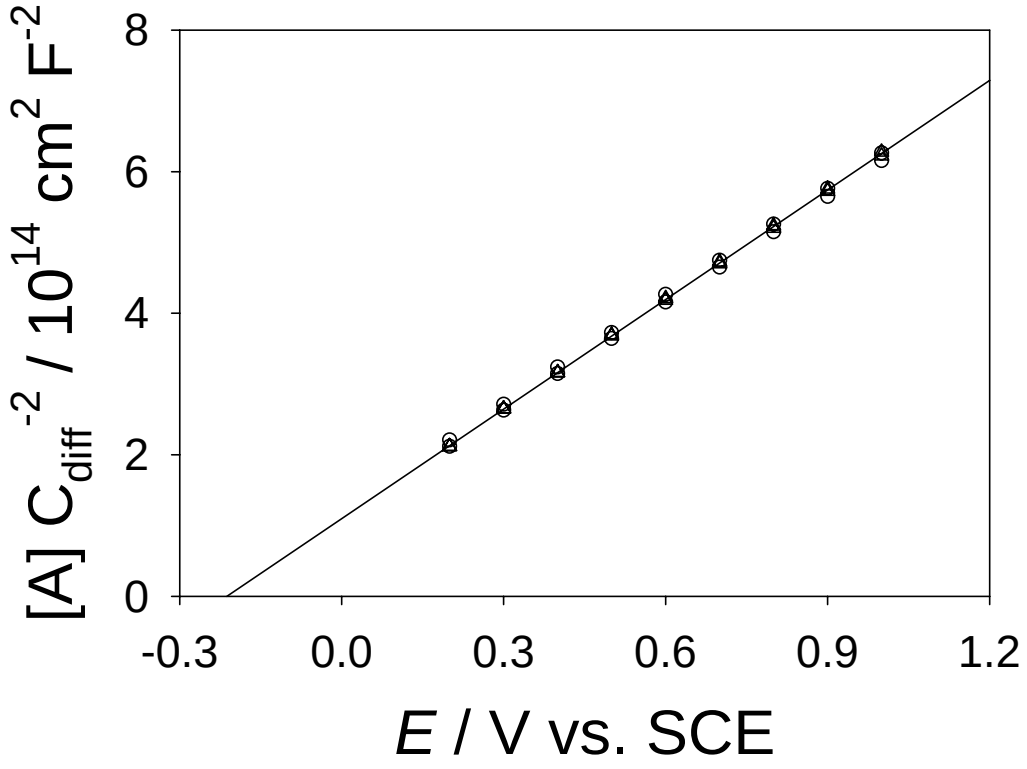

Figure 4.4 Mott-Schottky plots of ZnO electrode in contact with $Os(Me_2bpy)_3^{3+/2+}$ (open circles) and $Os(t\text{-}Bu_2bpy)_3^{3+/2+}$ (open triangles) at two concentrations each. The line indicates the least-squares fit of all of the data.

4.4 displays Mott-Schottky plots, in the form of A_s^2/C_{diff}^2 vs. E, where A_s is the projected area of the electrode, for all contacts. All data were fitted to a straight line in accord with the Mott-Schottky equation:[45]

$$\frac{A_s^2}{C_{sc}^2} = \frac{2}{q\varepsilon_{ZnO}\varepsilon_o N_d}\left(E - E_{fb} - \frac{k_B T}{q}\right) \quad (4)$$

where ε_{ZnO} is the static dielectric constant of ZnO (8.65),[53] ε_o is the permittivity of free space, N_d is the dopant density of the semiconductor, and E_{fb} is the flat-band potential of the semiconductor/liquid contact. The slope and intercept of a linear least-squares fit were used to extract values for N_d and E_{fb}, respectively. The standard errors resulting from the fit were used to calculate the errors in N_d and E_{fb}, producing values of E_{fb} = -0.25 ± 0.01 V vs. SCE and $N_d = (6.5 \pm 0.7) \times 10^{16}$ cm^{-3}. The constant value of the capacitance at a given electrode potential in response to changes in the identity and/or concentration of the redox species, confirms that the band-edge position of the ZnO was fixed during these experiments.

4.4 DISCUSSION

A. Rate Constants and Reorganization Energies for $[Os(Me_2bpy)_3]^{3+/2+}$ Electron Transfer Self-Exchange Reactions

The self-exchange rate constant of $[Os(Me_2bpy)_3]^{3+/2+}$ in acetonitrile has been measured previously by Wahl and co-workers.[49] A rate constant of $k_{ex} = 2 \times 10^7$ M^{-1}s^{-1} was determined at 31 ºC at an ionic strength of ~ 0.05 M with PF_6^- as the counter ion. The value determined herein of $k_{ex} = (3.7 \pm 0.6) \times 10^5$ M^{-1}s^{-1} (CD_3CN, 22º C) for $[Os(t\text{-}Bu_2bpy)_3]^{3+/2+}$ is thus ≈ 50 times smaller than that of the methyl-substituted analog.

The self-exchange rate constant can be described by the expression[54-58]

$$k_{ex} = K_A \kappa_{el} \nu_n e^{-\lambda_{se}/4k_B T} \quad (5)$$

where K_A is the equilibrium constant for the formation of the precursor complex, κ_{el} is the electronic transmission coefficient, ν_n is the effective nuclear vibration frequency of the activated complex, and the exponential term is referred to as the Frank-Condon factor. Changes in any of these terms when the substituent R is varied from Me to t-Bu could account for the observed decrease in k_{ex}.

The total reorganization energy in self-exchange reactions is comprised of changes in electronic configuration and in the bond lengths and angles in the inner-coordination sphere of the complexes, $\lambda_{se,in}$, and of changes in the polarization of the solvent in the outer-coordination sphere, $\lambda_{se,out}$. For osmium complexes that involve bipyridyl ligands, however, the inner-sphere does not undergo significant changes upon electron transfer.[59] The total reorganization energy can therefore be estimated to be equal to the outer-sphere reorganization energy, λ_{se}. The value of λ_{se} for two spherical reactants in solution can be calculated using eq (6):[54]

$$\lambda_{se} = \frac{(\Delta zq)^2}{4\pi\varepsilon_0}\left[\left(\frac{1}{a}-\frac{1}{R}\right)\left(\frac{1}{n^2}-\frac{1}{\varepsilon}\right)\right] \qquad (6)$$

where Δz is the change in charge for the molecule during the self-exchange process, ε_0 is the vacuum permittivity, a is the radius of the reactant, R is the center-to-center distance of the reactant separation, n is the refractive index of the solvent (1.3441 for CH_3CN), and ε is the static dielectric constant of the solvent (37.5 for CH_3CN). Values of a = 6 Å and R = 12 Å were estimated for $[Os(Me_2bpy)_3]^{3+/2+}$, assuming that the methyl groups do not completely block the solvent from the bipyridyl rings. Use of these values in eq (6) produces a value of $\lambda_{se} \approx 0.63$ eV, which is in good agreement with a previous report.[47] Estimating that the tert-butyl group increases the radius by ≈1.2 Å compared to a methyl group yields a = 7.2 Å and R = 14.4 Å for $[Os(t\text{-}Bu_2bpy)_3]^{3+/2+}$, and hence a value from eq (6) of $\lambda_{se} \approx 0.53$ eV.

The decrease in the reorganization energy of $[Os(t\text{-}Bu_2bpy)_3]^{3+/2+}$ compared to $[Os(Me_2bpy)_3]^{3+/2+}$ should therefore result, according to eq (5), in a small increase of k_{ex},

on the order of 2-3, assuming constant values of K_A and κ_{el}. For a series of ruthenium compounds, a linear dependence of ln k_{ex} has been observed as a function of $1/r$, indicating that the charge-transfer process is adiabatic (i.e., $\kappa_{el} = 1$) and thus controlled by the outer-sphere reorganization energy.[60] The measured value of k_{ex} for $[Os(t\text{-}Bu_2bpy)_3]^{3+/2+}$ is however ~ 50 times smaller than that of $[Os(Me_2bpy)_3]^{3+/2+}$, rather than somewhat larger, indicating that the reorganization energy is not the dominant factor in determining this reduction in k_{ex}.

The pre-exponential term is thus ≈ 100 times smaller for $[Os(t\text{-}Bu_2bpy)_3]^{2+/3+}$ compared to $[Os(Me_2bpy)_3]^{2+/3+}$, suggesting that either K_A or $\kappa_{el}\nu_n$ has changed. Relatively small changes in complex size are not expected to have a significant effect on K_A. Therefore, the observed decrease in k_{ex} is attributed to $\kappa_{el}\nu_n$ which indicates that the reaction is not adiabatic, i.e., $\kappa_{el} < 1$. In the non-adiabatic limit, the electron hopping frequency between initial and final states is given by

$$\kappa_{el}\nu_n = \frac{4\pi^2}{h}\frac{1}{\sqrt{4\pi k_B T}}\overline{H_0^2}e^{-\beta(r-r_0)} \qquad (7)$$

where h is Planck's constant and the quantity $\overline{H_0^2}$ represents the square of the electronic coupling matrix element (in units of eV^2 $state^{-1}$) that couples reactant and product states at closest contact. The electronic coupling is assumed to decrease exponentially with distance, r, from the distance of closest approach, r_0, of the redox couples, with the electronic coupling attenuation coefficient, β. A value of ~1 $Å^{-1}$ for β is typically found for tunneling through alkyl chains. Taking the ratio of eq (7) for the two complexes, and assuming $\beta = 1$ $Å^{-1}$, the separation difference is approximately 4.8 Å. This distance corresponds to four carbon carbon bonds, two on each redox couple. The methyl groups on $[Os(Me_2bpy)_3]^{2+/3+}$, therefore, may not prevent the pyridyl rings from coming into close contact, which is consistent with the observation that the self-exchange rate constant is the same, within error, for $[Os(Me_2bpy)_3]^{2+/3+}$ and $[Os(bpy)_3]^{2+/3+}$.[49] Thus, the

bulk of the tert-butyl groups effectively act as spacers, preventing the bipyridyl rings from coming into close contact.

The results of this first-order analysis is in good agreement with a prior report of the self-exchange rate constants for a series of $Mn(CNR)_6^{+/2+}$ compounds, in which k_{ex} was ~ 200 times lower when R = t-Bu than when R = Me. This behavior has been attributed to steric effects effecting a decrease in the electron transfer rate due to the increased separation distance between the redox centers in the transition state of the reaction.[61]

B. Interfacial Rate Constants for $[Os(Me_2bpy)_3]^{3+/2+}$ and $[Os(t\text{-}Bu_2bpy)_3]^{3+/2+}$ at n-ZnO Electrodes

An electronic coupling model, based on the Fermi Golden Rule applied to a semiconductor electrode in contact with a random distribution of acceptor species in solution, has produced the following expression for the interfacial charge-transfer rate constant:[62]

$$k_{et} = k_{et,max} \exp\left\{\frac{-(\Delta G^{o\prime} + \lambda_{sc})^2}{4\lambda_{sc} k_B T}\right\} \tag{8}$$

where the prefactor, $k_{et,max}$, is the rate constant at optimal exoergicity, obtained when the standard free energy for interfacial charge transfer, $\Delta G°'$, is equal to $-\lambda_{sc}$. The value of $k_{et,max}$ can be estimated by

$$k_{et,max} = \frac{2\pi}{\hbar}(4\pi k_B T \lambda_{sc})^{-1/2}\left(\overline{H^2_{AB,sc}}\right)\beta_{sc}^{-1}\left\{\frac{l_{sc}}{d_{sc}^{2/3}(6/\pi)^{1/3}}\right\} \tag{9}$$

where l_{sc} is the effective coupling length in the semiconductor, d_{sc} is the atomic density of the solid, and the quantity $\overline{H^2_{AB,sc}}$ represents the square of the matrix element that couples reactant and product states at an energy **E**, averaged over all degenerate states in the semiconductor in a plane parallel to the electrode surface.[62] The subscript "sc" indicates parameters for a semiconductor electrode.

A theoretical value for the reorganization energy of a redox couple at a ZnO electrode, λ_{sc} , can be calculated using eq (10):[63,64]

$$\lambda_{sc} = \frac{(\Delta zq)^2}{8\pi\varepsilon_0}\left[\frac{1}{a}\left(\frac{1}{n_{Sol}^2}-\frac{1}{\varepsilon_{Sol}}\right)-\frac{1}{2R_e}\left(\left(\frac{n_{ZnO}^2-n_{Sol}^2}{n_{ZnO}^2+n_{Sol}^2}\right)\frac{1}{n_{Sol}^2}-\left(\frac{\varepsilon_{ZnO}-\varepsilon_{Sol}}{\varepsilon_{ZnO}+\varepsilon_{Sol}}\right)\frac{1}{\varepsilon_{Sol}}\right)\right] \quad (10)$$

where n_{ZnO} and n_{Sol} are the refractive index of ZnO (1.9[53,65]) and the aqueous solution, respectively, ε_{ZnO} and ε_{Sol} are the static dielectric constant of ZnO (8.65[53]) and the solution, respectively, and here R_e is the distance from the acceptor to the electrode. Using a = 6 Å and R_e = 6 Å produces a value of λ_{sc} = 0.53 eV for $[Os(Me_2bpy)_3]^{2+/3+}$, whereas using a value of 7.2 Å for a, and 7.2 Å for R_e produces a value of λ_{sc} = 0.45 eV for $[Os(t\text{-}Bu_2bpy)_3]^{2+/3+}$.

The observed interfacial electron-transfer rate constant for $[Os(t\text{-}Bu_2bpy)_3]^{3+/2+}$ at a ZnO electrode is approximately 100 times smaller than the value of k_{et} observed for $[Os(Me_2bpy)_3]^{3+/2+}$. The redox couple $[Os(t\text{-}Bu_2bpy)_3]^{3+/2+}$ showed reversible behavior with a formal potential of 0.43 V vs. SCE which is ~ 50 mV positive of $[Os(Me_2bpy)_3]^{3+/2+}$.[47] According to eqs (8) and (10), assuming a constant value of $k_{et,max}$, $[Os(t\text{-}Bu_2bpy)_3]^{3+/2+}$ can be expected to have a 5-fold smaller k_{et} than $[Os(Me_2bpy)_3]^{3+/2+}$, due the approximately 50 mV increase in driving force and the 0.08 eV smaller calculated reorganization energy for the $[Os(t\text{-}Bu_2bpy)_3]^{3+/2}$ system. The expected dependence of k_{et} on the Frank-Condon nuclear terms has been demonstrated.[46,47] The magnitude of the estimated change in the Frank-Condon nuclear terms may have a significant uncertainty due to the accuracy with which the absolute value of the energy of the conduction band of the ZnO is known. Assuming that the conduction band edge energy is accurate to within 100 mV, however, a range for the decrease in k_{et} by a factor of 2-10 is estimated upon changing from $[Os(Me_2bpy)_3]^{3+/2+}$ to $[Os(t\text{-}Bu_2bpy)_3]^{3+/2+}$. Assuming the estimated 5-fold decrease due to the Frank-Condon factor is accurate, the additional 20-fold decrease of k_{et} observed for $[Os(t\text{-}Bu_2bpy)_3]^{3+/2+}$ is therefore indicative of a smaller value of $k_{et,max}$. While $k_{et,max}$ is not independent of the reorganization energy,

this variation is very small for the reorganization energy values considered here. The approximate 20-fold decrease in $k_{et,max}$ is thus consistently attributed to the attenuation of the coupling by the tert-butyl group acting as a spacer between the redox couple and the ZnO electrode. The attenuation of the coupling at close contact is given by

$$\overline{H_{AB,sc}^2} = \overline{H_{0,sc}^2} e^{-\beta(r-r_0)} \quad (11)$$

Taking the ratio of eq (11) for the two complexes, using the value of $\beta = 1$ Å^{-1} estimated above, the 20-fold decrease in coupling indicates an increased separation distance from the electrode of ~ 3 Å, which is consistent with the length of a tert-butyl group. The magnitude of the coupling attenuation of interfacial electron-transfer reactions by the tert-butyl group is consistent with the 100-fold attenuation of k_{ex} in the self-exchange reaction, because in the interfacial charge-transfer process one t-Bu group acts as an intervening spacer, while in the self-exchange process two t-Bu groups, one on each redox couple, serve as spacers between the donor and acceptor centers.

The expected rate constant behavior as a function of $\Delta G°'$ and λ_{sc} has been shown for analogous Os and Ru bipyridyl complexes at n-type ZnO electrodes.[46,47] Figure 4.5 shows a plot of the electron-transfer rate constant for $Os(Me_2bpy)_3^{3+/2+}$ and $Os(t\text{-}Bu_2bpy)_3^{3+/2+}$ as a function of $-\Delta G°'$. The theoretically predicted k_{et} vs. $\Delta G°'$ behavior, according to eq (8), is also shown, assuming $k_{et,max} = 1\times10^{-17}$ cm^4 s^{-1} for the values of λ_{sc} = 0.53 eV and λ_{sc} = 0.46 eV. It appears that differences in the Frank-Condon nuclear terms are very unlikely to account for the 100-fold smaller k_{et} of $Os(t\text{-}Bu_2bpy)_3^{3+/2+}$ compared to $Os(Me_2bpy)_3^{3+/2+}$. Including an estimated 20-fold decrease in coupling, however, shown by the predicted k_{et} vs. $\Delta G°'$ behavior for $k_{et,max} = 5\times10^{-19}$ cm^4 s^{-1} and λ_{sc} = 0.46 eV, is in good agreement with the measured k_{et} values.

The results reported herein are therefore in agreement with previous observations of sterically hindered cobalt polypyridyl complexes being successfully employed as redox mediators in dye-sensitized solar cells.[33,35,36] When $[Co(Me_2bpy)_3]^{3+/2+}$ was employed as a mediator, the DSSC exhibited very small values of the short-circuit

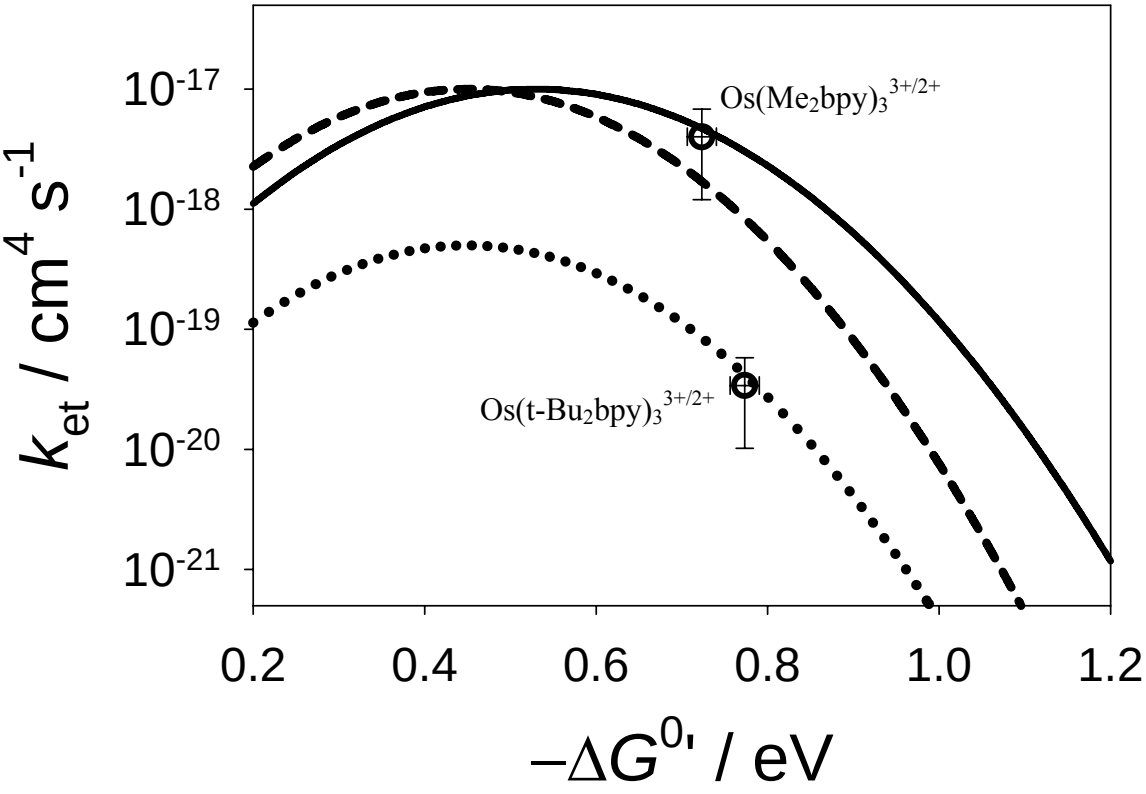

Figure 4.5 Plot of the electron-transfer rate constant for Os(Me$_2$bpy)$_3^{3+/2+}$ and Os(t-Bu$_2$bpy)$_3^{3+/2+}$ as a function of the standard driving force, $-\Delta G^{o\prime} = qE^{o\prime}(A/A^-) - \mathbf{E}_{cb}$. The solid line represents the predicted k_{et} vs. $\Delta G^{o\prime}$ behavior for $k_{et,max} = 1\times10^{-17}$ cm^4 s^{-1} and $\lambda_{sc} = 0.53$ eV, the dashed line represents the predicted k_{et} vs. $\Delta G^{o\prime}$ behavior for $k_{et,max} = 1\times10^{-17}$ cm^4 s^{-1} and $\lambda_{sc} = 0.46$ eV, and the dotted line represents the predicted k_{et} vs. $\Delta G^{o\prime}$ behavior for $k_{et,max} = 5\times10^{-19}$ cm^4 s^{-1} and $\lambda_{sc} = 0.46$ eV.

photocurrent density, J_{ph}, open-circuit voltage, V_{oc}, and overall efficiency.[36] However, when $[Co(t\text{-}Bu_2bpy)_3]^{3+/2+}$ was used as the mediator, the DSSC was ~ 80% as efficient as the analogous system with $I_3^{-/}$ I^- as the mediator.[36] This result is consistent with the observations reported herein that the 4,4'-t-Bu bipyridyl ligands can reduce interfacial electron-transfer rates by over an order of magnitude compared to the 4,4'-methyl substituted bipyridyl ligands, and are thus expected to reduce the charge-recombination rate at TiO_2 surfaces by decreasing the electronic coupling of the redox species to the electrode surface. These results therefore offer insight into the design of new redox mediators for use in DSSCs as well as insight into the factors that fundamentally control interfacial charge-transfer reactions at semiconductor electrodes.

4.5 CONCLUSIONS

Introduction of tert-butyl groups onto the bipyridyl ligand decreased the self-exchange rate constant by a factor of 50 compared to that of the analogous methyl substituted Os(III/II) trisbipyridine system. The observed reduction in the self-exchange rate constant is consistent with a decrease in the electronic coupling due to steric effects increasing the closest approach distance between the reactants. Steady-state current density vs. potential measurements on ZnO electrodes similarly revealed that the interfacial electron-transfer rate constant for $[Os(t\text{-}Bu_2bpy)_3]^{3+/2+}$ decreased 100-fold compared to that for $[Os(Me_2bpy)_3]^{3+/2+}$. These results therefore collectively indicate that the tert-butyl group can act as an efficient intervening spacer, decreasing the electronic coupling in both interfacial and solution-based self-exchange electron transfer reactions, and opening up a strategy for reducing deleterious back charge-transfer processes in semiconductor/liquid junction-based solar energy conversion systems.

4.6 ACKNOWLEDGMENTS

We thank the Department of Energy, Office of Basic Energy Sciences, for support of this work.

4.7 REFERENCES

(1) Gray, H. B.; Winkler, J. R. *Annu. Rev. Biochem.* **1996**, *65*, 537.

(2) Langen, R.; Chang, I. J.; Germanas, J. P.; Richards, J. H.; Winkler, J. R.; Gray, H. B. *Science* **1995**, *268*, 1733-1735.

(3) Mayo, S. L.; Ellis, W. R.; Crutchley, R. J.; Gray, H. B. *Science* **1986**, *233*, 948-952.

(4) Wuttke, D. S.; Bjerrum, M. J.; Winkler, J. R.; Gray, H. B. *Science* **1992**, *256*, 1007-1009.

(5) Jia, Y. W.; Dimagno, T. J.; Chan, C. K.; Wang, Z. Y.; Du, M.; Hanson, D. K.; Schiffer, M.; Norris, J. R.; Fleming, G. R.; Popov, M. S. *J. Phys. Chem.* **1993**, *97*, 13180-13191.

(6) Franzen, S.; Goldstein, R. F.; Boxer, S. G. *J. Phys. Chem.* **1993**, *97*, 3040-3053.

(7) Elkabbani, O.; Chang, C. H.; Tiede, D.; Norris, J.; Schiffer, M. *Biochemistry* **1991**, *30*, 5361-5369.

(8) Boxer, S. G. In *Annual Review of Biophysics and Biophysical Chemistry*, 1990; Vol. 19, pp 267-299.

(9) Franzen, S.; Goldstein, R. F.; Boxer, S. G. *J. Phys. Chem.* **1990**, *94*, 5135-5149.

(10) Closs, G. L.; Miller, J. R. *Science* **1988**, *240*, 440.

(11) Closs, G. L.; Calcaterra, L. T.; Green, N. J.; Penfield, K. W.; Miller, J. R. *J. Phys. Chem.* **1986**, *90*, 3673-3683.

(12) Beebe, J. M.; Engelkes, V. B.; Liu, J. Q.; Gooding, J.; Eggers, P. K.; Jun, Y.; Zhu, X. Y.; Paddon-Row, M. N.; Frisbie, C. D. *J. Phys. Chem. B* **2005**, *109*, 5207-5215.

(13) Lokan, N. R.; Paddon-Row, M. N.; Koeberg, M.; Verhoeven, J. W. *J. Am. Chem. Soc.* **2000**, *122*, 5075-5081.

(14) Paulson, B. P.; Curtiss, L. A.; Bal, B.; Closs, G. L.; Miller, J. R. *J. Am. Chem. Soc.* **1996**, *118*, 378-387.

(15) Paulson, B.; Pramod, K.; Eaton, P.; Closs, G.; Miller, J. R. *J. Phys. Chem.* **1993**, *97*, 13042-13045.

(16) Johnson, M. D.; Miller, J. R.; Green, N. S.; Closs, G. L. *J. Phys. Chem.* **1989**, *93*, 1173-1176.

(17) Smalley, J. F.; Feldberg, S. W.; Chidsey, C. E. D.; Linford, M. R.; Newton, M. D.; Liu, Y. P. *J. Phys. Chem.* **1995**, *99*, 13141.

(18) Smalley, J. F.; Finklea, H. O.; Chidsey, C. E. D.; Linford, M. R.; Creager, S. E.; Ferraris, J. P.; Chalfant, K.; Zawodzinsk, T.; Feldberg, S. W.; Newton, M. D. *J. Am. Chem. Soc.* **2003**, *125*, 2004-2013.

(19) Smalley, J. F.; Sachs, S. B.; Chidsey, C. E. D.; Dudek, S. P.; Sikes, H. D.; Creager, S. E.; Yu, C. J.; Feldberg, S. W.; Newton, M. D. *J. Am. Chem. Soc.* **2004**, *126*, 14620-14630.

(20) Sikes, H. D.; Smalley, J. F.; Dudek, S. P.; Cook, A. R.; Newton, M. D.; Chidsey, C. E. D.; Feldberg, S. W. *Science* **2001**, *291*, 1519-1523.

(21) Sachs, S. B.; Dudek, S. P.; Hsung, R. P.; Sita, L. R.; Smalley, J. F.; Newton, M. D.; Feldberg, S. W.; Chidsey, C. E. D. *J. Am. Chem. Soc.* **1997**, *119*, 10563-10564.

(22) Robinson, D. B.; Chidsey, C. E. D. *J. Phys. Chem. B* **2002**, *106*, 10706-10713.

(23) Finklea, H. O.; Liu, L.; Ravenscroft, S.; Punturi, S. *J. Phys. Chem.* **1996**, *100*, 18852-18858.

(24) Chidsey, C. E. D.; Bertozzi, C. R.; Putvinski, T. M.; Mujsce, A. M. *J. Am. Chem. Soc.* **1990**, *112*, 4301-4306.

(25) Chidsey, C. E. D. *Science* **1991**, *251*, 919-922.

(26) Finklea, H. O.; Hanshew, D. D. *J. Am. Chem. Soc.* **1992**, *114*, 3173.

(27) Nazeeruddin, M. K.; Pechy, P.; Renouard, T.; Zakeeruddin, S. M.; Humphry-Baker, R.; Comte, P.; Liska, P.; Cevey, L.; Costa, E.; Shklover, V.; Spiccia, L.; Deacon, G. B.; Bignozzi, C. A.; Gratzel, M. *J. Am. Chem. Soc.* **2001**, *123*, 1613-1624.

(28) Nazeeruddin, M. K.; Kay, A.; Rodicio, I.; Humphrybaker, R.; Muller, E.; Liska, P.; Vlachopoulos, N.; Gratzel, M. *J. Am. Chem. Soc.* **1993**, *115*, 6382-6390.

(29) Gratzel, M. *Nature* **2001**, *414*, 338-344.

(30) Frank, A. J.; Kopidakis, N.; van de Lagemaat, J. *Coord. Chem. Rev.* **2004**, *248*, 1165-1179.

(31) Kopidakis, N.; Benkstein, K. D.; van de Lagemaat, J.; Frank, A. J. *J. Phys. Chem. B* **2003**, *107*, 11307-11315.

(32) Gregg, B. A.; Pichot, F.; Ferrere, S.; Fields, C. L. *J. Phys. Chem. B* **2001**, *105*, 1422-1429.

(33) Nusbaumer, H.; Moser, J. E.; Zakeeruddin, S. M.; Nazeeruddin, M. K.; Gratzel, M. *J. Phys. Chem. B* **2001**, *105*, 10461-10464.

(34) Nusbaumer, H.; Zakeeruddin, S. M.; Moser, J. E.; Gratzel, M. *Chem.-Eur. J.* **2003**, *9*, 3756-3763.

(35) Cameron, P. J.; Peter, L. M.; Zakeeruddin, S. M.; Gratzel, M. *Coord. Chem. Rev.* **2004**, *248*, 1447-1453.

(36) Sapp, S. A.; Elliott, C. M.; Contado, C.; Caramori, S.; Bignozzi, C. A. *J. Am. Chem. Soc.* **2002**, *124*, 11215-11222.

(37) Clifford, J. N.; Palomares, E.; Nazeeruddin, M. K.; Gratzel, M.; Nelson, J.; Li, X.; Long, N. J.; Durrant, J. R. *J. Am. Chem. Soc.* **2004**, *126*, 5225-5233.

(38) Galoppini, E.; Guo, W. Z.; Qu, P.; Meyer, G. J. *J. Am. Chem. Soc.* **2001**, *123*, 4342-4343.

(39) Galoppini, E.; Guo, W. Z.; Zhang, W.; Hoertz, P. G.; Qu, P.; Meyer, G. J. *J. Am. Chem. Soc.* **2002**, *124*, 7801-7811.

(40) Piotrowiak, P.; Galoppini, E.; Wei, Q.; Meyer, G. J.; Wiewior, R. *J. Am. Chem. Soc.* **2003**, *125*, 5278-5279.

(41) Gaal, D. A.; McGarrah, J. E.; Liu, F.; Cook, J. E.; Hupp, J. T. *Photochem. Photobiol. Sci.* **2004**, *3*, 240-245.

(42) Gerischer, H. *Z. Phys. Chem.* **1960**, *26*, 223.

(43) Gerischer, H. In *Advances in Electrochemistry and Electrochemical Engineering*; Delahay, P., Ed.; Wiley-Interscience: New York, 1961; Vol. 1, pp 139-232.

(44) Lewis, N. S. *J. Phys. Chem. B* **1998**, *102*, 4843.

(45) Morrison, S. R. *Electrochemistry at Semiconductor and Oxidized Metal Electrodes*; Plenum: New York, 1980.

(46) Hamann, T. W.; Gstrein, F.; Brunschwig, B. S.; Lewis, N. S. *J. Am. Chem. Soc.* **2005**, *127*, 13949-13954.

(47) Hamann, T. W.; Gstrein, F.; Brunschwig, B. S.; Lewis, N. S. *J. Am. Chem. Soc.* **2005**, *127*, 7815-7824.

(48) Hamann, T. W.; Gstrein, F.; Brunschwig, B. S.; Lewis, N. S. *Chem. Phys*. **2006**, *326*, 15-23.

(49) Chan, M. S.; Wahl, A. C. *J. Phys. Chem.* **1978**, *82*, 2542-2549.

(50) Bryant, G. M.; Fergusso, J. *Aust. J. Chem.* **1971**, *24*, 275-&.

(51) Tan, M. X.; Laibinis, P. E.; Nguyen, S. T.; Kesselman, J. M.; Stanton, C. E.; Lewis, N. S. *Progress in Inorganic Chemistry* **1994**, *41*, 21-144.

(52) Lewis, N. S.; Rosenbluth, M. L. In *Photocatalysis: Fundamentals and Applications*; Serpone, N., Pelizzetti, E., Eds.; John Wiley & Sons: New York, 1989.

(53) Bhargava, R. *Properties of Wide Bandgap II-VI Semiconductors*; Inspec: London, 1997; Vol. Series No. 17.

(54) Marcus, R. A.; Sutin, N. *Biochim. Biophys. Acta* **1985**, *811*, 265.

(55) Meyer, T. J.; Taube, H. In *Comprehensive Coordination Chemistry*; Wilkinson, S. G., Gilliard, R. D., McCleverty, J. A., Eds.; Pergamon Press: New York, 1987; Vol. 1, p 331.

(56) Sutin, N. *Acc. Chem. Res.* **1982**, *15*, 275.

(57) Sutin, N. *Prog. Inorg. Chem.* **1983**, *30*, 441.

(58) Brunschwig, B. S.; Logan, J.; Newton, M. D.; N., S. *J. Am. Chem. Soc.* **1980**, *102*, 5798.

(59) Biner, M.; Burgi, H.-B.; Ludi, A.; C., R. *J. Am. Chem. Soc.* **1992**, *114*, 5197-5203.

(60) Brown, G. M.; Sutin, N. *J. Am. Chem. Soc.* **1979**, *101*, 883-892.

(61) Nielson, R. M.; Wherland, S. *J. Am. Chem. Soc.* **1985**, *107*, 1505-1510.

(62) Royea, W. J.; Fajardo, A. M.; Lewis, N. S. *J. Phys. Chem. B* **1997**, *101*, 11152.

(63) Kuciauskas, D.; Freund, M. S.; Gray, H. B.; Winkler, J. R.; Lewis, N. S. *J. Phys. Chem. B* **2001**, *105*, 392-403.

(64) Marcus, R. A. *J. Phys. Chem.* **1991**, *95*, 2010.

(65) Ashkenov, N.; Mbenkum, B. N.; Bundesmann, C.; Riede, V.; Lorenz, M.; Spemann, D.; Kaidashev, E. M.; Kasic, A.; Schubert, M.; Grundmann, M.; Wagner, G.; Neumann, H.; Darakchieva, V.; Arwin, H.; Monemar, B. *J. App. Phys.* **2003**, *93*, 126-133.

Chapter 5

Control of the Stability, Electron-Transfer Kinetics, and pH-Dependent Energetics of Si/H_2O Interfaces Through Methyl Termination of Si(111) Surfaces

5.1 INTRODUCTION

The positions of the band edges of photoelectrodes must be controlled to enable water splitting and other desirable photoelectrochemical reactions at semiconductor/liquid interfaces.[1,2] To allow water splitting to be possible thermodynamically under standard state conditions, the semiconductor electrode must produce a photovoltage in excess of 1.23 V. In addition, the energies of the bottom of the conduction band and the top of the valence band, respectively, need to be positioned appropriately with respect to the electrochemical potentials of the H^+/H_2 and O_2/H_2O redox couples (Scheme 5.1).[1] An analogous energy-matching constraint applies to photoelectrolysis of HI, HBr, and of many other fuel-forming redox processes. The electrochemical potentials of the H^+/H_2 and O_2/H_2O systems can, of course, be manipulated by changing the pH of the solution.[3] It is well-documented, however, that such pH variation does not, in general, affect the energetics of the semiconductor/liquid interface because the band-edge positions of the semiconductor surface are also sensitive to pH.[4-6] The need to manipulate the band-edge positions energetically has prompted "band-edge engineering" approaches in which materials with different band gaps are layered onto desired photoactive materials, in attempts to shift the energetics of the semiconductor into the appropriate positions.[7] We describe herein another approach to control the interfacial energetics of photoelectrodes, in which covalent chemical modification of the surface is used to eliminate the pH dependence of the band edges, allowing manipulation of the energetics of the bands of the solid relative to the redox potentials of the solution through pH control of the electrolyte.

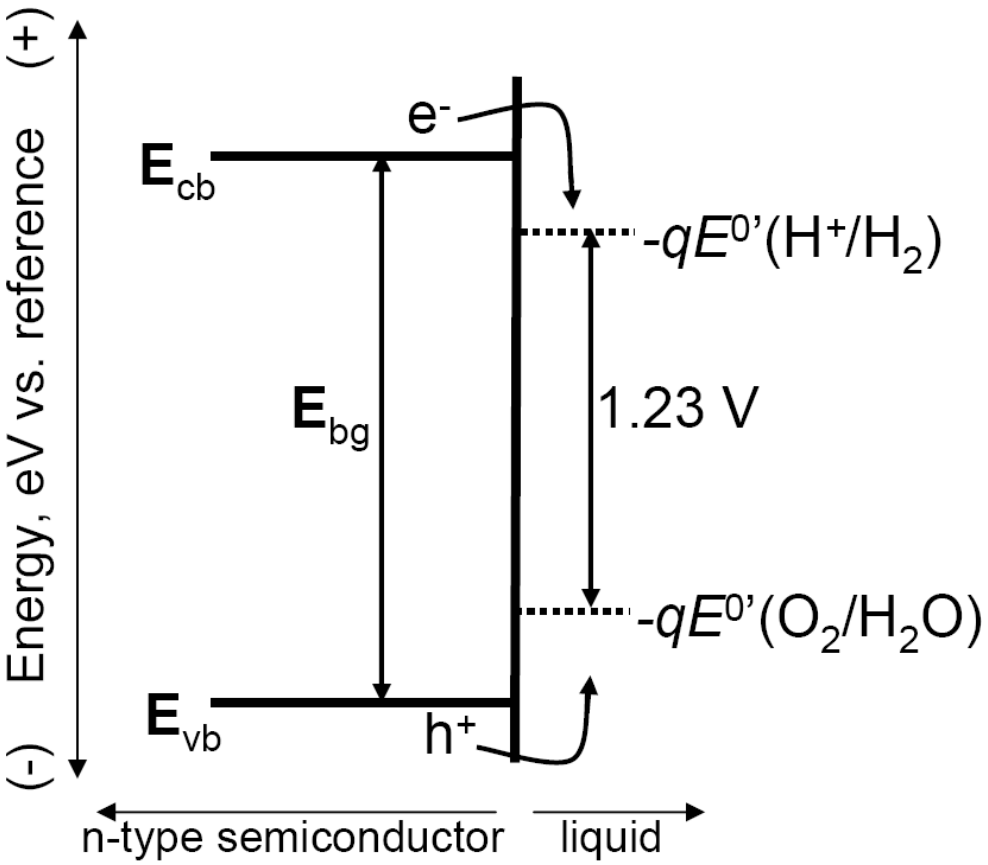

Scheme 5.1 Energy vs. distance for an idealized n-type semiconductor for water splitting in contact with an aqueous solution. The conduction-band and valence-band edges, $\mathbf{E}_{cb}$ and $\mathbf{E}_{vb}$, respectively, separated by a band gap energy, $\mathbf{E}_{bg}$, straddle the formal potentials $E^{o\prime}(H^+/H_2)$ and $E^{o\prime}(O_2/H_2O)$ for the reduction and oxidation, respectively, of water.

Metal oxide photoelectrodes are well-known to display a Nernstian dependence of their flat-band potential, E_{fb}, on pH.[4-6,8] The 1.1 eV band-gap of Si is better matched to the solar spectrum than that of most metal oxides,[2] and Si could be used in a dual-junction- or heterojunction-type system for water splitting if its band-edge positions could be appropriately controlled. Si, however, readily oxidizes in the presence of mildly oxidizing redox species in water,[9] introducing both electrochemical instability and an oxide layer whose protonation/deprotonation equilibrium imparts pH sensitivity to the band-edge positions of Si/H_2O interfaces. For example, shifts of E_{fb} of 33 mV/pH unit,[10] 59 mV/pH unit,[11] as well as non-linear shifts of E_{fb} with variations in pH,[9] have been reported for Si/H_2O interfaces.

In this work, we describe the covalent modification of Si surfaces via a two-step chlorination-methylation method[12] to introduce kinetically stable CH_3-Si bonds onto Si surfaces. This process eliminates the pH dependence of the Si band-edge positions, and additionally facilitates use of the Si under conditions in which it otherwise would be rapidly oxidized to produce pH-dependent surface potentials. This methylation process additionally allows for the experimental measurement of the interfacial electron-transfer kinetics in media which cannot be probed at reactive, oxidizable, H-terminated Si surfaces, and has produced a system that reveals "ideal" kinetics behavior at the semiconductor/liquid contact. The ability to control the band-edge positions, and to introduce, or eliminate, a pH dependence of Si surfaces through molecular level control, without introducing deleterious levels of surface states, is of obvious relevance to Si chem-FET (field-effect transistor)'s,[13] light-addressable potentiometric sensor devices,[7]

Si nanowire sensors used in chemical and biological applications,[14] and has implications in a variety of other applications of semiconductor/liquid interfaces.

5.2 EXPERIMENTAL

The (111)-oriented, n-type, Si single crystals (Crysteco Inc.) had a resistivity of 3.7 Ω cm, as determined from four-point probe measurements. The samples were H-terminated by etching for 20 min in a 40% NH_4F solution that was purged with Ar.[12] CH_3-terminated Si samples were prepared by chlorinating H-Si(111) surfaces with PCl_5 in chlorobenzene at 100 °C for 1 hr followed by heating at 70 °C for 14-18 hr in a 1 M CH_3MgBr solution, as described previously.[12,15] Ga-In eutectic was used as an ohmic contact and silver print was used to connect the Ga-In to a tinned copper wire. Paraffin wax was used to seal the electrode assembly in a glass tube. The resulting electrode areas, typically 0.2-0.5 cm^2, were determined by digitizing photographs of a microruler and of the exposed Si surface.

Methyl viologen (MV) dichloride was purchased from Aldrich and used as received. All buffers (phthalate, phosphate, borax, and imidazole) were prepared by literature methods.[16] The ionic strength of all solutions was adjusted to 1.0 M by the addition of KCl. The pH was measured using a VWR Scientific model 8010 pH meter.

Electrochemical measurements were performed with a Schlumberger Instruments model SI1287 potentiostat. All potentials are referenced to a standard calomel electrode (SCE). All solutions were purged with Ar before each measurement, and measurements

were performed under an Ar atmosphere in the dark. X-ray photoelectron spectroscopic (XPS) data were obtained as described previously.[15]

5.3 RESULTS AND DISCUSSION

Figure 5.1 depicts the current density, *J*, vs. applied potential, *E*, observed for CH_3-Si(111) and H-Si(111) electrodes, respectively, in the dark, in contact with 10 mM MV^{2+}(aq). The initial scan of the H-terminated electrode displayed in Figure 5.1 was very similar to that of the CH_3-terminated electrode, but the current density of the H-Si(111) surface decayed quite rapidly thereafter. In fact, most H-terminated Si electrodes studied initially displayed *J-E* curves with lower current densities at a given potential, being similar to the later scans of the *J-E* curve shown in Figure 5.1.

Figure 5.2a displays high-resolution XPS data in the Si 2p region of H-Si(111) samples before and after collection of the *J-E* data. Si oxide was clearly observed after two scans of the *J-E* measurements, even though extensive precautions were taken to prevent deliberate illumination of the electrode. The extent of oxidation was estimated by dividing the ratio of the SiO_x:Si 2p peak areas by the normalization constant 0.21, as described previously.[15] Values of oxide coverage of greater than one equivalent monolayer were observed after two *J-E* scans at either 10 mM or 100 mM MV^{2+} in the solution. This growth of an oxide peak is in agreement with the decay of the current during successive *J-E* scans. Oxide was still formed even when the electrode was scanned only at relatively negative potentials (-0.5 to -0.75 V vs. SCE). These results

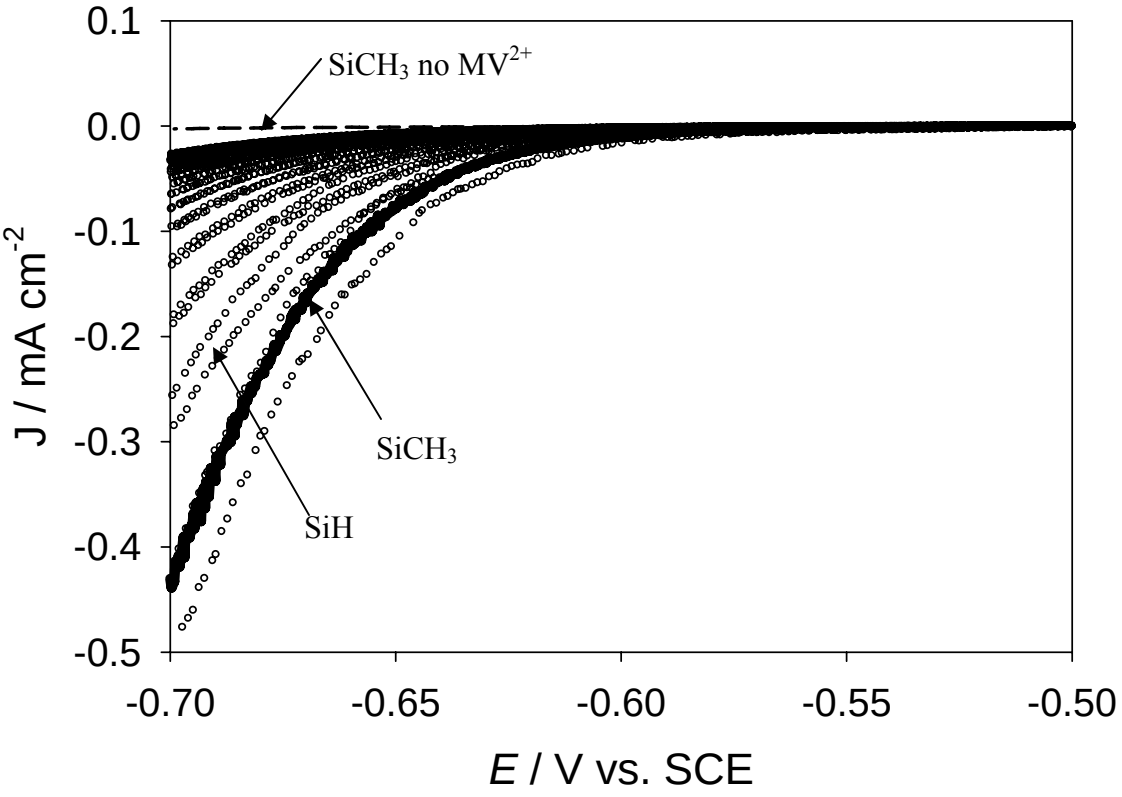

Figure 5.1 Plots of the dark current density, *J*, vs. applied potential, *E*, for H-terminated and methyl-terminated Si in a 10 mM MV^{2+} pH 11 buffer solution. Also shown is a *J*-*E* curve for methyl-terminated Si in contact with aqueous solution without MV^{2+} present.

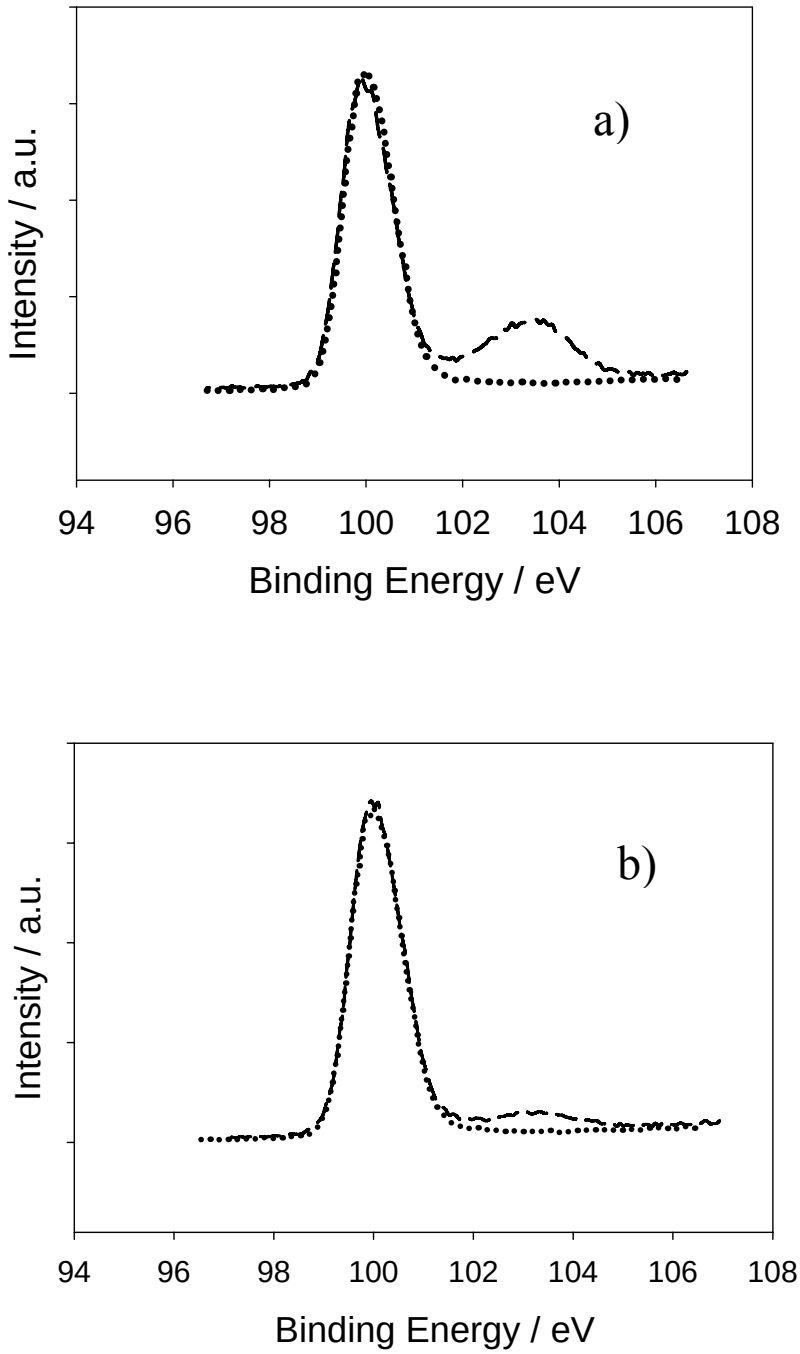

Figure 5.2 High-resolution XP spectra of the Si 2p region of a) a freshly etched H-terminated electrode (dotted line) and the electrode following *J-E* measurements (dashed line) and b) freshly etched H-terminated electrode (dotted line) and a methyl-terminated electrode following *J-E* measurements (dashed line).

highlight the challenge of making reliable electrochemical measurements of H-Si(111) surfaces in contact with aqueous solution. The pH dependence of Si electrodes reported previously[9-11] is then consistently ascribed to the presence of an oxide overlayer on the Si surface after it is initially used as an electrode in such aqueous solutions.

Figure 5.2b compares the high-resolution XP spectra of the Si 2p region of CH_3-Si(111) samples with those of freshly prepared H-Si(111) surfaces. 0.2-0.5 monolayer equivalents of silicon oxide were observed following 2 to 10 *J-E* scans at either [MV^{2+}] = 10 or 100 mM. The introduction of methyl functionality onto the silicon surface clearly protects the Si from oxidation, in accord with the stability of the *J-E* curves for the CH_3-Si(111) surfaces displayed in Figure 5.1.

The protection against oxidation allowed for the measurement of interfacial electron-transfer reactions, which are in accord with the ideal model of electron transfer at the semiconductor/liquid interface. The rate law for an electron-transfer process from the conduction band of an n-type semiconductor to an acceptor species, A, in solution, is given by

$$J(E) = -qk_{et}[\mathrm{A}]n_s \qquad (1)$$

where q is the charge of an electron (1.6022×10^{-19} C), k_{et} is the electron-transfer rate constant ($cm^4\ s^{-1}$), [A] is the acceptor concentration (cm^{-3}), and n_s is the electron concentration (cm^{-3}) at the surface of the semiconductor.[2] The above rate law can be shown to apply by verifying the first-order dependence of J on [A] and n_s.[17]

According to eq (1), an increase in [A] by a factor of 10 should produce a potential shift, ΔE, by $(k_B T/q)\ln(10)$ (with k_B being Boltzmann's constant), i.e., by 59 mV

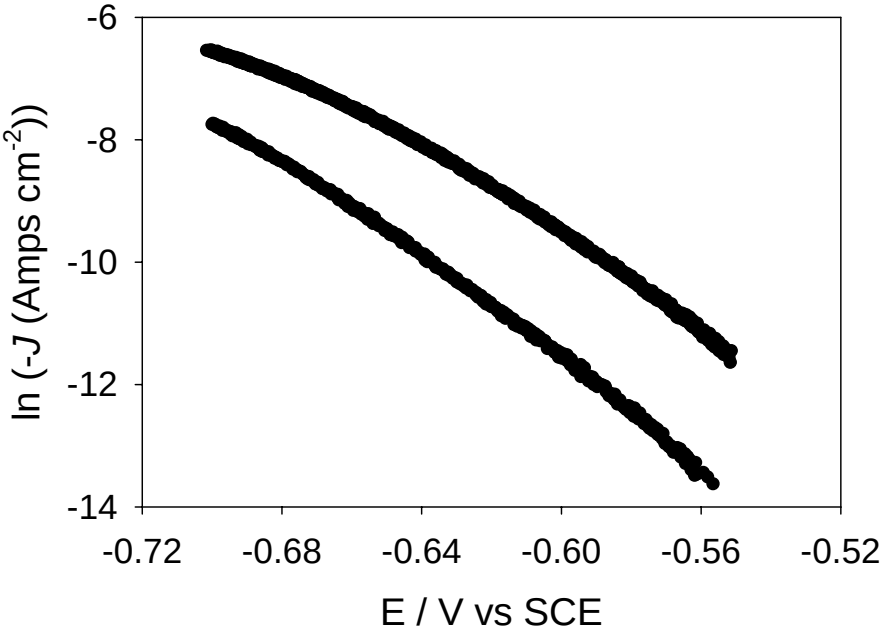

Figure 5.3 Logarithmic plots of *J* vs *E* for a methyl-terminated Si electrode at 10 mM (triangles) and 100 mM (circles) MV^{2+} concentrations. As noted in the text, an increase in [*A*] should result in a shift of the *J*-*E* curve by approximately ΔE = 59 mV.

at room temperature, to produce a given value of J. Figure 5.3 displays a semi-logarithmic plot of J-E for a CH_3-Si(111) electrode in contact with solutions having $[MV^{2+}]$ = 10 mM and $[MV^{2+}]$ = 100 mM. The ten-fold increase in [A] resulted in a 50 mV shift of the J-E curve, verifying the first-order dependence of J on [A].

All of the junctions showed rectifying behavior in accord with the diode equation:

$$J = -J_0\left(e^{\frac{-qE}{\gamma k_B T}} - 1\right) \tag{2}$$

where J_o is the exchange current density and γ is the diode quality factor. The diode quality factors were typically 1.1-1.3 at low concentrations of acceptor, in accord with the expectation of $\gamma = 1$ for a process that is kinetically first-order in the concentration of electrons at the surface of the semiconductor. Large acceptor concentrations, while favoring direct electron transfer, typically had higher diode quality factors, indicating the presence of non-ideal recombination pathways attributed to the small growth of oxide, because these measurements followed measurements at low acceptor concentration. As noted above, the current density of H-Si(111) electrodes either displayed, or quickly decayed to, a value of $\gamma \approx 2$. In addition, measurements of CH_3-Si(111) electrodes in contact with the stronger oxidant, $Ru(NH_3)_6^{3+/2+}$, exhibited $\gamma \approx 2$. A correlation between the value of the diode quality factor and Si oxide growth was thus observed, underscoring the necessity of using carefully prepared CH_3-terminated electrodes to probe the kinetics of interfacial electron transfer at n-type (111)-oriented silicon electrodes in aqueous solution.

Since the kinetics of interfacial electron transfer are strongly dependent on the interfacial energetics,[8,18] the kinetics are a good, although indirect, probe of energetic

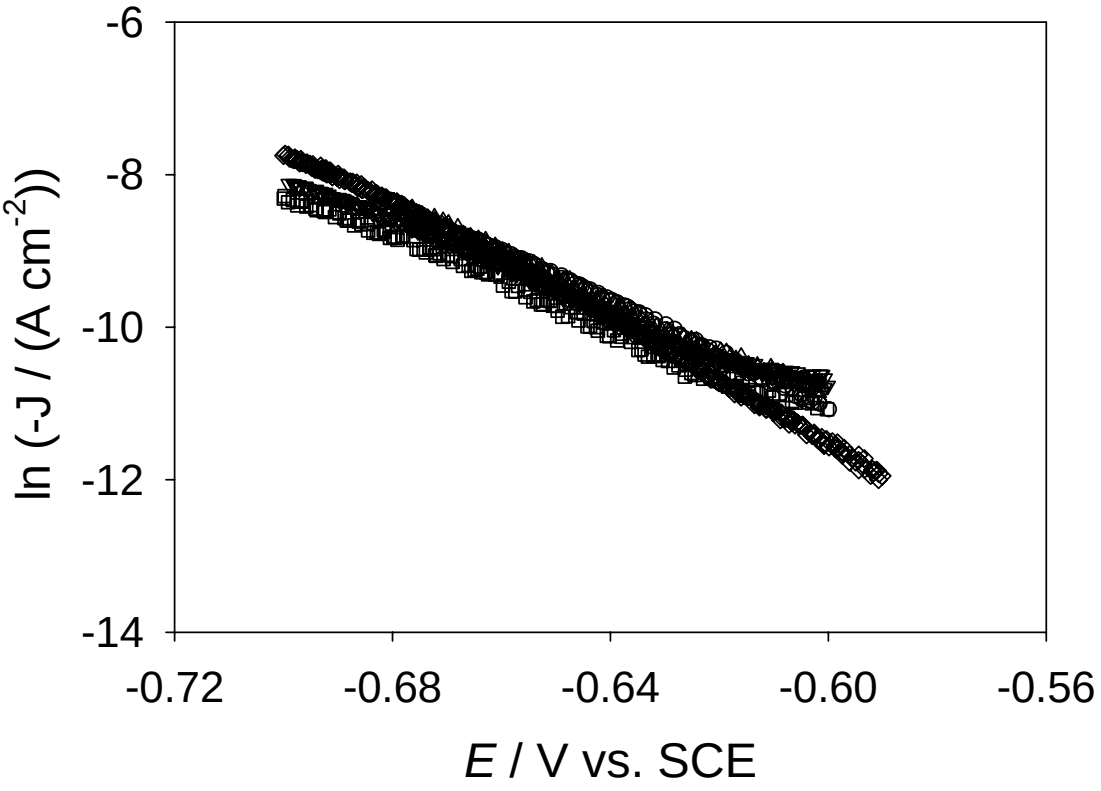

Figure 5.4 Logarithmic plots of *J* vs. *E* for methyl-terminated Si electrodes in contact with 10 mM MV^{2+} at pH = 1.4 (upside down triangle), pH = 3.8 (square), pH = 6.8 (triangle), pH = 9.0 (circle), and pH = 11 (diamond).

variations. Figure 5.4 displays *J-E* data obtained at pH values ranging from 1.5 to 11. If the band edges shifted with pH, a corresponding change in the applied potential would be needed to produce a given value of the interfacial current density, as has been observed for n-ZnO electrodes in contact with outer-sphere redox couples.[8] The invariance of the *J-E* curves despite the nearly 10 pH unit variation in the solution and the formal potential of the H^+/H_2 and O_2/H_2O redox couples, is strong evidence that the band edges of CH_3-Si(111) electrodes are fixed with respect to pH changes, in contrast to the pH dependence of the band edges observed for metal oxides and for unmodified Si electrodes in aqueous solution. The data thus indicate that the energetics of the band-edge positions relative to a pH-dependent redox couple can be manipulated by pH changes at the CH_3-Si(111)/H_2O interface.

5.4 CONCLUSIONS

Methyl-terminated Si(111) electrodes are effective at preventing the oxidation of Si in contact with MV^{2+} dissolved in aqueous solutions. Such surface modification allowed for measurements of the current density vs. applied potential, which are in accord with the ideal model of interfacial electron-transfer reactions at a semiconductor/ liquid junction. The kinetics were observed to be independent of pH over approximately 10 pH units. Since the kinetics are dependent on the interfacial energetics, the invariance of the kinetics with respect to pH implies that the band-edge energetics of these modified Si surfaces are also independent of pH.

5.5 ACKNOWLEDGMENTS

We acknowledge the NSF, grant CHE-021358, for support of this work. XPS data were collected at the Molecular Materials Research Center of the Beckman Institute of the California Institute of Technology.

5.6 REFERENCES

(1) Gerischer, H. In *Solar Energy Conversion. Solid-State Physics Aspects*; Seraphin, B. O., Ed.; Springer-Verlag: Berlin, 1979; Vol. 31, p 115.

(2) Tan, M. X.; Laibinis, P. E.; Nguyen, S. T.; Kesselman, J. M.; Stanton, C. E.; Lewis, N. S. *Prog. Inorg. Chem.* **1994**, *41*, 21-144.

(3) Bard, A. J.; Faulkner, L. R. *Electrochemical Methods, Fundamentals and Applications*; 2nd edition ed.; John Wiley & Sons, Inc.: New York, Chichester, Weinheim, Brisbane, Singapore, Toronto, 2001.

(4) Bolts, J. M.; Wrighton, M. S. *J. Phys. Chem.* **1976**, *80*, 2641-2645.

(5) Lohmann, F. *Ber. Bunsenges. Phys. Chem.* **1966**, *70*, 428-434.

(6) Morrison, S. R. *Electrochemistry at Semiconductor and Oxidized Metal Electrodes*; Plenum: New York, 1980.

(7) Khaselev, O.; Turner, J. A. *Science* **1998**, *280*, 425-427.

(8) Hamann, T.; Gstrein, F.; Brunschwig, B. S.; Lewis, N. S. *Chem. Phys.* **2006**, *326*, 15-23.

(9) Nakato, Y.; Ueda, T.; Egi, Y.; Tsubomura, H. *J. Electrochem. Soc.* **1987**, *134*, 353-358.

(10) Madou, M. J.; Loo, B. H.; Frese, K. W.; Morrison, S. R. *Surf. Sci.* **1981**, *108*, 135-152.

(11) Schlichthorl, G.; Peter, L. M. *J. Electrochem. Soc.* **1994**, *141*, L171-L173.

(12) Bansal, A.; Li, X. L.; Lauermann, I.; Lewis, N. S.; Yi, S. I.; Weinberg, W. H. *J. Am. Chem. Soc.* **1996**, *118*, 7225-7226.

(13) Blackburn, G. F. In *Biosensors Fundamentals and Applications*; Turner, A. P. F., Karube, I., Wilson, G. S., Eds.; Oxford Univ. Press: Oxford, 1987, pp 481-530.

(14) Cui, Y.; Wei, Q. Q.; Park, H. K.; Lieber, C. M. *Science* **2001**, *293*, 1289-1292.

(15) Webb, L. J.; Lewis, N. S. *J. Phys. Chem. B* **2003**, *107*, 5404-5412.

(16) Lide, D. R., Ed. *CRC Handbook of Chemistry and Physics*; 81 ed.; CRC Press, 2001.

(17) Fajardo, A. M.; Lewis, N. S. *J. Phys. Chem. B* **1997**, *101*, 11136-11151.

(18) Hamann, T.; Gstrein, F.; Brunschwig, B. S.; Lewis, N. S. *J. Am. Chem. Soc.* **2005**, *127*, 7815-7824.